2015-08-20

The Shape of Silence: The Solution-State Conformation of Sir Heterochromatin: A Dissertation

Sarah G. Swygert
University of Massachusetts Medical School

THE SHAPE OF SILENCE: THE SOLUTION-STATE CONFORMATION OF SIR HETEROCHROMATIN

A Dissertation Presented

By

SARAH G. SWYGERT

Submitted to the Faculty of the University of Massachusetts Graduate School of Biomedical Sciences, Worcester in partial fulfillment of the requirements for the degree of

DOCTOR OF PHILOSOPHY

August 20th, 2015

Biochemistry and Molecular Pharmacology

THE SHAPE OF SILENCE: THE SOLUTION-STATE CONFORMATION OF SIR HETEROCHROMATIN

A Dissertation Presented By

SARAH G. SWYGERT

The signatures of the Dissertation Defense Committee signify completion and approval as to style and content of the Dissertation

_____

Craig L. Peterson, Ph.D., Thesis Advisor

_____

Job Dekker, Ph.D., Member of Committee

_____

Kendall L. Knight, Ph.D., Member of Committee

_____

Jeffrey J. Hayes, Ph.D., Member of Committee

The signature of the Chair of the Committee signifies that the written dissertation meets the requirements of the Dissertation Committee

_____

Paul D. Kaufman, Ph.D., Chair of Committee

The signature of the Dean of the Graduate School of Biomedical Sciences signifies that the student has met all graduation requirements of the school.

_____

Anthony Carruthers, Ph.D., Dean of the Graduate School of Biomedical Sciences

Biochemistry and Molecular Biology

August 20th, 2015

To my family,

for making all of this possible, even when it wasn't easy.

ACKNOWLEDGEMENTS

Surviving graduate school would have been impossible were it not for my Peterson lab family. Specifically, I would like to thank Mayuri Rege for being a constant source of inspiration and awe, Benjamin Manning for serving as a playmate and human punching bag, Christopher Van for all the baked goods and moral support, Salih Topal for being a bright spot in my days, Shinya Watanabe for all the help and laughing at my terrible jokes, Nicholas Adkins for teaching me a few things (I guess), and Gwendolyn Bennett for showing me it was possible to get out. Special thanks to Kimberly Crowley, who instructed me in the use of the AUC (my baby) and patiently dealt with all of my maternal neuroses, among many other things.

Many faculty members at UMMS have helped me in countless ways. I would like to acknowledge Daniel Bolon and Job Dekker for serving on my TRAC, Osman Bilsel and Jill Zitzewitz for assistance with biophysical experiments, Bill Kobertz for navigating me through the BMP program, Ollie Rando for being a cool dude, Paul Kaufman for being an extremely supportive chair of my committees, and Kendall Knight and Anthony Carruthers for making the graduate school such an excellent place to learn. I would also like to thank Jeffrey Hayes at the University of Rochester Medical Center for taking the time to act as the external member of my defense committee.

I am grateful to Benjamin Roscoe, who gave me a tremendous amount of advice on everything from academic politics to experimental troubleshooting, and a lot of emotional support.

Timothy Finco at Agnes Scott College taught me a million good scientific habits, a few of which I still have.

I am particularly indebted to all of the wonderful teachers who taught me in the Dekalb County public schools in Atlanta, Georgia. Specifically, the biology and chemistry departments at Lakeside High School did an amazing job of laying a deep foundation for science careers while fostering the joys of discovery.

My eternal gratitude goes to my family for being endlessly and overwhelmingly supportive, and for tirelessly listening to my whining. Thank you so much, and I am so sorry!

Finally, I would like to thank my advisor Craig Peterson for his friendly guidance and brilliant ideas. In the challenging and often cutthroat world of science, he makes an incredibly difficult job look like a piece of cake, and I would like to be him when I grow up.

ABSTRACT

Heterochromatin is a silenced chromatin region essential for maintaining genomic stability in eukaryotes and for driving developmental processes in higher organisms. A hallmark of heterochromatin is the presence of specialized architectural proteins that alter chromatin structure to inhibit transcription and recombination. Although it is generally assumed that heterochromatin is highly condensed, surprisingly little is known about the structure of heterochromatin or its dynamics in solution. In budding yeast, heterochromatin assembly at telomeres and the HM silent mating type loci requires the Sir proteins: Sir3, believed to be the major structural component of SIR heterochromatin, and the Sir2/4 complex, responsible for SIR recruitment to silencing regions and deacetylation of lysine 16 of the histone H4 tail, a mark associated with active chromatin. A combination of sedimentation velocity, atomic force microscopy, and nucleosomal array capture was used to characterize the stoichiometry and conformation of SIR nucleosomal arrays. The results indicate that Sir3 interacts with nucleosomal arrays with a stoichiometry of two Sir3 monomers per nucleosome, and that Sir2/4 may additionally bind at a ratio of one per nucleosome. Despite Sir3's ability to repress transcription *in vivo* and homologous recombination *in vitro* in the absence of Sir2/4, Sir3 fibers were found to be significantly less compact than canonical magnesium-induced 30 nanometer fibers. However, heterochromatin fibers composed of all three Sir

proteins did adopt a more condensed, globular structure. These results suggest that heterochromatic silencing is mediated both by the creation of more stable nucleosomes and by the steric exclusion of external factors.

TABLE OF CONTENTS

LIST OF FIGURES

PREFACE

Chapter II of this work was initially published in *Nature Communications* as:

Swygert, S.G., Manning, B.J., Senapati, S., Kaur, P., Lindsay, S., Demeler, B., Peterson, C.L. Solution-state conformation and stoichiometry of yeast Sir3 heterochromatin fibres. *Nature Communications* **5,** 4751 (2014).

CHAPTER I: AN INTRODUCTION TO SILENCE

Why Does Chromatin Exist?

Chromatin is often presented as nature's solution to a complicated storage problem. As if cramming two meters of genetic material into a several hundred cubic micrometer nucleus were not already a seemingly-Herculean task, DNA's strong electronegative charge creates repulsion between neighboring regions and molecules, rendering it stiff and unwieldy (Pepenella et al. 2014; Maeshima et al. 2014; Ozer et al. 2015). Thus, the wrapping of DNA around positively-charged proteins allows the cell to overcome this electrostatic barrier to efficient packaging (Nishino et al. 2012; Pepenella et al. 2014). However, to view chromatin simply as a molecular scaffold is to miss its overall purpose; it is one thing to shove twenty-four miles of fine wire into a tennis ball (Alberts et al. 2002), and quite another to locate a specific region of that wire again when it is needed. In fact, not only do the genomes of eukaryotic cells manage to fit comfortably within the nucleus, but they are organized by chromatin in an intricate and dynamic way which facilitates all nuclear processes.

On the local scale, the presence of chromatin dictates the accessibility of the underlying DNA sequence to interactions with the enzymes responsible for mediating transcription, replication, and repair (Rando & Winston 2012; Papamichos-Chronakis & Peterson 2013). On a broad scale, chromatin allows

the cell to arrange the genome into active compartments wherein high local concentrations of proteins such as transcription factors promote rapid gene expression, and silent compartments in which repetitive elements and unnecessary developmental genes are wrapped up and placed out of the way (Woodcock & Ghosh 2010; Saksouk et al. 2015). The organization of DNA into chromosomes ensures the successful transfer of each into daughter cells during mitosis, chromatin structures such as telomeres protect DNA from degradation, and chromatin remodeling mediates the dynamic movement of DNA through the nucleus during repair by homologous recombination (Woodcock & Ghosh 2010; Neumann et al. 2012). Inversely, the misregulation of chromatin can lead to aberrant gene expression, faulty DNA repair, chromosomal translocations, developmental errors, oncogenesis, and cell death (Hargreaves & Crabtree 2011).

The Building Blocks of Chromatin

The basic unit of chromatin is the nucleosome core particle, which consists of 147 base pairs of DNA wrapped 1.7 times around an octamer composed of two copies each of the canonical core histone proteins H2A, H2B, H3, and H4 (Figure 1.1) (Richmond et al. 1984; Luger et al. 1997). The contacts between DNA and histones are mediated primarily by interactions of basic side chains and main-chain amide groups with the phosphate backbone, as well as by

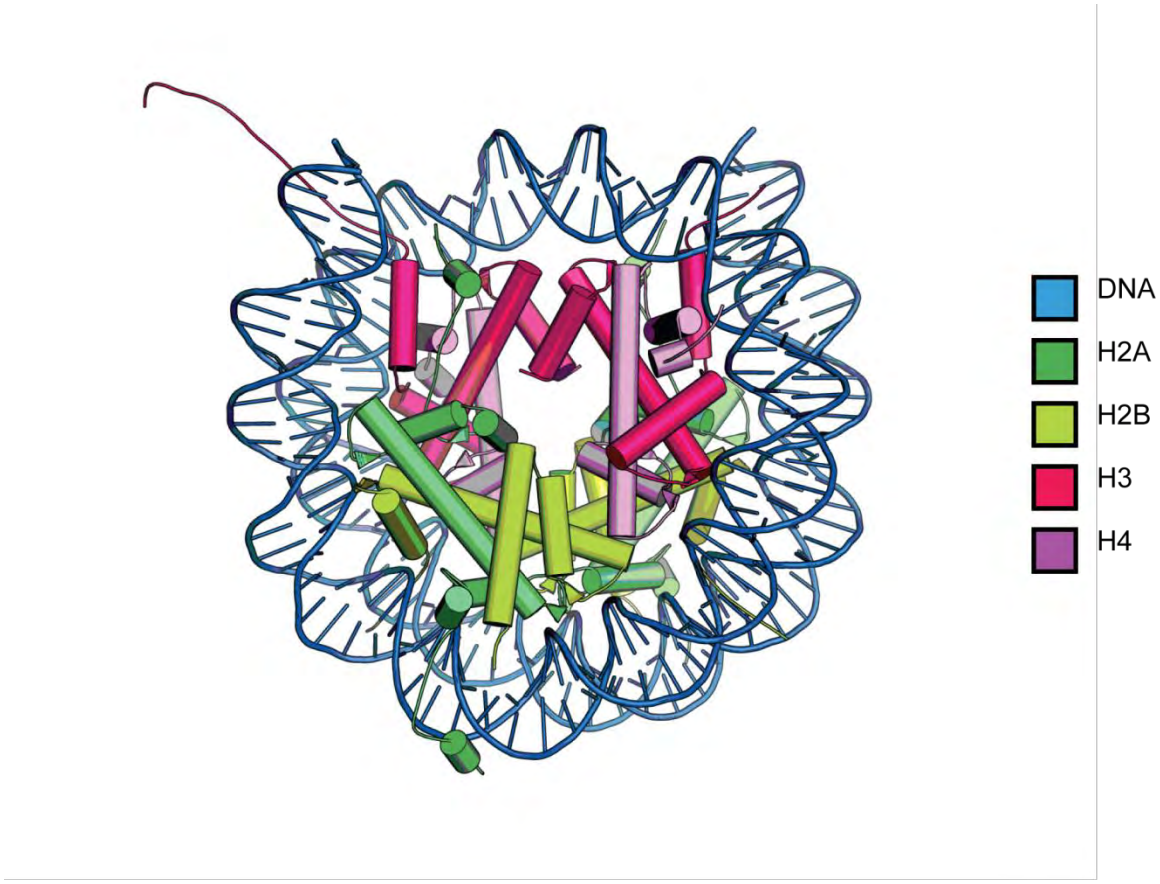
DNA
H2A
H2B
H3
H4

Figure 1.1 Crystal structure of the nucleosome. The crystal structure of the nucleosome at 2.8 Å resolution (PDB # 1aoi, Luger et al. 1997).

the intercalation of an arginine side chain into each of the 14 minor grooves (Luger et al. 1997; Davey et al. 2002). This association of DNA with the histone octamer represents the first level of compaction by chromatin; while the persistence length of DNA is approximately 150 base pairs, the DNA of the nucleosome is contorted into a turn of about 80 base pairs (Richmond et al. 2003; Cutter & Hayes 2015). Although nucleosomes form readily throughout the genome, some sequence-specificity clearly exists, with the need for greater distortion of the DNA structure of A-T rich regions leading to an apparent preference for G-C sequences (Bao et al. 2006; Hughes & Rando 2009), though the sequence patterns necessary to generate the strongest positioning are significantly more complex and involve 10 base pair periodic repeats likely conducive to bending (Lowary & Widom 1998).

The core histone proteins are highly conserved from yeast to humans. Each is a small, basic protein containing a histone fold motif composed of two shorter α-helices flanking a longer central α-helix, with the three helices separated by two short loops (Luger et al. 1997). Heterodimers are formed between H2A and H2B and H3 and H4 via anti-parallel interactions between central helices (Arents et al. 1991). Additionally, H3 and H4 exist as a stable tetramer mediated by contacts between H3 molecules across heterodimers (Arents et al. 1991). At physiological salt concentrations, the histone octamer is only stable when wrapped by DNA (Hansen et al. 1991; Cutter & Hayes 2015). Nucleosome formation is initiated by the binding of an H3/H4 tetramer, followed

by the separate binding of two H2/H2B dimers (Hansen et al. 1991), a process aided *in vivo* by a diverse set of histone chaperones (Kaufman & Botchan 1994).

In addition to the histone fold motif, each histone has a disordered N-terminal tail, with H2A also possessing a C-terminal tail, all of which extend from the nucleosome and represent popular sites for binding by chromatin regulators (Luger et al. 1997; Davey et al. 2002). The tails are especially frequent targets of post-translational modifications, though myriad modifications occur across the solvent-exposed faces of the nucleosome as well. Common modifications include lysine acetylation, the mono-, di-, or tri- methylation of lysines, mono- or di-methylation of arginines, the phosphorylation of serines, threonines, or tyrosines, as well as lysine ubiquitylation and SUMOylation (Zentner & Henikoff 2013). These marks often occur in complex patterns, and there are numerous ongoing studies focused on understanding how such patterns are interpreted by cellular machineries (Patel & Wang 2013). Surprisingly, very few histone marks appear to affect chromatin structure dramatically by themselves, with the large majority of histone modifications influencing either the binding or activity of other regulatory factors, such as chromatin architectural proteins and ATP-dependent chromatin remodeling enzymes (Shogren-knaak & Peterson 2006; Woodcock & Ghosh 2010; Zentner & Henikoff 2013; Swygert & Peterson 2014).

Higher-order Chromatin Structure

Nucleosomes occur periodically throughout eukaryotic genomes separated by free linker DNA, whose length varies between species, cell types, and locations within the nucleus (Simpson 1986; Wang et al. 2008; Woodcock & Ghosh 2010). Budding yeast primarily have short linkers of 15 or 25 base pairs, whereas most vertebrates have an average closer to 35 base pairs (Wang et al. 2008; Woodcock & Ghosh 2010; Brogaard et al. 2012). Linear strings of nucleosomes along the same DNA strand are referred to as nucleosomal arrays

Although detailed structural studies of chromatin are difficult to perform *in vivo*, a great deal of structural information has been discovered using chromatin isolated from nuclei and particularly *in vitro* reconstituted nucleosomal arrays. Two major strategies exist for array reconstitution: 1) Arrays can be generated by combining recombinant purified histone octamers and DNA template containing strong nucleosome positioning sequences with histone chaperone proteins such as Nap1, which will facilitate the binding of histones to DNA, and a chromatin remodeling enzyme capable of spacing nucleosomes evenly along the DNA strand, such as ISWI, and 2) Octamers and DNA template can be combined in two molar sodium chloride, then taken through a series of decreasing salt dialysis steps during which the octamers break apart into tetramers and dimers and stably reform at positioning sequences (Simpson et al. 1985; Hansen et al. 1991; Lu et al. 2006). These arrays are then suitable for analysis by experimental methods such as X-ray crystallography (for smaller particles),

electron or atomic force microscopy (EM or AFM), small angle x-ray scattering (SAXS), and sedimentation velocity analytical ultracentrifugation (SV-AUC).

From these *in vitro* studies, it has been determined that in low-salt conditions, a linear array of nucleosomes exists in an extended beads-on-a-string structure known as the 10 nanometer fiber (Olins & Olins 1974). This is due to the fact that despite the highly basic nature of histone proteins, the nucleosome is only capable of neutralizing about half of the negative charge of the DNA backbone, maintaining a significant level of electrostatic repulsion (Maeshima et al. 2014). However, when moderate salt is added to the buffer, particularly divalent cations such as Mg^{2+}, it functions to shield the backbone from repulsion, permitting compaction into the 30 nanometer fiber (Finch & Klug 1976; Widom 1986; Schwarz & Hansen 1994). The 30 nanometer fiber can additionally be stabilized in the presence of linker histone H1, which is ubiquitous in higher eukaryotes and appears to bind at a stoichiometry of one per nucleosome at the entry-exit point of DNA, where it shields an additional 20 base pairs of DNA from nuclease digestion (Simpson 1978; Thoma et al. 1979; Allan et al. 1980; Staynov & Crane-Robinson 1988).

The formation of the 30 nanometer fiber requires the N-terminal tails of histones, especially H3 and H4 tails (Garcia-Ramirez et al. 1992; Schwarz et al. 1996), and is believed to be mediated largely by binding interactions between the base of positively-charged H4 tails and an H2A/H2B acidic patch on the surface of adjacent nucleosomes (Dorigo et al. 2003; Dorigo et al. 2004; Shogren-Knaak

et al. 2006; Kan et al. 2009). This contact was initially recognized in the packing of the crystal lattice in the X-ray crystal structure of the nucleosome (Luger et al. 1997), and was confirmed by cross-linking studies of folded *in vitro* reconstituted arrays (Kan et al. 2009). Importantly, the acetylation of a single residue in the H4 tail, lysine 16 (H4-K16), disrupts the H4 tail/acidic patch interaction and abrogates 30 nanometer fiber compaction to the same extent as deletion of the entire H4 tail (Shogren-Knaak et al. 2006).

The overall structure of the 30 nanometer fiber has been controversial, with some groups favoring a two-start zigzag model in which contacts occur between every-other nucleosome (Woodcock et al. 1984; Dorigo et al. 2004), and other groups advocating a one-start solenoid folding model stabilized by contacts between neighboring nucleosomes (Finch & Klug 1976; Widom 1985; Kruithof et al. 2009). However, this discussion was largely resolved by a careful EM study which demonstrated that arrays of shorter linker-length (167 base pairs) fold into zigzags, whereas arrays with longer linkers (197 base pairs) fold into one-start helices (Routh et al. 2008), though evidence exists that many 30 nanometer fibers may exist in some combination of both (Grigoryev et al. 2009). Interestingly, not only the length but also the periodicity of linkers affects the compaction of arrays with shorter linkers; formation of efficiently compacted structures was observed in arrays in which linkers contained 10*n* base pairs, but not in arrays where linker periodicity was 10*n* + 5 (Correll et al. 2012). Presumably this is due to the orientation of nucleosomes in relation to each other

on the DNA strand, as a complete turn of the DNA helix requires approximately ten base pairs, and thus a 10*n* + 5 linker periodicity would create rotational variability between nucleosomes.

Beyond 30 nanometer fiber compaction, the addition of greater concentrations of divalent cations to reconstituted chromatin leads to array oligomerization, forming very large structures that sediment at hundreds S and contain many array fibers (Schwarz et al. 1996). Although oligomerization is also disrupted by H4-K16 acetylation (Shogren-Knaak et al. 2006), the determinants of oligomerization vary from 30 nm folding (Schwarz et al. 1996; Tse & Hansen 1997), and in fact oligomerization is contrary to intra-array compaction (Sinha & Shogren-Knaak 2010). Instead, oligomerization is facilitated by contacts between H3 and H4 tails and the DNA and acidic patches of neighboring arrays, creating interdigitated fibers (Zheng et al. 2005; Kan et al. 2007; Kan et al. 2009; Sinha & Shogren-Knaak 2010). Surprisingly, despite the presence of a larger acidic patch, the incorporation of the histone variant H2A.Z into arrays decreases their ability to oligomerize *in vitro* (Fan et al. 2002), possibly reflective of H2A.Z's association with active chromatin *in vivo* (Gabrielli et al. 1981).

While the folding properties of reconstituted arrays are well-defined, their relevance to *in vivo* chromatin structure is unclear. However, a significant body of evidence has emerged suggesting that 30 nanometer fibers are not a dominant conformation in the nucleus (Maeshima et al. 2014). Even *in vitro*, compaction requires the regular spacing and consistent saturation of

nucleosomes (Schwarz & Hansen 1994), a state rarely found *in vivo* (van Holde & Zlatanova 2007). Additionally, chromatin within the cell is constantly bound and metabolized by a plethora of structural proteins and enzymes which logically must create steric hindrance to intra-array folding (Woodcock & Ghosh 2010). Consistently, recent cryo-EM, SAXS, and electron spectroscopic imaging (ESI) studies of purified chromatin failed to identify 30 nanometer fibers, even in mitotic chromosomes (Eltsov et al. 2008; Nishino et al. 2012; Fussner et al. 2012). Chromosome-conformation-capture (3C) based studies, which report on chromatin interactions within cells, have also failed to demonstrate the presence of 30 nanometer fibers in cells ranging from budding yeast to human, and within both interphase and mitotic chromatin (Dekker 2008; Lieberman-Aiden et al. 2009; Naumova et al. 2013). Instead, *in vivo* chromatin appears to exist as loops of 10 nanometer fibers, which may interdigitate in a manner similar to array oligomerization in more densely-packed regions (Grigoryev 2004; Eltsov et al. 2008; Maeshima et al. 2014). In support of this theory, physiological salt concentrations exist at levels that promote oligomerization rather than folding *in vitro*, and the increase in divalent cation concentration during mitosis has been shown to be necessary for the complete folding of chromosomes (Schwarz et al. 1996; Strick et al. 2001; Lu et al. 2006). These findings highlight the need for the implementation of controls in *in vitro* studies to ensure that structures made using reconstituted chromatin retain known properties of chromatin within the cell.

Further, these studies suggest that internal mechanisms of folding are insufficient to create repressive chromatin domains.

General Properties of Heterochromatin

Although the exact structural state of chromatin within the cell has yet to be conclusively determined, it is clear that *in vivo* chromatin exists in one of two major forms of distinct conformation and function. Euchromatin contains transcriptionally active genes, and thus maintains an accessible structure toward the interior of the nucleus where transcription factors, polymerases, and other regulatory machinery are abundant (Woodcock & Ghosh 2010). In contrast, heterochromatin consists of unexpressed, or silent, densely-packed regions of the genome and locates primarily around the nuclear periphery (Woodcock & Ghosh 2010; Beisel & Paro 2011; Saksouk et al. 2015).

Heterochromatin can be further classified into two types, constitutive and facultative. Constitutive heterochromatin exists largely at telomeres and centromeres, contains mostly repetitive DNA sequences, and is present in the same general location throughout the cells of an organism (Grewal & Jia 2007; Saksouk et al. 2015). This form of heterochromatin is essential for maintaining genome stability, as it protects chromosome ends, blocks aberrant homologous recombination between repetitive sequences that could lead to chromosomal translocations or deletions, and guards against the spreading of transposable

elements (Grewal & Jia 2007; Beisel & Paro 2011). Facultative heterochromatin forms in various genomic locations, where it functions to silence genes in a manner necessary for development (Grewal & Jia 2007; Beisel & Paro 2011; Simon & Kingston 2013). The formation of facultative heterochromatin is essential for the differentiation and maintenance of cell types (Simon & Kingston 2013). A central theme in the creation of both types of heterochromatin is the recruitment of heterochromatin proteins by sequence-specific DNA binding factors to silencing regions, a process known as nucleation, followed by the deacetylation of histones and in higher organisms the propagation of specific methylation marks, and the spreading of these proteins and histone modification states linearly outward generating repressive domains (Rusche et al. 2002; Rusche & Lynch 2009; Beisel & Paro 2011; Kueng et al. 2013). While heterochromatic silencing is believed to be mediated by the construction of a repressive chromatin conformation, the nature of this structure and thus its mechanism of silencing remains a mystery.

HP1 Heterochromatin

Most eukaryotes possess heterochromatin that relies on paralogs of Heterochromatin Protein 1 (HP1). HP1 was first discovered in *Drosophila melanogaster* when it was found to be responsible for mediating position effect variegation (PEV), a phenomenon in which genes located near heterochromatin

are variably silenced within a genetically identical population (James & Elgin 1986; Eissenberg et al. 1990). Since then, five HP1 paralogs have been identified in *D. melanogaster* (a, b, c, d, and e), three in humans (α, β, and γ), and two in *Schizosaccharomyces pombe* (Swi6 and Chp2) (Grewal & Jia 2007; Canzio et al. 2014). All HP1 proteins contain a chromodomain (CD) responsible for binding di- or tri-methylated histone H3 lysine 9 (H3K9), a disordered central hinge region that binds DNA and RNA sequence-independently, and a chromoshadow domain (CSD) that allows HP1 proteins to dimerize (Platero et al. 1995; Bannister et al. 2001; Cowieson et al. 2000; Smothers & Henikoff 2000; Lachner et al. 2001; Meehan et al. 2003; Canzio et al. 2013).

In *S. pombe*, heterochromatin is nucleated by DNA-binding factors such as Atf1 and Taz1, which recruit Clr3, a histone deacetylase (Jia et al. 2004; Kanoh et al. 2005; Yamada et al. 2005). Deacetylation then promotes binding of Clr4, the homolog of *D. melanogaster* Su(var)3-9, which both methylates H3K9 and binds methylated H3K9 via its chromodomain (Rea et al. 2000; Schotta et al. 2002). Heterochromatin spreading is then mediated by cycles of Clr4 and Swi6 binding and H3K9 methylation, with Swi6 generating a repressive structure (Grewal & Jia 2007; Beisel & Paro 2011; Al-Sady et al. 2013). A parallel form of nucleation occurs at repeat regions, in which the transcription of repetitive sequences generates small interfering RNAs (siRNAs) which bind to Argonaute protein (Ago1) in the RNA-induced initiation of transcriptional gene silencing (RITS) complex (Hall et al. 2002; Sugiyama et al. 2005; Bühler et al. 2006;

Grewal & Jia 2007). This in turn targets RITS to silencing regions, where it recruits Clr4. RITS, Clr4, and Swi6 then cooperatively propagate and bind H3K9 methylated chromatin, forming heterochromatin domains.

Silencing in HP1 heterochromatin requires the ability of HP1 proteins to oligomerize, presumably inducing chromatin compaction as HP1 molecules interact across nucleosomes. However, though HP1 proteins are competent to dimerize between adjacent nucleosomes, the resulting effect on chromatin structure is unknown (Brasher et al. 2000; Cowieson et al. 2000; Canzio et al. 2011). Interestingly, recent work on Swi6 has found that it preferentially binds H3K9 trimethyl nucleosomal arrays with 15 base pair linkers at a ratio of four Swi6 monomers per nucleosome (Canzio et al. 2011). This preference for small linkers may demonstrate the limit of Swi6 proteins to oligomerize between nucleosomes, as cooperative array binding is diminished when the length between nucleosomes is extended (Canzio et al. 2011). Further, flexibility in its hinge region allows it to exist in two distinct conformations; a closed state, in which CD domains of neighboring Swi6 proteins bind a histone mimic sequence on each other rather than H3K9, and an open state in which CD domains are capable of both H3K9 binding and oligomerization across chromatin (Canzio et al. 2013). This auto-inhibition function may provide an additional mechanism by which HP1 protein polymerization is regulated *in vivo*.

SIR Heterochromatin

The most thoroughly-characterized form of heterochromatin exists in the budding yeast *Saccharomyces cerevisiae*, which requires the silent information regulator, or Sir, proteins. Although SIR heterochromatin is relatively simple and involves proteins which are mostly unconserved, it operates under the same general principles of heterochromatin in higher eukaryotes. Specifically, SIR heterochromatin is hypoacetylated, exists largely at the nuclear periphery, is formed via nucleation and spreading, and maintains a heritably silent state (Rusche et al. 2003; Kueng et al. 2013; Oppikofer, Kueng & Gasser 2013). SIR heterochromatin occurs both at repetitive sequences at telomeres and at genes regulating cell type, making it a good model system for both constitutive and facultative heterochromatin (Rusche et al. 2003).

The Sir proteins were initially discovered via their role in facultative heterochromatin (Ivy et al. 1986; Rine & Herskowitz 1987). Haploid *S. cerevisiae* exist as one of two cell types, **a** or α, depending on the genes at the mating-type (*MAT*) locus located near the center of Chromosome III (Haber 1998; Rusche et al. 2003). *MAT**a*** and *MATα* encode for transcription factors which initiate **a**- or α-specific programs which allow for mating between cells of opposite type, forming an **a**/α diploid (Roman & Sands 1953; Mackay & Manney 1974; Haber 1998). Cells expressing both **a** and α factors are unable to mate. In addition to *MAT*, *S. cerevisiae* cells maintain copies of the α and **a** genes at the homothallic mating type loci, (*HML* and *HMR*, respectively) located on the left and right sides of

Chromosome III (Takano & Oshima 1970; Hicks et al. 1977; Hicks & Herskowitz 1977; Hicks et al. 1977; Rine et al. 1979; Haber & George 1979; Haber 1998). These genes must be silenced in cells functional for mating. However, homothallic strains expressing the *HO* endonuclease are able to switch between mating types (Kostriken & Heffron 1984). During switching, *HO* cuts at a specific site within the *MAT* locus, and homologous recombination between *MAT* and either *HML* or *HMR* leads to restoration of the original cell type or switching to the opposite type, depending on which *HM* locus is chosen as the repair template (Haber et al. 1980; Haber 1998). Although most laboratory strains are switching deficient, all contain both *MAT* and *HM* loci (Rusche et al. 2003). A screen for mutations leading to expression of *HM* and thus loss of mating identified three genes required for silencing, *Sir2*, *Sir3*, and *Sir4*, and a fourth with a partial effect, *Sir1* (Ivy et al. 1986; Rine et al. 1979; Rine & Herskowitz 1987).

The *sir* genes were also shown to be essential for constitutive heterochromatin formation at telomeres. The insertion of a reporter gene within or adjacent to subtelomeres can lead to silencing of that gene, a term referred to as telomere position effect (Gottschling et al. 1990). This is similar to the PEV phenomenon identified in flies. Specific mutations or deletions of *sir2*, *sir3*, and *sir4* lead to loss of silencing in subtelomeric regions (Aparicio et al. 1991). Consequently, silencing at the *HM* loci and at telomeres occur by the same mechanism of Sir-mediated repression (Aparicio et al. 1991; Rusche et al. 2003).

At both the *HM* loci and telomeres, SIR heterochromatin formation is initiated by the binding of sequence-specific DNA binding factors to silencing regions. *HML* and *HMR* contain E and I silencing elements which are required for *HM* repression and are composed of DNA sequences targeted by Rap1 and Abf1 transcription factors and the Origin Recognition Complex (ORC) (Abraham et al. 1984; Feldman et al. 1984; Brand et al. 1985; Brand et al. 1987). Likewise, telomeric repeat sequences are bound by Rap1, and telomeric ends are bound by the yeast Ku complex (*y*Ku) (Conrad et al. 1990; Palladino et al. 1993; Laroche et al. 1998). The Sir proteins are then recruited to these regions via direct interactions with these DNA binding proteins. Rap1 and Abf1 have been shown to bind both to Sir3 and Sir4, whereas *y*Ku interacts specifically with Sir4 (Diffley & Stillman 1989; Moretti et al. 1994; Mishra & Shore 1999; Roy et al. 2004). ORC is bound by Sir1, which further bridges Sir4 to silencing elements at the *HM* loc (Triolo & Sternglanz 1996). As Sir2 and Sir4 exist as a stable complex *in vivo*, these binding interactions are sufficient to recruit all three Sir proteins to nucleation regions (Moazed et al. 1997; Hoppe et al. 2002). Following initial recruitment, Sir2 deacetylates the histone tails of an adjacent nucleosome, promoting binding of Sir3 to the nucleosome and subsequent recruitment of additional Sir2/4 complex (Figure 1.2) (Hecht et al. 1995; Imai et al. 2000; Rusche et al. 2002). As this cycle of deacetylation and binding continues, the Sir proteins spread along the chromosome away from nucleation

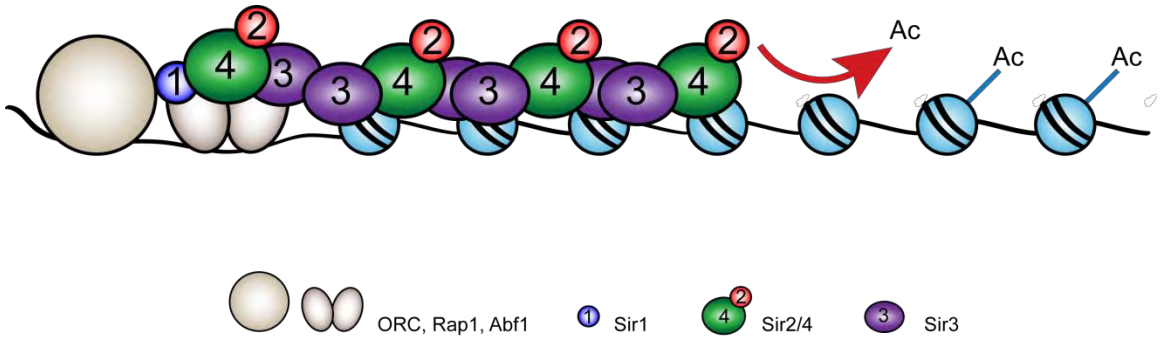
2
4
1
3
3
4
2
3
4
2
3
4
2
Ac
Ac
Ac
ORC, Rap1, Abf1
1
Sir1
2
4
Sir2/4
3
Sir3

Figure 1.2 Model of SIR heterochromatin nucleation and spreading. The Sir2/4 complex and Sir3 are recruited to silencing nucleation sites via interactions with DNA sequence-specific binding factors and Sir1. Sir2 deacetylates H4-K16, providing a high-affinity binding site for Sir3. Successive cycles of deacetylation and binding promote spreading of Sir proteins along the chromosome, forming repressive heterochromatin domains.

regions, forming extended heterochromatin domains (Rusche et al. 2003; Rusche & Lynch 2009).

The Sir2 protein is the founding member of the sirtuin family of deacetylases conserved from bacteria to humans. Sirtuins are NAD-dependent deacetylases which couple deacetylation to the hydrolysis of an NAD^+ molecule. In this reaction, NAD^+ is cleaved into nicotinamide and ADP-ribose, and the acetyl group removed from the modified lysine is transferred to the ADP-ribose molecule, forming *O*-acetyl-ADP-ribose (*O*-AADPR) (Tanny et al. 1999; Tanner et al. 2000; Tanny & Moazed 2001). *In vitro*, Sir2 specifically targets lysines 9 and 14 of the H3 tail and lysine 16 of H4, although *in vivo* SIR heterochromatin is fully hypoacetylated (Imai et al. 2000; Tanny & Moazed 2001; Suka et al. 2001). Sir2 has no documented affinity for DNA, histones, or nucleation factors, and thus its targeting to SIR heterochromatin requires its interaction with Sir4 (Figure 1.3) (Cubizolles et al. 2006; Kueng et al. 2013). Strong evidence suggests that Sir2 and Sir4 exist in a stable complex *in vivo* separate from Sir3. A Sir2/4 complex can be purified from yeast cells using a tandem affinity purification (TAP) strategy, however TAP-purified Sir2/4 does not contain Sir3, and similarly-purified Sir3 does not contain Sir2 or Sir4 (Moazed et al. 1997; Hoppe et al. 2002). Additionally, the Sir2/4 complex can be recruited to silencing nucleation regions independently of Sir3 (Hoppe et al. 2002). Sir2 contains a Sir4 interaction region located between its N-terminal regulatory domain and its C-terminal catalytic domain, which binds and possibly orders a central region of

Sir4, the Sir2-interaction domain (SID) (Figure 1.3) (Hsu et al. 2013). Sir4 binding stabilizes Sir2 in an orientation in which its N- and C-terminal domains are positioned for optimal activity, and in fact Sir4 binding has been shown to stimulate Sir2's enzymatic activity *in vitro* (Hsu et al. 2013). A mutation within the Sir4 interaction region of Sir2 has also been found to enhance the silencing defect of a *sir1Δ in vivo* (Garcia & Pillus 2002).

Unlike Sir2, the Sir4 protein has no enzymatic activity and is not conserved in higher organisms. Instead, it serves as a scaffold linking the nuclear envelope, silencers, Sir proteins, and chromatin together into heterochromatin. In addition to the interactions with silencing factors Rap1, Abf1, Sir1, and *y*Ku which recruit Sir proteins to nucleation sites, Sir4 binds the nuclear envelope associated protein Esc1 via its partitioning and anchoring domain (PAD) (Figure 1.3) (Andrulis et al. 2002; Taddei & Gasser 2004; Taddei et al. 2004). Sir4's PAD is both necessary and sufficient to tether telomeres to the nuclear envelope in the presence of either *y*Ku or Esc1, making it the most important factor in mediating heterochromatin positioning along the nuclear periphery (Taddei et al. 2004). Beyond the role of its SID in the Sir2/4 complex, Sir4 also contains a C-terminal coiled-coil domain which both allows it to homodimerize and to bind Sir3 (Figure 1.3) (Moretti et al. 1994; Murphy et al. 2003; Chang et al. 2003). A single amino acid substitution in this region, isoleucine 1311 to asparagine (Sir4-I1311N), disrupts the Sir3/Sir4 interaction, diminishing Sir3 recruitment to and silencing at both the *HM* loci and telomeres

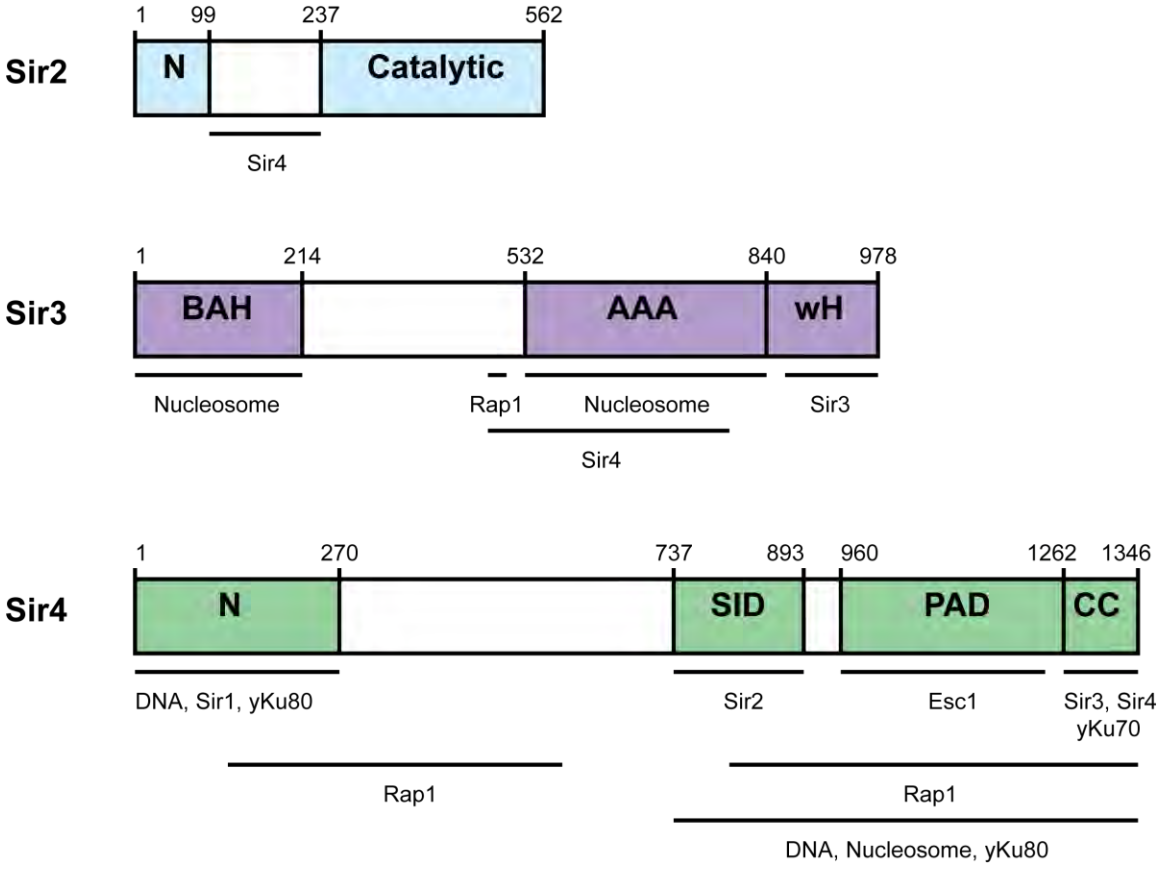
Sir2
1
99
237
562
N
Catalytic
Sir4
Sir3
1
214
532
840
978
BAH
AAA
wH
Nucleosome
Rap1
Nucleosome
Sir3
Sir4
Sir4
1
270
737
893
960
1262
1346
N
SID
PAD
CC
DNA, Sir1, yKu80
Sir2
Esc1
Sir3, Sir4
yKu70
Rap1
Rap1
DNA, Nucleosome, yKu80

Figure 1.3 Sir protein domains and binding interactions. Domains and mapped binding interactions of Sir2, Sir3, and Sir4.

(Chang et al. 2003; Rudner et al. 2005). Conversely, overexpression of the Sir4 coiled-coil domain also disrupts silencing (Cockell et al. 1995). The Sir4 protein also interacts directly with chromatin, with a high affinity for DNA and H3 and H4 tails (Hecht et al. 1995; Liou et al. 2005; Johnson et al. 2009; Martino et al. 2009; Oppikofer et al. 2011; Kueng et al. 2012).

Despite Sir4's ability to bind tails, the Sir3 protein is believed to be responsible for the bulk of SIR/histone interactions. Specifically, Sir3 contains an N-terminal bromo-adjacent homology (BAH) domain which binds to the face of the nucleosome and the base of the H4 tail (Figure 1.4) (Connelly et al. 2006; Onishi et al. 2007; Armache et al. 2011a). This binding is enhanced by the acetylation of the N-terminus of Sir3, which helps to position loop 3 and helix 8 of BAH within hydrogen bonding distance to the nucleosome, and is necessary for complete silencing *in vivo* (Wang et al. 2004; Wang et al. 2013). Additionally, Sir3 contains an AAA ATPase domain which also binds the nucleosome surface and the coiled-coil domain of Sir4 (Figure 1.3) (Moretti et al. 1994; Hecht et al. 1995; Rudner et al. 2005; Buchberger et al. 2008; Ehrentraut et al. 2011). Although the AAA domain lacks the necessary residues for ATP binding and hydrolysis (Bell et al. 1995), it was long hypothesized that it may bind the byproduct of Sir2 deacetylation, *O*-AADPR, inducing a conformational change that mediates silencing (Liou et al. 2005; Martino et al. 2009; Ehrentraut et al. 2011). However, *O*-AADPR has been shown to be unessential for silencing *in vivo* when nucleosome deacetylation is accomplished in a Sir2-independent

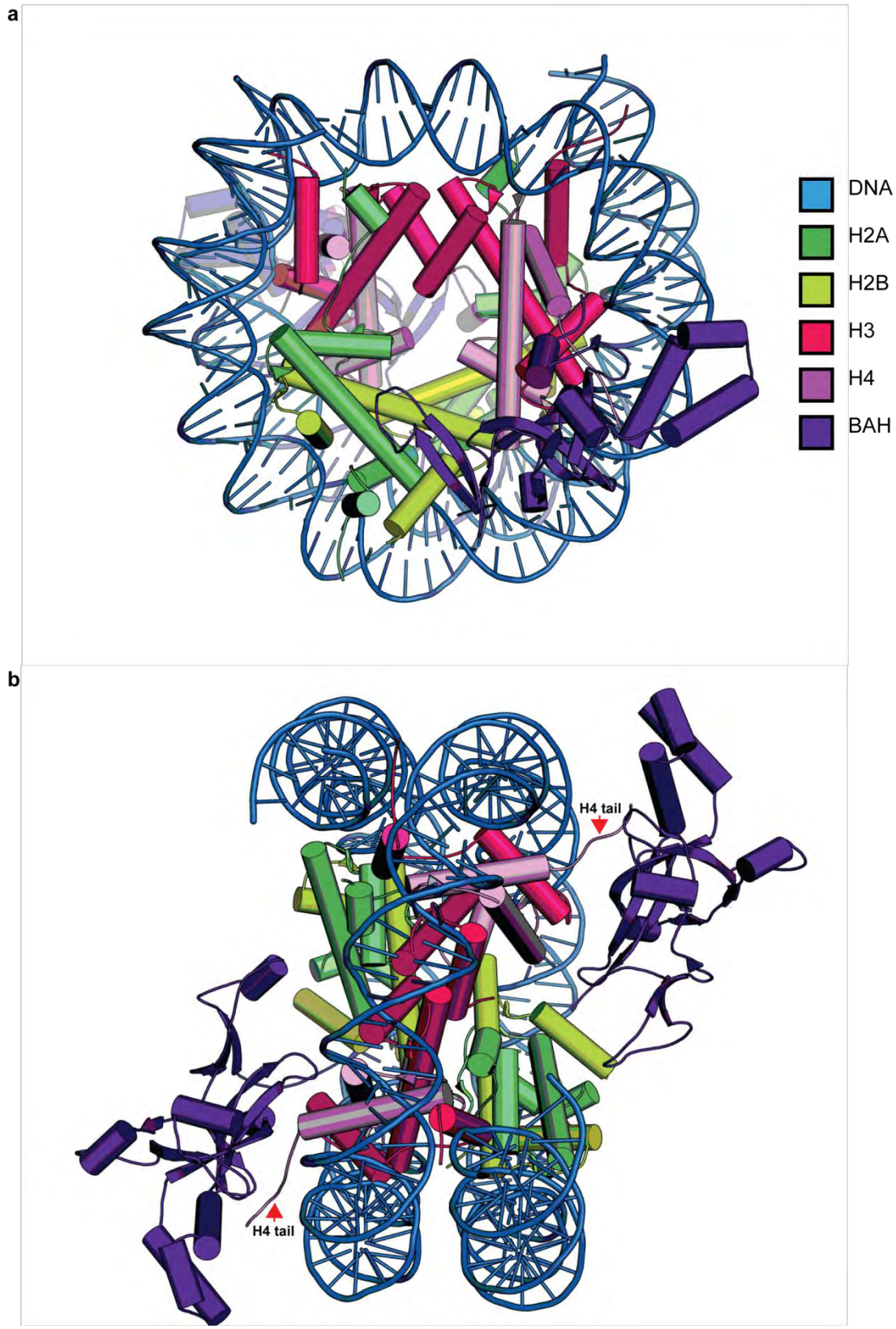
a
DNA
H2A
H2B
H3
H4
BAH
b
H4 tail
H4 tail

Figure 1.4 Crystal structure of the Sir3 BAH domain bound to a nucleosome. (a) The Sir3 BAH domain bound to the surface of the nucleosome. **(b)** Side view of BAH bound to the nucleosome. Sir3 BAH interacts with the base of the H4 tail. The position of the H4 tail is indicated by the arrow (PDB# 3tu4, Armache et al. 2011).

manner (Chou et al. 2008), a crystal structure of the AAA domain revealed a conformation wholly incompatible with nucleotide binding (Ehrentraut et al. 2011), and mutations within the putative nucleotide interacting region had no phenotype (Ehrentraut et al. 2011). Finally, Sir3 contains a winged helix-turn-helix (wH) domain that mediates homodimerization at its C-terminus (Figure 1.3) (Moretti et al. 1994; McBryant et al. 2006; King et al. 2006; Oppikofer, Kueng, Keusch, et al. 2013). This domain is essential for silencing *in vivo*, perhaps by promoting the spreading of Sir proteins across neighboring nucleosomes (Liaw & Lustig 2006; Oppikofer, Kueng, Keusch, et al. 2013).

While Sir2, Sir3, and Sir4 are all required for silencing, significant evidence points to Sir3 as being the predominant component of the repressive SIR heterochromatin structure. Overexpression of Sir3 leads to the extension of silenced domains at telomeres, despite low levels of Sir2/4, and can restore silencing in a Sir4-I1311N mutant in which Sir3/Sir4 interactions are lost (Hecht et al. 1996; Strahl-Bolsinger et al. 1997; Wang et al. 2013). Additionally, Sir3 alone can block the early stages of homologous recombination *in vitro*, and is sufficient to make nucleosomes resistant to most chromatin remodeling enzymes (Sinha et al. 2009; Manning & Peterson 2014).

The formation and regulation of SIR heterochromatin is mediated through several chromatin modifications, most crucially H4-K16 acetylation. The importance of H4-K16 was first recognized when its mutation to glutamine (H4-K16Q) was found to abrogate mating, and compensatory mutations in Sir3

(including D205N, which dramatically increases the affinity of the BAH domain for the nucleosome) were identified (Johnson et al. 1990; Connelly et al. 2006; Buchberger et al. 2008). Further, *in vitro* studies showed that Sir3 is unable to immunoprecipitate histones bearing an H4-K16Q substitution, or to bind acetylated histone tail peptides or reconstituted H4-K16Q or H4-K16A chromatin (Carmen et al. 2002; Liou et al. 2005; Onishi et al. 2007; Johnson et al. 2009; Sinha et al. 2009). The crystal structure of Sir3's BAH domain bound to a nucleosome subsequently revealed an electronegative patch of BAH that interacts with the H4 tail and contains a specific binding pocket for H4-K16, making it one of the key SIR/nucleosome contacts (Figure 1.4) (Armache et al. 2011b; Wang et al. 2013; Arnaudo et al. 2013). Surprisingly, deletion of the H4-K16 histone acetyltransferase *Sas2* leads to loss of silencing, as it promotes ubiquitous Sir3 binding throughout the genome (Suka et al. 2002). Thus, H4-K16 acetylation is both necessary for SIR heterochromatin formation and inhibitory to its aberrant spreading; silencing requires the specific recruitment of the Sir2/4 complex to nucleation sites where the deacetylation of H4-K16 by Sir2 is necessary to direct Sir3 to silencing regions, while widespread H4-K16 acetylation prevents Sir3 binding within euchromatin (Suka et al. 2002; Oppikofer et al. 2011).

A similar, but weaker effect is seen when H3-K79 is methylated. This residue is also contacted by the Sir3 BAH domain (Armache et al. 2011b; Wang et al. 2013; Arnaudo et al. 2013), and its mutation has been shown to disrupt Sir3

binding to reconstituted chromatin (Onishi et al. 2007; Johnson et al. 2009; Sinha et al. 2009; Ehrentraut et al. 2011). *In vivo*, overexpression of the methyltransferase responsible for methylating H3-K79, Dot1, was found to impair silencing (Singer et al. 1998; Van Leeuwen et al. 2002). However, no enzyme responsible for the removal of H3-K79 methylation has been identified, making it an unlikely mechanism for heterochromatin targeting (Rusche et al. 2003; Oppikofer, Kueng & Gasser 2013; Kueng et al. 2013). Instead, Dot1 preferentially binds H4-K16 acetylated nucleosomes, where H3-K79 methylation may aid in the formation of boundaries between heterochromatic and euchromatic domains (Altaf et al. 2007). Likewise, the incorporation of the histone variant H2A.Z has also been recognized as an important boundary element, as H2A.Z nucleosomes are inhibitory to Sir3 binding *in vitro* and subject to rapid histone exchange *in vivo* (Meneghini et al. 2003; Shia et al. 2006; Dion et al. 2007; Johnson et al. 2009). Interestingly, in the presence of both Sir2/4 and Sir3, all three Sir proteins are capable of binding chromatin with a modified H4-K16 or H3-K79 residue; however, these interactions are not sufficient for silencing (Johnson et al. 2009; Kitada et al. 2012; Johnson et al. 2013).

Although the mechanism of silencing by SIR heterochromatin is believed to be the formation of a repressive chromatin structure, the nature of this structure remains highly controversial. Early work demonstrating a decrease in DNA accessibility in heterochromatic domains led to the hypothesis that heterochromatin is highly condensed and sterically incompatible with the binding

of external factors (Gottschling 1992; Loo & Rine 1994; Ansari & Gartenberg 1999). However, transcription factors and even RNA Polymerase II (Pol II) are frequently found bound within heterochromatic sites, and promoters within *HM* loci are accessible to micronuclease digestion despite the silencing of their associated genes (Weiss & Simpson 1998; Sekinger & Gross 2001; Chen & Widom 2005; Johnson et al. 2013; Thurtle & Rine 2014). *In vitro* investigations of DNA accessibility have also disagreed, with some finding Sir proteins to repress digestion of linker DNA, while others saw no effect (Georgel et al. 2001; Martino et al. 2009; Oppikofer et al. 2011). Interestingly, a recent study found that although Sir proteins can prevent the formation of the entire pre-initiation complex (PIC) on arrays presumably through steric means, a single SIR-bound nucleosome is capable of blocking *in vitro* transcription, arguing against condensation as the mechanism of silencing (Johnson et al. 2013). Although an SV-AUC and EM study argued that Sir3 binding led to the compaction of reconstituted arrays in a manner cooperative with 30 nm fiber folding (McBryant et al. 2008), the crystal structure of Sir3 BAH bound to the nucleosome clearly demonstrates that Sir3 binding to the H4 tail must inhibit the H4 tail/acidic patch interactions necessary for the intrinsic folding pathway (Armache et al. 2011b). Further, EM analysis of all three Sir proteins bound to purified chromatin fragments showed the formation of long, linear filaments incompatible with chromatin compaction (Onishi et al. 2007; Johnson et al. 2009). These

conflicting results indicate a need for the implementation of controls ensuring heterochromatin structures generated *in vitro* recapitulate *in vivo* behavior.

In This Work

The mechanism of heterochromatic silencing remains a crucial question in biology. Although a great deal of effort has been made to uncover the repressive structure responsible for silencing, current *in vivo* methods are not yet sufficiently powerful to provide detailed structural information, and *in vitro* methods are highly subject to artifacts. Here, I describe the development of experimental conditions in which *in vitro* reconstituted SIR fibers are sensitive to histone octamers bearing an H4-K16Q mutation, known to abrogate silencing *in vivo* (Johnson et al. 1990). These physiologically-relevant heterochromatin fibers were analyzed via a variety of biophysical methods, including SV-AUC, modeling, and AFM to reveal the structure of SIR heterochromatin. Sir3 was found to bind arrays at a stoichiometry of two molecules per nucleosome. Although some occlusion of linker DNA was observed, Sir3 fibers were nowhere near as compacted as 30 nm fibers. This result suggests that Sir3 mediates silencing by creating stable nucleosomes resistant to processes such as chromatin remodeling. Further work revealed that in the presence of all three Sir proteins, arrays do adopt a more sterically restrictive structure in which Sir proteins likely exist at a stoichiometry of two Sir3's to one Sir2/4 per nucleosome. That the

formation of this structure required unmodified H4-K16, the C-terminus of Sir3 containing its dimerization domain, and the interaction between Sir3 and Sir4 strongly supports the *in vivo* relevance of this silencing mechanism.

CHAPTER II: SOLUTION-STATE CONFORMATION AND STOICHIOMETRY OF YEAST SIR3 HETEROCHROMATIN FIBERS

Abstract

Heterochromatin is a repressive chromatin compartment that is essential for maintaining genomic integrity. A hallmark of heterochromatin is the presence of specialized nonhistone proteins that alter chromatin structure to inhibit transcription and recombination. It is generally assumed that heterochromatin is highly condensed. However, surprisingly little is known about the structure of heterochromatin or its dynamics in solution. In budding yeast, the formation of heterochromatin at telomeres and the HM silent mating type loci require the Sir3 protein. Here, we use a combination of sedimentation velocity, atomic force microscopy, and nucleosomal array capture to characterize the stoichiometry and conformation of Sir3 nucleosomal arrays. The results indicate that Sir3 interacts with nucleosomal arrays with a stoichiometry of two Sir3 monomers per nucleosome. We also find that Sir3 fibers are less compact than canonical – magnesium-induced 30 nm fibers. We suggest that heterochromatin proteins promote silencing by "coating" nucleosomal arrays, stabilizing interactions between nucleosomal histones and DNA.

Introduction

Eukaryotic genomes are assembled into a complex assembly of proteins and DNA known as chromatin. The basic unit of chromatin is the nucleosome, which consists of 147 base pairs of DNA wrapped approximately twice around an octamer of histones containing two copies each of histones H2A, H2B, H3, and H4 (Luger et al. 1997). Within the nucleus, long linear arrays of nucleosomes are organized into two functionally distinct compartments, termed euchromatin and heterochromatin. Euchromatic regions are often referred to as “active” chromatin, since they harbor transcriptionally active gene loci, whereas heterochromatin contains “inactive” chromatin domains that are generally repressive for transcription and typically localize to the nuclear periphery (Woodcock & Ghosh 2010). Heterochromatin is required for the organization and function of centromeres (White & Allshire 2008), as well as the protection of telomeres (Savitsky et al. 2002). In addition, heterochromatin protects genome integrity by repressing the transposition of abundant transposable elements and by preventing extensive or illicit recombination between dispersed repetitive DNA elements (Peng & Karpen 2007; Peng & Karpen 2008). Although heterochromatin assembly is known to require interactions between heterochromatin-specific architectural proteins and nucleosomes, the way in which these proteins organize a nucleosomal array into the overall repressive conformation remains poorly understood (Hecht et al. 1995; Suka et al. 2002; Sinha et al. 2009).

In *Saccharomyces cerevisiae*, heterochromatin formation requires the Silent Information Regulator proteins, Sir2, Sir3, and Sir4 (Hecht et al. 1996; Rusche et al. 2002; Rusche et al. 2003). Assembly of Sir-dependent heterochromatin is believed to be a step-wise process in which silencing is initiated by binding of Sir4 to telomeres or the HM silent mating type loci via interactions with sequence-specific DNA binding proteins, such as Rap1 (Moretti et al. 1994; Rusche et al. 2002). Sir4 interacts directly with Sir2 (Hoppe et al. 2002), which is an NAD^+-dependent histone deacetylase that targets lysine 16 of histone H4 (H4-K16) (Imai et al. 2000). The Sir2-dependent deacetylation of H4-K16 promotes the subsequent nucleosome binding of the Sir3 protein (Suka et al. 2002; Rusche et al. 2003; Onishi et al. 2007). Multiple cycles of histone deacetylation and Sir2, Sir3, and Sir4 binding are believed to control the spreading of the heterochromatic domain from the initial point of recruitment (Hecht et al. 1996; Hoppe et al. 2002; Rusche et al. 2002; Buchberger et al. 2008).

Both *in vivo* and *in vitro* studies indicate that Sir3 may be the primary structural component of yeast heterochromatin and that it can function, at least in part, independently of Sir2 and Sir4. For instance, overexpression of Sir3 can extend a domain of transcriptional silencing at telomeres in which Sir2 is largely absent and Sir4 is only detected at low levels (Strahl-Bolsinger et al. 1997). Likewise, Sir3 overexpression allows formation of repressive heterochromatin at the HMR locus in a *sir4-I1311N* mutant that eliminates Sir4-Sir3 interactions

(Wang et al. 2013). *In vitro*, Sir3 binds to DNA and to nucleosomes, and the addition of Sir3 to recombinant nucleosomal arrays is sufficient to create a heterochromatin fiber that blocks early steps of homologous recombination *in vitro* (Georgel et al. 2001; Onishi et al. 2007; McBryant et al. 2008; Adkins et al. 2009; Sinha et al. 2009).

Biochemical and genetic studies have led to the identification of a nucleosomal surface that plays a key role in Sir3 heterochromatin assembly. Notably, substitution of histone H4-K16 with a glutamine residue (H4-K16Q) eliminates the binding of Sir3 to heterochromatic loci *in vivo*, and mutations within Sir3 were identified as genetic suppressors of an H4-K16Q substitution allele (Johnson et al. 1990). Furthermore, the importance of H4-K16 for Sir3 nucleosomal recognition has been highlighted by several high-resolution structures of Sir3-nucleosome complexes (Armache et al. 2011b; Wang et al. 2013; Arnaudo et al. 2013; Yang et al. 2013). These studies demonstrate that H4-K16 occupies a central cavity within the nucleosome binding domain of Sir3, consistent with previous biochemical data showing that high affinity binding of Sir3 to histone peptides (Liou et al. 2005) and to mononucleosomes is disrupted by H4-K16 acetylation or glutamine substitution (Johnson et al. 2009; Sinha et al. 2009). These results contrast with several *in vitro* studies indicating that Sir3 has a high nonspecific binding affinity for DNA (McBryant et al. 2008; Adkins et al. 2009), and that the binding of Sir3 to 6-mer nucleosomal arrays is relatively insensitive to a H4-K16Q substitution (Oppikofer et al. 2011). Notably, these

biochemical studies employed rather low salt binding buffers that are likely to promote nonspecific DNA binding at the expense of specific nucleosomal interactions.

Here, we describe ionic conditions that diminish the nonspecific DNA binding activity of Sir3, resulting in binding to recombinant 12-mer nucleosomal arrays that is highly sensitive to the integrity of H4-K16. Using these conditions, we characterized the structure and subunit stoichiometry of Sir3 nucleosomal arrays by a combination of sedimentation velocity analytical ultracentrifguation (SV-AUC), atomic force microscopy (AFM), and a nucleosomal array capture assay. Notably, we have adapted a grid-based modeling method, called two-dimensional spectrum analysis (2DSA) (Brookes et al. 2010), coupled with a genetic algorithm (GA) and Monte Carlo analysis (Brookes 2006; Demeler & Brookes 2007), to fit sedimentation and diffusion parameters to the SV-AUC data. These modeling methods have allowed determination of both the native molecular weight and shape parameters of Sir3 nucleosomal arrays. Our results indicate that Sir3 binds to recombinant nucleosomal arrays at a stoichiometry of two Sir3 monomers per nucleosome, and that Sir3 binding leads to structures that are distinct from, and less compact than, canonical 30 nm fibers.

Results

Reconstitution of Sir3 nucleosomal arrays

Our goal was to develop *in vitro* assay conditions in which Sir3 binding to nucleosomal arrays is highly sensitive to the substitution of histone H4-K16 with glutamine (H4-K16Q), a substitution that eliminates assembly of Sir heterochromatin *in vivo* (Johnson et al. 1990). To this end, nucleosomal arrays were reconstituted using recombinant wildtype (WT) or H4-K16Q histone octamers and DNA templates that contained 12 tandem copies of a nucleosome positioning sequence. Full-length Sir3 was purified from yeast and used in several binding assays. First, Sir3 binding was monitored by nucleosomal array capture (Figure 2.1a). For this assay, a small concentration of octamers that contained a biotin group covalently attached to an engineered cysteine residue at the histone H2A C-terminus was added to chromatin, such that arrays contained ~2 biotinylated nucleosomes per 12-mer array. Sir3 was then bound to arrays in buffers containing increasing NaCl concentrations, arrays were captured on streptavidin magnetic beads, and the amount of bound Sir3 was determined by western blot. At low concentrations of NaCl, Sir3 bound almost equivalently to the wildtype and H4-K16Q nucleosomal arrays, consistent with previous studies (Figure 2.1a) (McBryant et al. 2008; Martino et al. 2009; Oppikofer et al. 2011). In contrast, Sir3 bound almost exclusively to the WT arrays when the NaCl concentration was increased to 40-50 mM. Likewise, Sir3 strongly preferred the WT arrays when binding was performed in 20 mM phosphate buffer (~40 mM Na^+; Figure 2.2). Furthermore, adding increasing amounts of Sir3 to WT and Q arrays under these conditions showed saturation binding, with

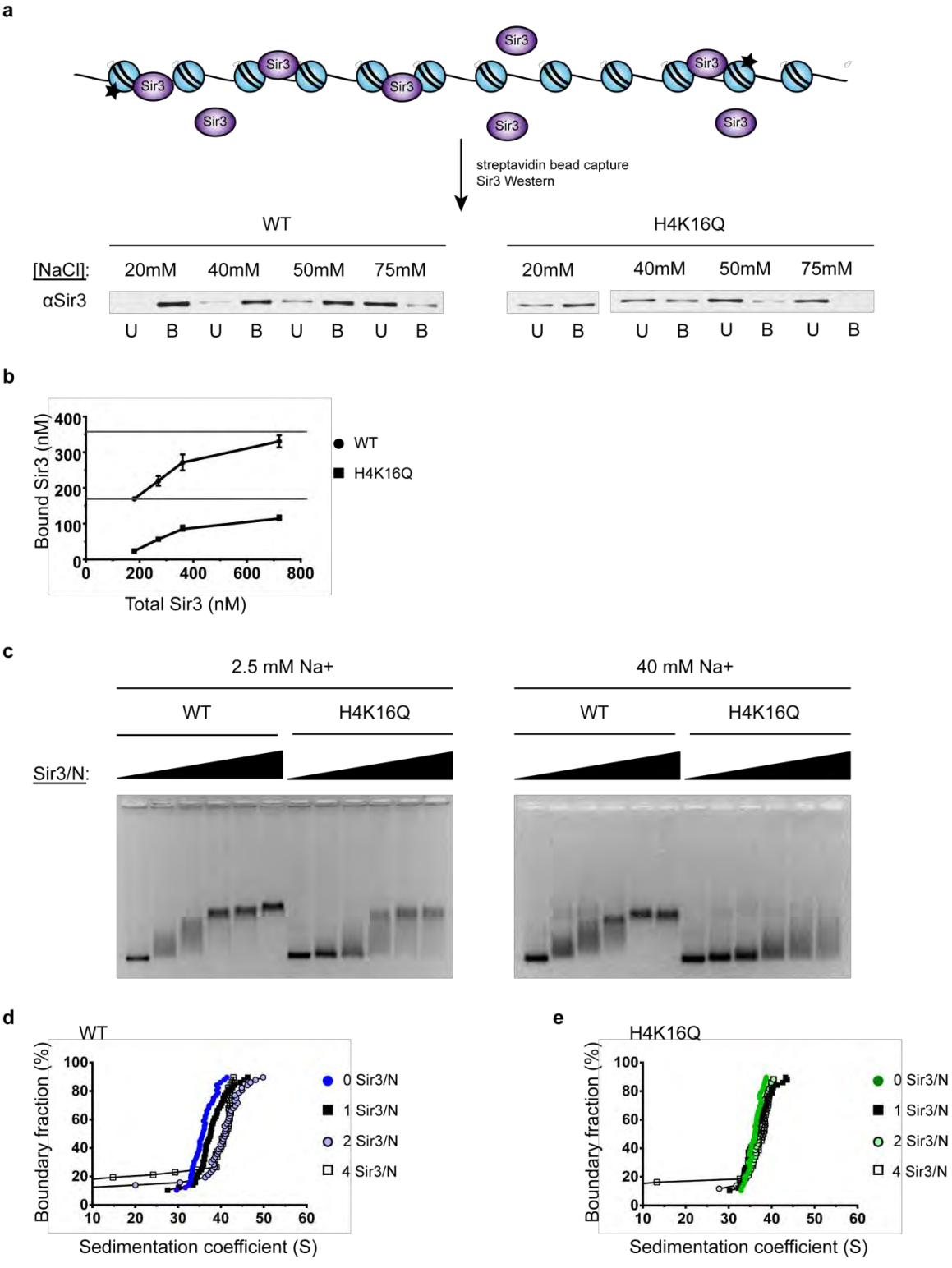
a
Sir3
streptavidin bead capture
Sir3 Western
WT
H4K16Q
[NaCl]:
20mM
40mM
50mM
75mM
αSir3
U B U B U B U B
b
Bound Sir3 (nM)
Total Sir3 (nM)
WT
H4K16Q
c
2.5 mM Na+
40 mM Na+
WT
H4K16Q
Sir3/N:
d
WT
Boundary fraction (%)
Sedimentation coefficient (S)
0 Sir3/N
1 Sir3/N
2 Sir3/N
4 Sir3/N
e
H4K16Q
Boundary fraction (%)
Sedimentation coefficient (S)
0 Sir3/N
1 Sir3/N
2 Sir3/N
4 Sir3/N

Figure 2.1 Increased ionic strength buffer enhances the nucleosome-specific binding of Sir3. (a) Nucleosomal array capture and Western blot analysis of Sir3 unbound (U) and bound (B) to WT and H4-K16Q arrays. **(b)** Quantification of bound vs. unbound Sir3 to WT and H4-K16Q arrays of an experiment performed as in (**a**) using increasing Sir3 concentrations in 40 mM NaCl. **(c)** EMSA of Sir3 binding to WT and H4-K16Q 12-mer arrays in Tris containing 2.5 mM NaCl buffer (left) and phosphate buffer at ~40 mM Na^+ (right). Sir3/N is the number of Sir3 monomers per nucleosome positioning sequence, ranging from 0 to 8. **(d,e)** SV-AUC analyses. vHW plots of Sir3 binding to WT and H4-K16Q arrays, respectively. Sir3/N is the number of Sir3 monomers per nucleosome positioning sequence.

a

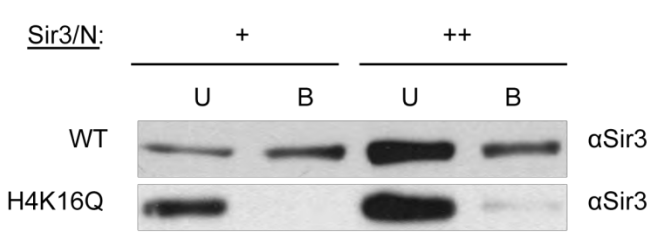

Figure 2.2 Sir3 specifically binds to WT over H4-H16Q arrays in phosphate buffer containing ~40 mM Na+. (a) Nucleosomal array capture assay as in **Fig. 1a-b** showing a titration of Sir3 on WT and H4-K16Q arrays in 20 mM phosphate buffer.

Sir3 binding to the wildtype arrays with an approximate maximum of two Sir3 monomers per nucleosome (Figure 2.1b). In contrast, less than one monomer of Sir3 bound to each H4-K16Q nucleosome when assayed in 40 mM Na^+ buffer, even at high concentrations of Sir3 (Figure 2.1b).

Sir3 binding to 12-mer arrays was also monitored by an electrophoretic mobility shift assay (EMSA). As in the array capture assay in Fig. 2.1a, when assayed in low salt Tris buffer (2.5 mM Na+), Sir3 binding showed only a slight preference for WT versus H4-K16Q arrays (Figure 2.1c, left panel). Under these conditions, the addition of increasing quantities of Sir3 led to formation of heterogeneous, slow migrating complexes, as previously observed (McBryant et al. 2008; Martino et al. 2009; Oppikofer et al. 2011). However, when binding reactions were performed in 20 mM sodium phosphate buffer (~40 mM Na^+), Sir3 demonstrated a strong preference for WT over H4-K16Q arrays (Figure 2.1c, right panel). Furthermore, under these conditions, increasing Sir3 concentrations led to the formation of a discrete complex of stable mobility.

We next analyzed Sir3 binding to arrays using SV-AUC. Phosphate buffer was used in these assays, as its Na^+ concentration (approximately 40 mM at pH 8.0) is within the ideal range of specific Sir3 binding (see Figure 2.1a and 2.1c), but unlike Tris buffer, phosphate does not absorb in the low UV range. In the absence of Sir3, both WT and H4-K16Q 12-mer nucleosomal arrays sedimented as fairly uniform species at ~34-36 S (Figure 2.1d, e). Addition of Sir3 to the WT arrays shifted the distribution to larger S values, with maximal shifts at a ratio of

two Sir3 monomers per nucleosome, leading to a structure that sedimented with a midpoint at ~42-45 S (Figure 2.1d, see also Figure 2.9a). A corresponding shift in S was not seen when Sir3 was added to H4-K16Q arrays (Figure 2.1e), consistent with the binding specificity observed by both EMSA and array capture assays. In contrast to previous studies (McBryant et al. 2008), extensive aggregation or oligomerization was not observed when high concentrations of Sir3 were added to the arrays under these ionic conditions (Figure 2.1d).

Implementation of SV-AUC modeling

The sedimentation behavior of a macromolecule in an SV-AUC experiment is proportional to both its buoyant molecular weight and frictional properties governed by its overall shape. Consequently, the observed Sir3-induced changes in the S distribution of nucleosomal arrays in Figure 2.1d could be due to an increased molecular weight, an altered conformation of the nucleosomal fiber, or a combination of both. To separate these two parameters, we applied a set of modeling methods implemented in UltraScan3 software, beginning with two-dimensional spectrum analysis (2DSA), which uses a grid-based method to fit sedimentation and diffusion parameters to the SV-AUC data. The 2DSA analysis yields a set of solutes of specific sedimentation and diffusion properties that are likely to describe the experimental data set (Brookes et al. 2010). In order to distinguish between truly present solutes and false positives, a genetic algorithm (GA) is used to refine the 2DSA solution (Brookes 2006). GA is

based on an evolutionary paradigm, using random cross-over, mutation, and deletion events to alter the sedimentation and diffusion characteristics of the 2DSA solutes, and to eliminate false positive solutes by parsimonious regularization. The ultimate goal is to obtain a solution that satisfies Occam's razor. According to Occam's razor, from the many solutions possible for the lowest root-mean-square-deviation the preferred solution is the one with the fewest solutes (Brookes & Demeler 2007). In such a solution only solutes representing intrinsic sedimentation signal will remain. Finally, Monte Carlo (MC) analysis of the GA solution is performed to further refine the fit and to obtain statistical descriptors of the final solutes (Demeler & Brookes 2007). This overall modeling process is termed 2DSA/GA-MC. When the partial specific volume is constant and known from other sources, the resulting solution gives fits for the sedimentation coefficient, partial concentration, molecular weight, and frictional ratio (f/f_0) of solutes present in the experimental sample. The f/f_0 value is the ratio of the frictional coefficient of an unknown molecule to the frictional coefficient of a perfect sphere of the same volume and density, and is thus a numerical descriptor of the particle's anisotropy (Demeler 2010). As the f/f_0 increases from 1.0, the molecule becomes more asymmetric, moving from spherical, to globular, and then to rod-like, with most proteins falling between 1 and 4 (Demeler 2010).

While the 2DSA/GA-MC modeling approach has been successfully used to predict the molecular weight and shape of proteins and small nucleic acids, this method has not been previously applied to complex macromolecules, such

as chromatin fibers. For an initial probe of this approach, 2DSA/GA-MC was employed to examine a DNA template containing twelve tandem copies of the 601 nucleosome positioning sequence separated by a 30 bp linker (601-177-12 DNA). van Holde Weischet (vHW) analysis of the SV-AUC data indicates that this ~ 2 Kb DNA fragment sediments as a homogenous species of ~11 S (Figure 2.3a). In agreement with vHW analysis, 2DSA/GA-MC shows the presence of a single solute at 10.65 S (Figure 2.3a, d). The fit molecular weight of this solute also matched the predicted molecular weight (1.34 vs 1.31 MDa expected), and the f/f_0 ratio of 7.5 correctly indicated the presence of an extended rod (Figure 2.3a, d).

As a further proof of principle, nucleosomal arrays were assembled with two concentrations of recombinant histone octamers to generate nucleosomal arrays that contained an average of ~6 or ~12 nucleosomes. Analysis of the SV-AUC data by either vHW analysis (Figure 2.3b, c) or 2DSA/GA-MC (Figure 2.3b-d) indicated the presence of relatively homogenous populations of solutes, and furthermore, the 2DSA/GA-MC modeling yielded reasonable fits for both the sedimentation coefficients (S) and the f/f_0 ratios. Likewise, the residuals for the 2DSA fits were largely random, indicating that this modeling method is appropriate for the analysis of chromatin fibers (Figure 2.4a). In contrast, the fit molecular weights, as determined by 2DSA/GA-MC, were much lower than the predicted molecular weights (1.17 vs 1.96 MDa and 2.3 vs 2.6 MDa). Likewise, 2DSA/GA-MC analysis of Sir3 nucleosomal arrays yielded molecular weights that

a

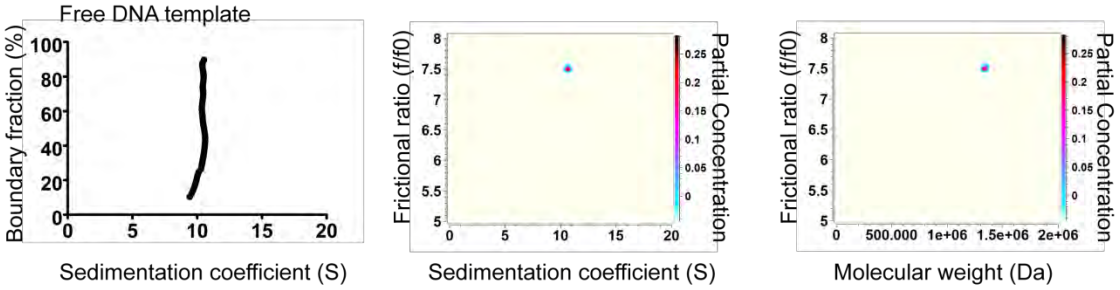

b

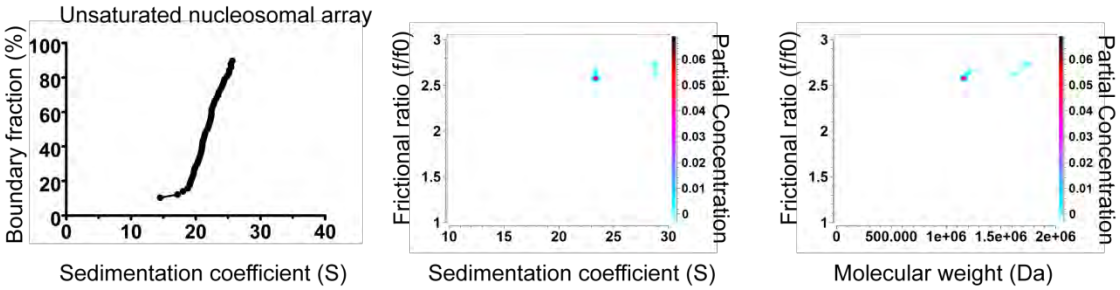

c

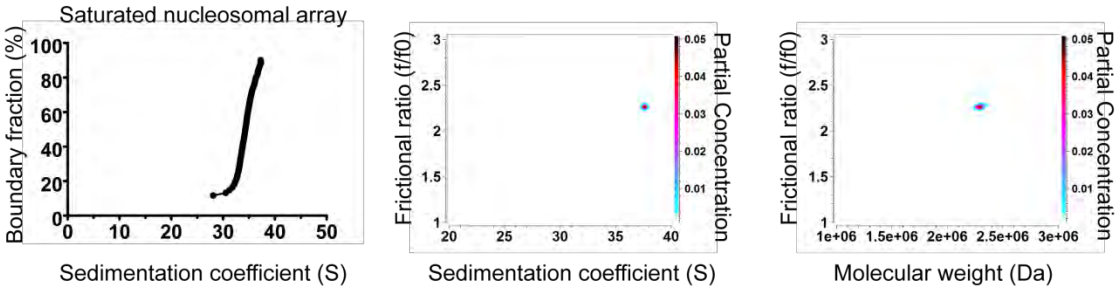

d

	Mol. Weight (MDa)	Sed. Coefficient (s^{-13})	Frictional Ratio
DNA template	1.335 [1.313] (1.333, 1.347)	10.654 (10.648, 10.668)	7.499 (7.486, 7.540)
Unsaturated array	1.167 [1.964] (1.140, 1.195)	23.341 (23.324, 23.358)	2.587 (2.546, 2.627)
Saturated array	2.296 [2.614] (2.272, 2.321)	37.594 (37.561, 37.627)	2.269 (2.252, 2.285)

Figure 2.3 2DSA/GA-MC modeling using predicted partial specific volumes does not accurately determine the molecular weights of complex chromatin macromolecules. (a-c) vHW and 2DSA/GA-MC plots of free 601-177-12 template DNA, an approximately half-saturated 12mer nucleosomal array, and a saturated 12mer nucleosomal array, respectively. **(d)** The molecular weight, sedimentation coefficient, and frictional ratio of samples in **(a-c)** as determined by 2DSA/GA-MC. Numbers in parentheses are 95% confidence intervals. Numbers in brackets represent theoretical molecular weights calculated by a sequence-based algorithm implemented in UltraScan3.

a

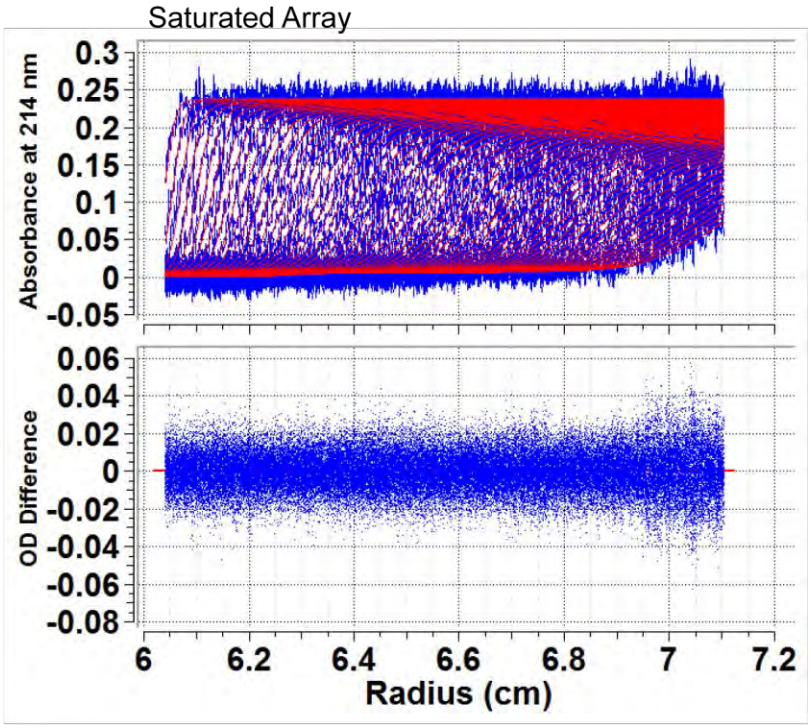
Saturated Array
Absorbance at 214 nm
0.3
0.25
0.2
0.15
0.1
0.05
0
-0.05
OD Difference
0.06
0.04
0.02
0
-0.02
-0.04
-0.06
-0.08
6
6.2
6.4
6.6
6.8
7
7.2
Radius (cm)

b

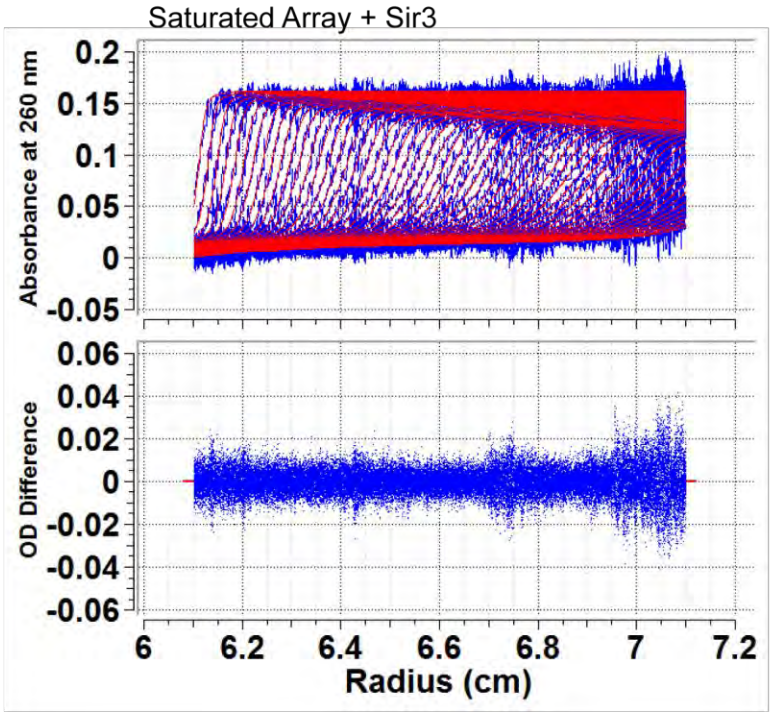
Saturated Array + Sir3
Absorbance at 260 nm
0.2
0.15
0.1
0.05
0
-0.05
OD Difference
0.06
0.04
0.02
0
-0.02
-0.04
-0.06
6
6.2
6.4
6.6
6.8
7
7.2
Radius (cm)

Figure 2.4 2DSA fitting is appropriate for chromatin samples. (a-b) 2DSA experimental vs. model scans (top, model is in red) and residuals (bottom) demonstrate good fits and random residuals for a WT array unbound **(a)** and bound by Sir3 **(b)**.

were much smaller than expected (data not shown). Notably, an accurate determination of molecular weight by 2DSA/GA-MC analysis is dependent not only on the experimentally determined *S* and f/f_0 values, but also on the partial specific volume ($\bar{\nu}$). $\bar{\nu}$ is the solvated volume of a macromolecule, defined in milliliters per gram, and is essential for describing the hydrodynamic behavior of molecules in solution (Gohon et al. 2004; Demeler 2010; Brown et al. 2011). The $\bar{\nu}$ of proteins can be accurately predicted based on sequence and knowledge of the solvent components, however there is no accurate method for predicting the $\bar{\nu}$ of DNA or a complex of protein and DNA, which is also strongly dependent on the ionic strength of the solvent conditions (Hearst 1962; Edelstein & Schachman 1967; Gorbet et al. 2014). UltraScan3 uses a weighted, average $\bar{\nu}$ for protein-nucleic acid complexes, based on predicted stoichiometry ($\bar{\nu}$ is predicted to be 0.65 for 12-mer arrays). Since SV-AUC experiments can only determine the buoyant MW [$MW_b = MW(1-\bar{\nu}\rho)$, where ρ is the solvent density] the $\bar{\nu}$ value has a dominant role in absolute MW determination. Small changes in the $\bar{\nu}$ parameter lead to considerable changes on the molecular weights determined by SV-AUC (Gorbet et al. 2014). These results indicate that analysis of chromatin fibers by 2DSA/GA-MC requires that the $\bar{\nu}$ be experimentally determined.

$\bar{\nu}$ determination by density-contrast sedimentation

We adapted a recently described method of experimentally measuring $\bar{\nu}$ using SV-AUC that allows for the use of much less sample mass than traditional

methods, such as measurement in a density balance (Gohon et al. 2004; Brown et al. 2011). In this method, samples are sedimented in three solvents containing either 0, 30, or 60% $H_2{}^{18}O$. The resulting sedimentation coefficients are plotted as a function of solvent density, and the $\bar{v}$ is calculated from the resulting plot (see Materials and Methods). We first applied this "density contrast" method to a well-characterized protein, lysozyme, and to both a 177 bp DNA fragment and the 601-177-12 DNA template (Figure 2.5). As expected, increasing concentrations of $H_2{}^{18}O$ led to a decrease in the sedimentation coefficients, and plotting the obtained S values against the solution density yielded experimental $\bar{v}$'s that were remarkably similar to the predicted $\bar{v}$ for both lysozyme and DNA. Indeed our experimental $\bar{v}$ for lysozyme (0.726 mL/g) is identical to the $\bar{v}$ measured previously with a vibrating densitometer (Ward 1976).

This density contrast method was then applied to nucleosomal arrays. First, a range of histone octamer concentrations were reconstituted on the 601-177-12 template to yield arrays with differing nucleosome density (Figure 2.6a). Each sample was then subjected to density contrast sedimentation (Figure 2.7), and the experimentally-derived $\bar{v}$'s are shown in Figure 2.6. Interestingly, as more nucleosomes were reconstituted onto the DNA, both the sedimentation coefficient and the $\bar{v}$ increased in a linear relationship (Figure 2.6b, c), indicative of both an increased molecular weight and an increased volume occupied by the chromatin fiber. Notably, the experimentally determined $\bar{v}$ for the fully saturated, 35 S array (0.695 mL/g) is consistent with the inverse of the previously

a

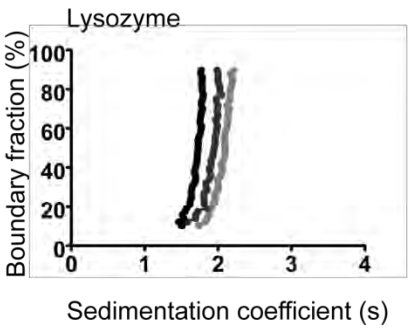

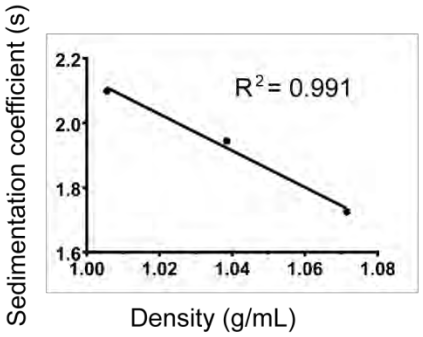

$\overline{v}$ = 0.726 mL/g
[0.724]

b

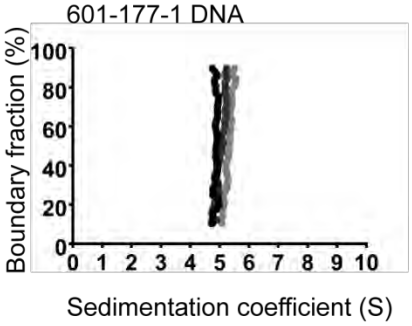

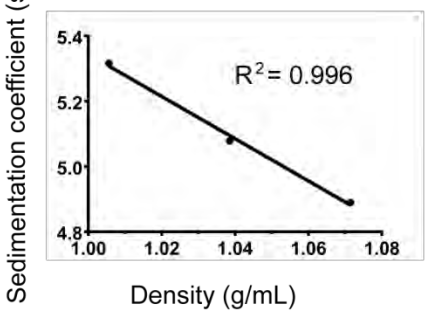

$\overline{v}$ = 0.548 mL/g
[0.55]

c

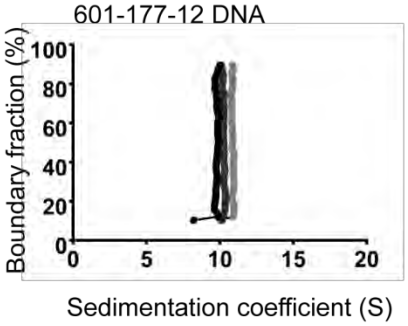

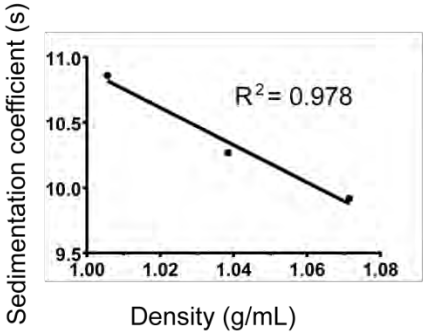

$\overline{v}$ = 0.568 mL/g
[0.55]

Figure 2.5 The partial specific volume of molecules can be determined via sedimentation in solvents of known density. (a-c) vHW plots showing the sedimentation of molecules in 0% (light gray), 30% (dark gray), and 60% H2O18 (black) and plots of sedimentation coefficient vs. density for **(a)** lysozyme, **(b)** 601-177-1 template DNA, and **(c)** 601-177-12 template DNA. The $\bar{v}$ is calculated by dividing the slope of the fit line by the y-intercept. Numbers in brackets represent the *v* of the respective molecule as predicted by UltraScan3.

a

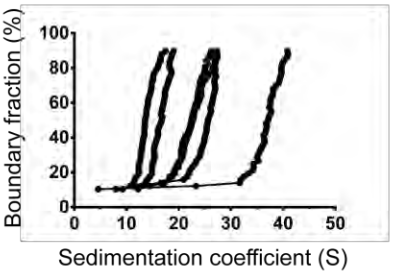

b

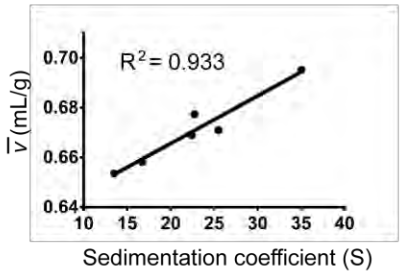

slope = 0.00192

y-intercept = 0.627

c

Sed. Coefficient (s^{-13})	$\overline{v}$ (mL/g)	Mol. Weight (MDa)	Frictional Ratio
13.517	0.654	1.871 (1.831, 1.912)	5.160 (5.084, 5.235)
16.737	0.658	2.083 (2.015, 2.152)	5.297 (5.181, 5.413)
22.444	0.669	2.227 (2.222, 2.233)	4.243 (4.239, 4.247)
22.753	0.677	2.263 (2.231, 2.294)	3.737 (3.702, 3.773)
26.670	0.671	2.229 (2.197, 2.262)	3.096 (3.065, 3.126)
35.043	0.695	2.585 [2.614] (2.490, 2.681)	2.471 (2.408, 2.535)

Figure 2.6 The partial specific volume of variably saturated 601-177-12 nucleosomal arrays is directly proportional to the sedimentation coefficient. **(a)** vHW plots of 601-177-12 nucleosomal arrays at varying nucleosome saturation. **(b)** The $\bar{\nu}$ of the arrays in (**a**) plotted against their sedimentation coefficient. $\bar{\nu}$'s were determined in Figure 7. **(c)** *S* and $\bar{\nu}$ of arrays in (**a**), and the molecular weight and f/f_0 ratio as determined by 2DSA/GA-MC, using experimental $\bar{\nu}$ numbers determined in Figure 4. Numbers in parenthesis are 95% confidence intervals, and the number in brackets is the expected molecular weight for a 601-177-12 DNA template reconstituted with 12 histone octamers.

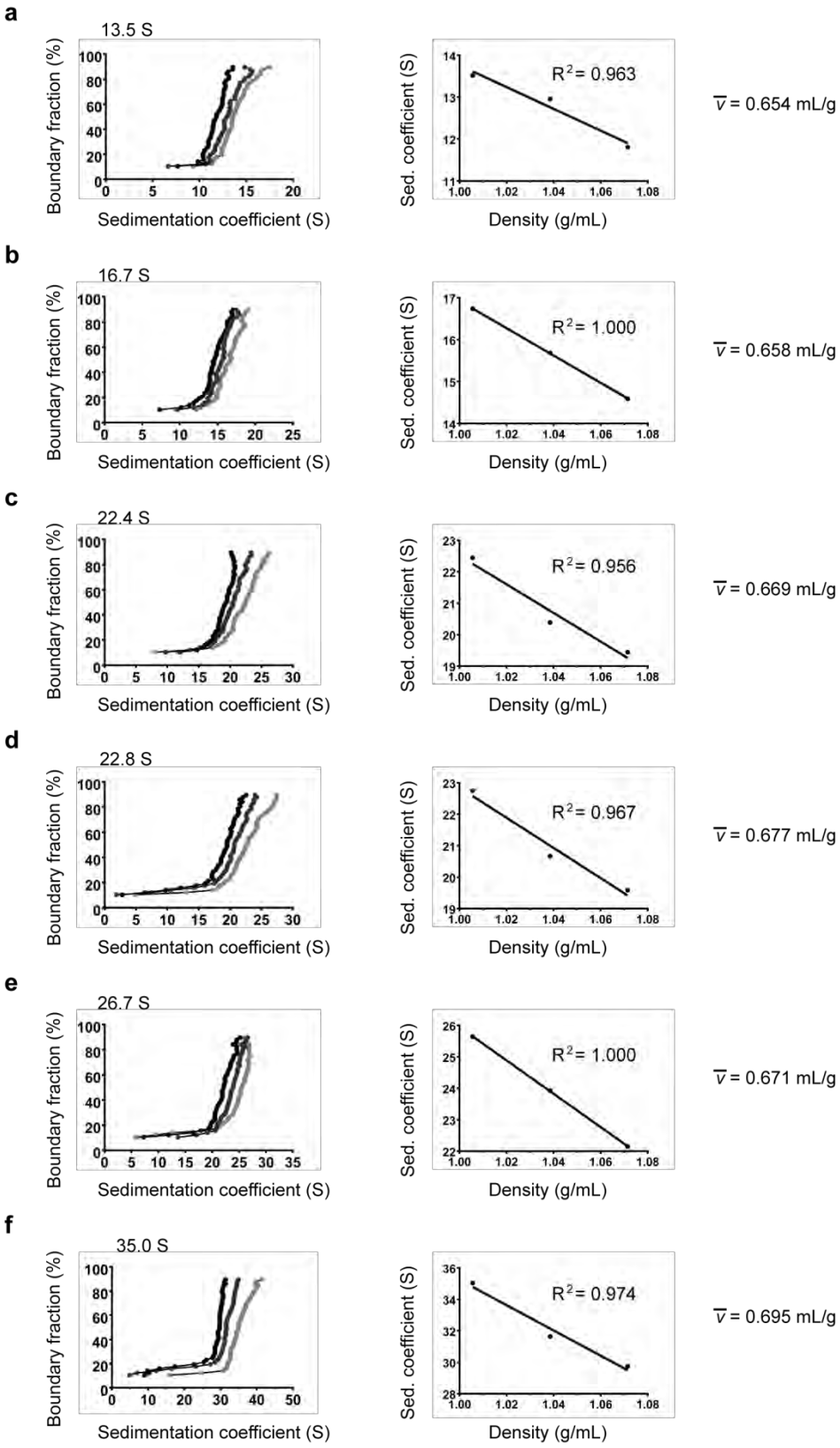
a
13.5 S
Boundary fraction (%)
Sedimentation coefficient (S)
Sed. coefficient (S)
Density (g/mL)
R² = 0.963
v̄ = 0.654 mL/g
b
16.7 S
R² = 1.000
v̄ = 0.658 mL/g
c
22.4 S
R² = 0.956
v̄ = 0.669 mL/g
d
22.8 S
R² = 0.967
v̄ = 0.677 mL/g
e
26.7 S
R² = 1.000
v̄ = 0.671 mL/g
f
35.0 S
R² = 0.974
v̄ = 0.695 mL/g

Figure 2.7 The partial specific volume of nucleosomal arrays increases with histone octamer saturation and S. (a-f) Determination of the $\bar{v}$ of arrays in Figure 6 as in Figure 5.

determined buoyant density of chromatin fragments isolated from chicken cells (0.706 mL/g) (Ghirlando & Felsenfeld 2008). Importantly, the $\bar{v}$ determinations were independent of the viscosity of the three separate solutions, and correcting the solutions for density led to vHW plots that overlayed closely, indicating that the sedimentation profiles of the samples in the three different buffers were highly reproducible (Figure 2.8).

Experimentally-determined $\bar{v}$'s were used in 2DSA/GA-MC fits for each nucleosomal array sample (Figure 2.6c). In striking contrast to our results with an estimated $\bar{v}$, the fit molecular weights increased in direct proportion with nucleosome saturation, from a molecular weight corresponding to a 12-mer template with approximately four nucleosomes (1.87 MDa), to one corresponding to a nearly saturated 12-mer array (2.59 MDa). Additionally, as the DNA template wrapped around an increasing number of histone octamers, the f/f_0 ratio decreased, indicating the transition from an extended linear DNA molecule to a shorter, more globular chromatin fiber.

This analysis was then applied to WT and H4-K16Q arrays assembled at a ratio of two Sir3 monomers per nucleosome (Figure 2.9). Density-contrast sedimentation was used to determine $\bar{v}$ values from an average of three independent experiments (examples in Figure 2.10a, b), and these values were used in 2DSA/GA-MC fitting of the SV-AUC data (Figure 2.9a, b). 2DSA/GA-MC modeling indicated that WT and H4-K16Q nucleosomal arrays without Sir3 were similar in molecular weight, ~2.6 MDa, consistent with arrays containing ~ 12

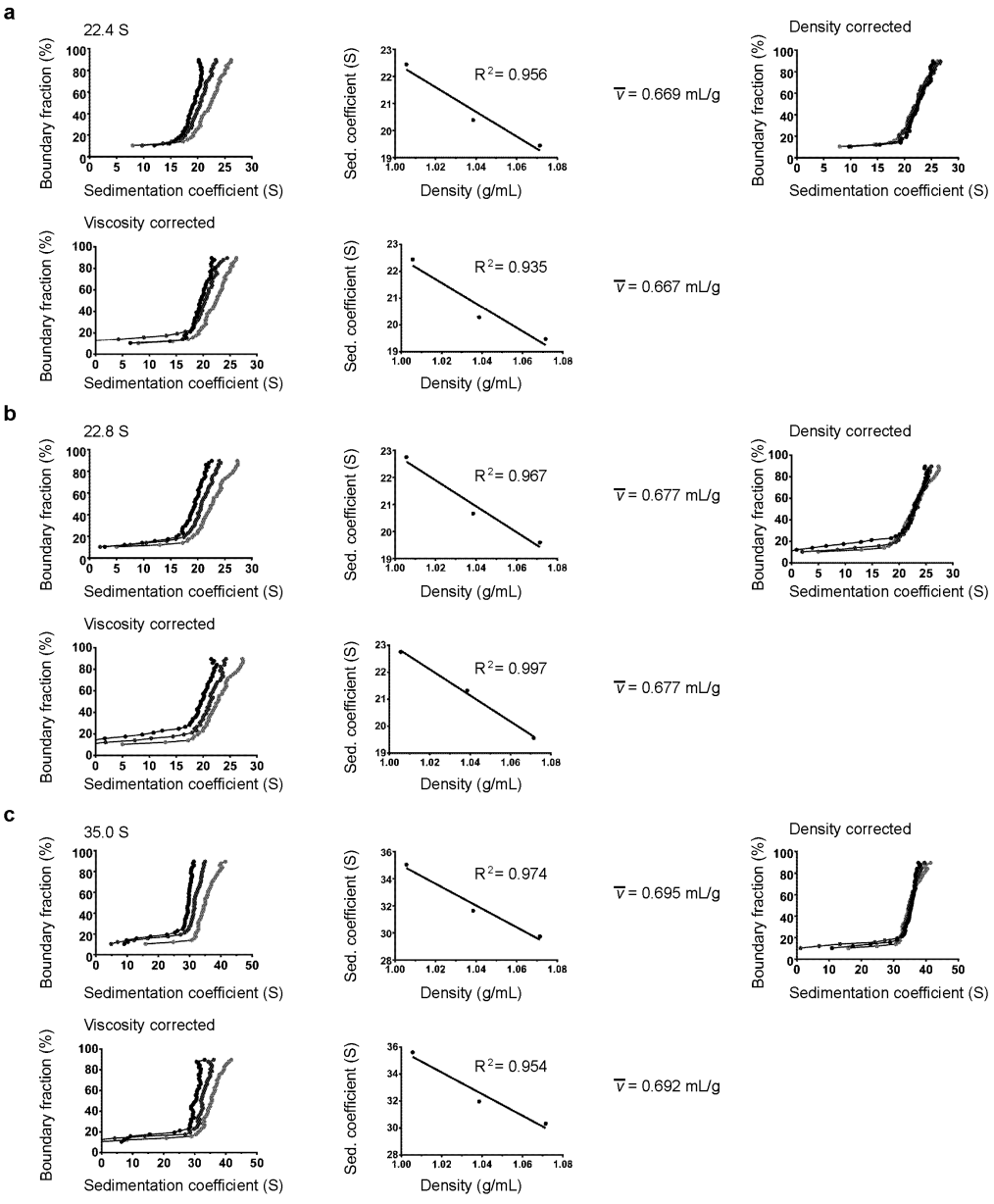
a
22.4 S
Boundary fraction (%)
Sedimentation coefficient (S)
Sed. coefficient (S)
Density (g/mL)
R2= 0.956
v̄ = 0.669 mL/g
Density corrected
Viscosity corrected
R2= 0.935
v̄ = 0.667 mL/g
b
22.8 S
R2= 0.967
v̄ = 0.677 mL/g
R2= 0.997
v̄ = 0.677 mL/g
c
35.0 S
R2= 0.974
v̄ = 0.695 mL/g
R2= 0.954
v̄ = 0.692 mL/g

Figure 2.8 The partial specific volume of nucleosomal arrays is independent of viscosity, and the sedimentation distribution of chromatin samples is highly reproducible. (a-c) The $\bar{v}$ determination of array samples in Figure 7c,d,f shown as used in Figure 6 (top panels) and corrected for viscosity (bottom panels). The vHW distributions corrected for density are in the top right panels.

a

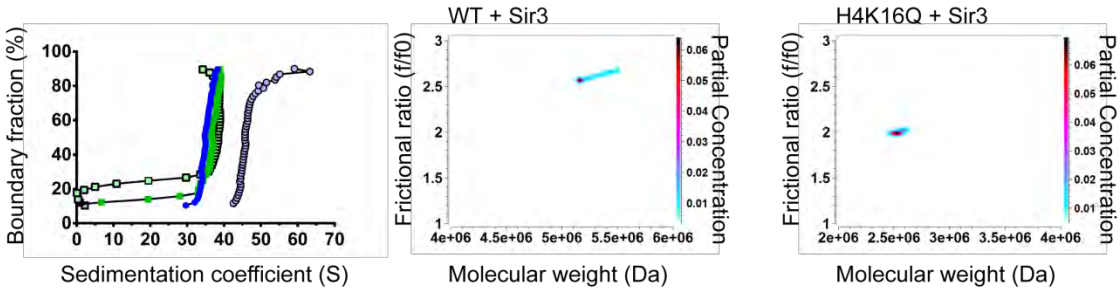

b

	$\overline{v}$ (mL/g)	Mol. Weight (MDa)	Sir3	Frictional Ratio
WT	0.694	2.566 [2.614] (2.553, 2.580)	N/A	2.230 (2.222, 2.238)
H4K16Q	0.697	2.667 [2.614] (2.636, 2.698)	N/A	2.162 (2.145, 2.179)
WT + Sir3	0.715	5.271 (5.230, 5.312)	23.9	2.582 (2.569, 2.595)
H4K16Q + Sir3	0.702	2.538 (2.494, 2.582)	N/A	1.998 (1.975, 2.022)

Figure 2.9 Sir3 binds at two monomers per nucleosome and stabilizes the rod-like structure of chromatin. (a) Left panel, vHW of WT and H4-K16Q 12mer arrays +/- 2 Sir3 monomers per nucleosome. WT array is represented by dark blue closed circles, H4-K16Q by green closed squares, WT + Sir3 by light blue open circles, and H4-K16Q + Sir3 by light green open squares. Middle and right panels, GA-MC plots showing f/f_0 vs. molecular weight for WT and H4-K16Q with Sir3. **(b)** 2DSA/GA-MC data of samples in (**a**) using experimentally-determined $\bar{v}$ values (see Figure 10 for examples). Numbers in brackets represent the expected molecular weight of a 601-177-12 array, and numbers in parentheses are 95% confidence intervals. Sir3 stoichiometry was calculated by subtracting the molecular weight of the array from the molecular weight of the array containing Sir3, divided by the molecular weight of 3xFLAG-tagged Sir3 (113 kDa).

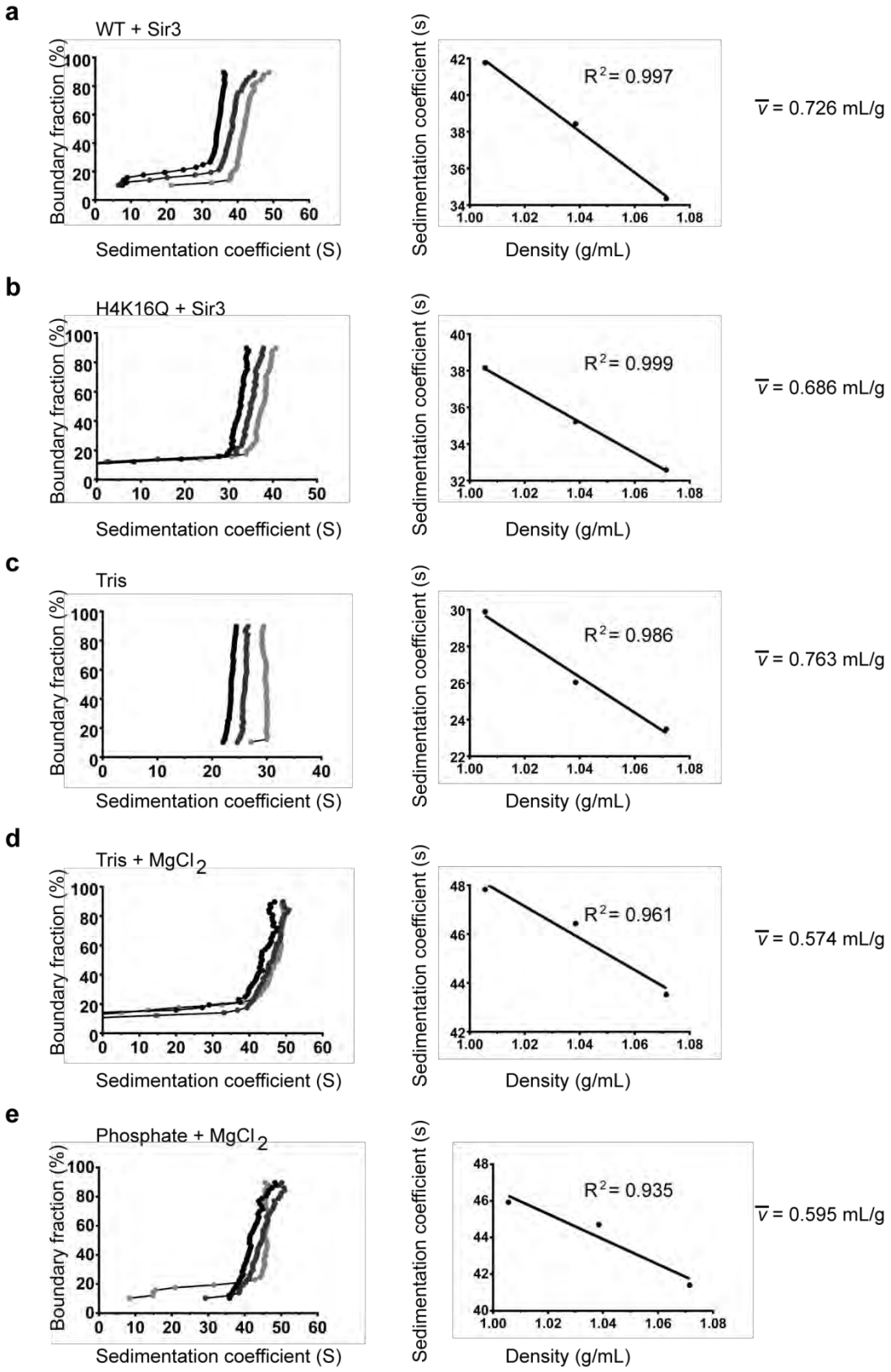
a
WT + Sir3
Boundary fraction (%)
Sedimentation coefficient (S)
Sedimentation coefficient (s)
Density (g/mL)
R2= 0.997
v̄ = 0.726 mL/g
b
H4K16Q + Sir3
Boundary fraction (%)
Sedimentation coefficient (S)
Sedimentation coefficient (s)
Density (g/mL)
R2= 0.999
v̄ = 0.686 mL/g
c
Tris
Boundary fraction (%)
Sedimentation coefficient (S)
Sedimentation coefficient (s)
Density (g/mL)
R2= 0.986
v̄ = 0.763 mL/g
d
Tris + MgCl2
Boundary fraction (%)
Sedimentation coefficient (S)
Sedimentation coefficient (s)
Density (g/mL)
R2= 0.961
v̄ = 0.574 mL/g
e
Phosphate + MgCl2
Boundary fraction (%)
Sedimentation coefficient (S)
Sedimentation coefficient (s)
Density (g/mL)
R2= 0.935
v̄ = 0.595 mL/g

Figure 2.10 The partial specific volume of arrays decreases during Mg++-induced folding but increases upon Sir3 binding. (a-b) Example $\bar{v}$ determinations of WT and H4K16Q arrays with Sir3. Average $\bar{v}$'s from three experiments were used for 2DSA/GA-MC in Figure 9. **(c-d)** Example $\bar{v}$ determinations of extended and folded WT arrays in Tris. Average $\bar{v}$'s from three experiments were used for 2DSA/GA-MC in Figure 13. **(e)** Example $\bar{v}$ determinations of folded WT arrays in phosphate buffer.

nucleosomes on the 12mer template (Figure 2.9b). Analysis of three independent WT and H4-K16Q arrays demonstrated remarkable reproducibility of the MW determinations (WT, 2.59 +/- 0.25 x 10^6, H4-K16Q, 2.61 +/- 0.089 x 10^6). Likewise, these analyses yielded similar frictional coefficient ratios (f/f_0), consistent with similar structures between WT and H4-K16Q arrays (WT, 2.16 +/- 0.19; H4-K16Q, 2.16 +/- 0.24). On addition of Sir3, the molecular weight of the WT fiber increased significantly, corresponding to the binding of ~24 monomers of Sir3 per nucleosomal array (Figure 2.9b). Analysis of three independent Sir3 array reconstitutions support a stoichiometry of 21 +-/ 4 molecules of Sir3 per nucleosome, consistent with an average ratio of ~2 monomers per nucleosome. In contrast, the addition of Sir3 to the H4-K16Q array did not lead to a significant shift in molecular weight (Figure 2.9b). These data are fully consistent with Sir3-nucleosome stoichiometry measurements determined by the nucleosomal array capture assay (Figure 2.1b), and they suggest that the 2DSA/GA-MC method can predict the molecular weight of complex protein-DNA complexes.

Sir3 binds to nucleosomal arrays as a monomer or dimer

Several previous studies have shown that Sir3 forms oligomers in solution (Liou et al. 2005; King et al. 2006; McBryant et al. 2006; Martino et al. 2009; Oppikofer, Kueng, Keusch, et al. 2013). Sir3 contains a dimerization domain at its C-terminus (King et al. 2006; Oppikofer, Kueng, Keusch, et al. 2013), and measurements of Sir3-Sir3 interactions indicates that Sir3 interacts with itself

with low nanomolar affinity (Liou et al. 2005; King et al. 2006). Our Sir3-nucleosome stoichiometry measurements are consistent with either the independent binding of two Sir3 monomers or the binding of a preformed Sir3 dimer. To evaluate the oligomeric state of Sir3 at the concentrations and buffer conditions employed here, SV-AUC analyses were performed. When analyzed in phosphate buffer (~40 mM Na^+) at 171 nM protein (the same concentration used in Figure 2.9), Sir3 was clearly heterogeneous, with at least two species apparent from the vHW distribution (Figure 2.11a). Analysis of the SV-AUC data by 2DSA/GA-MC modeling indicates that Sir3 is composed of a mixture of a monomer species that sediments at ~5 S and a population of dimers that sediment at ~8S (Figure 2.11a, b). Furthermore, this distribution was not altered when Sir3 was analyzed in phosphate buffer containing 150 mM Na^+ (Figure 2.12a). These data suggest that Sir3 may bind to each nucleosome within the array as either two monomers that subsequently dimerize or as a preformed dimer.

Sir3 chromatin fibers are less condensed than 30 nm fibers

The combination of density contrast sedimentation and 2DSA/GA-MC modeling yields two parameters, $\bar{\nu}$ and f/f_0 ratio, that describe the shape of a macromolecule. In order to test whether these parameters can describe chromatin folding events, nucleosomal arrays were sedimented in the presence or absence of $MgCl_2$, which promotes folding of an extended 12-mer array into

a

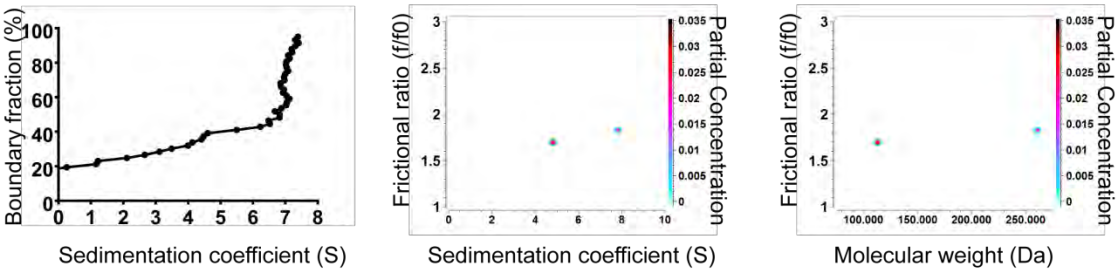

b

	Relative Percent	Sed. Coefficient (S)	Mol. Weight (kDa)	Frictional Ratio
Monomer	68.97 %	4.824 (4.815, 4.832)	113.43 (112.48, 114.38)	1.701 (1.693, 1.708)
Dimer	31.03 %	7.819 (7.806, 7.832)	260.53 (258.73, 262.33)	1.826 (1.819, 1.834)

Figure 2.11 Sir3 exists as a mixture of monomers and dimers in solution. **(a)** Left panel, vHW analysis of Sir3 at 171 nM (corresponding to the concentration used for 2 monomers of Sir3 per nucleosome in Figure 1d-e and 9) in phosphate buffer. Middle and right panels, GA-MC plots of S vs. molecular weight and *f/f0* vs. molecular weight. **(b)** 2DSA/GA-MC statistics show 69% of Sir3 in solution is a monomer (113 kDa), and 31% exists as an oligomer with a molecular weight most closely corresponding to a dimer (theoretical molecular weight is 226 kDa).

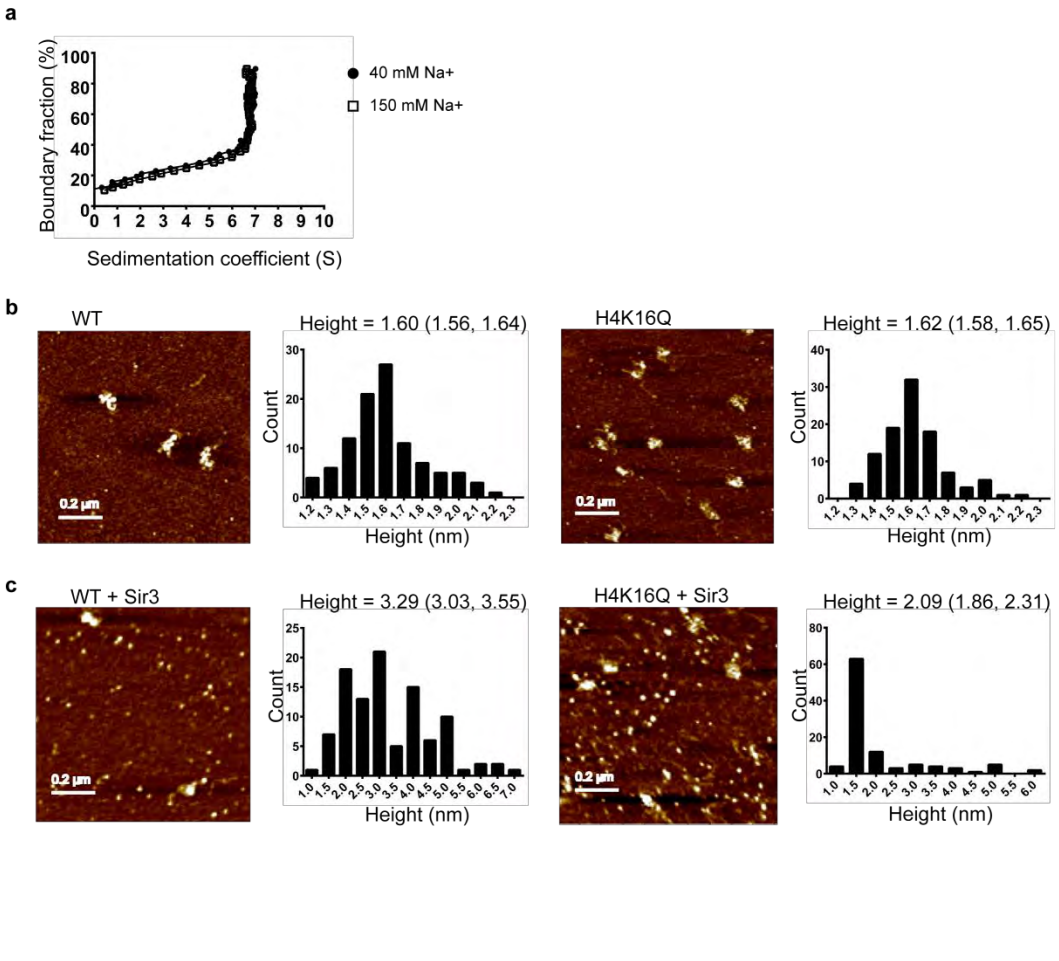
a
Boundary fraction (%)
100
80
60
40
20
0
0 1 2 3 4 5 6 7 8 9 10
Sedimentation coefficient (S)
40 mM Na+
150 mM Na+
b
WT
0.2 µm
Height = 1.60 (1.56, 1.64)
Count
Height (nm)
H4K16Q
0.2 µm
Height = 1.62 (1.58, 1.65)
Count
Height (nm)
c
WT + Sir3
0.2 µm
Height = 3.29 (3.03, 3.55)
Count
Height (nm)
H4K16Q + Sir3
0.2 µm
Height = 2.09 (1.86, 2.31)
Count
Height (nm)

0.2 µm

Figure 2.12 Sir3-array structure in 150 mM Na+ closely resembles Sir3-array structure in 40 mM Na+. (a) vHW analysis of 171 nM Sir3 in phosphate buffer containing ~40 mM Na+ or in phosphate buffer brought to 150 mM Na+. **(b)** WT and H4-K16Q arrays in phosphate buffer brought to 150 mM Na+ are equivalent in structure and height to arrays in phosphate buffer alone (compare to Figure 14b). **(c)** WT and H4-K16Q arrays in phosphate buffer brought to 150 mM Na+ are similar in structure and height to arrays in phosphate buffer alone in the presence of 2 Sir3 monomers/nucleosome (compare to Figure 14c).

structures resembling 30 nm chromatin fibers (Hansen & Wolffe 1992; Shogren-Knaak et al. 2006). Samples were analyzed in both low salt (2.5 mM Na+) Tris buffer and 20 mM phosphate (~40 mM Na+) buffer conditions. Consistent with previous studies, addition of low concentrations of $MgCl_2$ to 12-mer arrays promoted formation of fibers that sediment at ~55 S (Figure 2.13a, b). Density-contrast sedimentation was used to determine $\bar{\nu}$ values in all buffer conditions from three independent experiments (examples in Figure 2.10c, d), and the SV-AUC data was analyzed by 2DSA/GA-MC (Figure 2.13a-c). Strikingly, Mg^{++}-dependent folding was associated with an increased asymmetry of the fibers (i.e. higher f/f_0 ratio) and a dramatic decrease in the solvated volume (i.e. lower $\bar{\nu}$; Figure 2.13c). These altered biophysical parameters are consistent with a Mg^{++}-dependent transition from a flexible chromatin array to a more asymmetric, condensed chromatin fiber. Importantly, the fit molecular weights for the extended and folded samples were quite similar, demonstrating that 2DSA/GA-MC can distinguish contributions to *S* resulting from changes in shape versus changes in molecular weight.

Addition of Sir3 to 12-mer arrays (two monomers per nucleosome) led to small changes in both the $\bar{\nu}$ parameter and the f/f_0 ratio (Figure 2.9b). The asymmetry of the Sir3 chromatin fibers was quite similar to the Mg^{++}-induced structures (f/f_0 ratio of 2.54 +/- 0.19, n=4) and the values were larger than the WT arrays in the same phosphate buffer (2.16 +/- 0.19, n=6). Interestingly, the solvated volume ($\bar{\nu}$) did not decrease, as observed for Mg++-induced

a

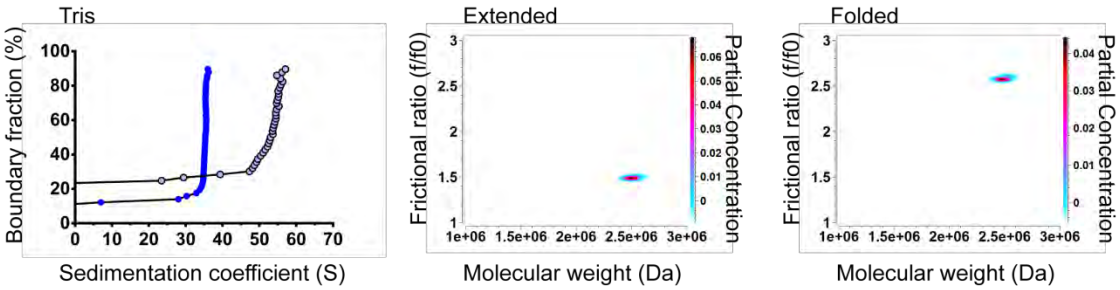

b

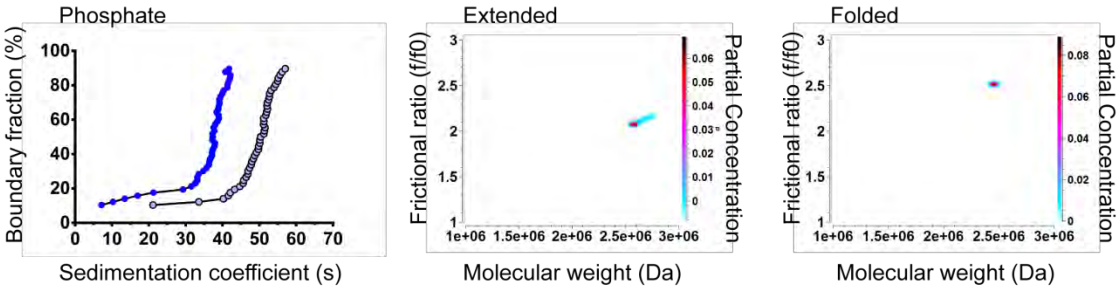

c

	$\overline{v}$ (mL/g)	Mol. Weight (MDa)	Frictional Ratio
Tris	0.775	2.511 [2.614] (2.473, 2.549)	1.493 (1.477, 1.507)
Tris + $MgCl_2$	0.576	2.494 [2.614] (2.454, 2.535)	2.584 (2.555, 2.614)
Phosphate	0.699	2.616 [2.614] (2.500, 2.733)	2.097 (2.034, 2.159)
Phosphate + $MgCl_2$	0.595	2.456 [2.614] (2.438, 2.474)	2.516 (2.503, 2.528)

0.2 μm 0.2 μm

Figure 2.13 2DSA/GA-MC can distinguish between the shape and molecular weights of 10 nm and 30 nm fibers. (a) Left panel, vHW analysis of a saturated nucleosomal array in low salt Tris buffer and in 1 mM $MgCl_2$ folding buffer. The extended sample is represented by closed blue circles, and the sample in folding buffer by open light blue circles. Middle and right panels, GA-MC plots of f/f_0 vs. molecular weight for extended and folded samples. **(b)** Same as in (**a**), using samples prepared in phosphate buffer containing ~ 40 mM Na+ (extended), and in this buffer supplemented with 8 mM $MgCl_2$ (folded). **(c)** GA-MC data of samples in (**a**) and (**b**) using experimentally-determined $\bar{\nu}$ values (for examples, see Figure 10). Number in brackets is the expected molecular weight of a 12mer array, and numbers in parentheses are 95% confidence intervals.

condensation, but rather it increased slightly (0.694 to 0.715 mL/g). Notably, these changes in the $\bar{v}$ or f/f_0 parameters were not observed when Sir3 was added to the H4-K16Q arrays (Figure 2.9b). These data indicate that the binding of Sir3 to nucleosomal arrays leads to an asymmetric structure that is distinct from, and less condensed, than a Mg^{++}-induced, 30 nm fiber.

Visualization of Sir3 arrays by AFM

To assess independently the structure of Sir3 chromatin fibers, samples were analyzed by AFM (Figure 2.14). In low salt Tris buffer (2.5 mM Na^+), WT arrays were highly extended, with an average height of 1.91 nm, consistent with a previous study indicating a height of ~ 2 nm for nucleosomes without linker histone (Leuba et al. 1998). The same arrays in 20 mM sodium phosphate buffer (~40 mM Na^+) were partially folded as expected in buffer with a moderate concentration of monovalent cation, with average heights of 1.60 and 1.84 nm for WT and H4-K16Q, respectively (Figure 2.14a, b). In agreement with the SV-AUC data, the addition of Mg^{++} led to formation of highly compact nucleosomal arrays with an average height of 5.62 nm (Figure 2.14a). In contrast, addition of Sir3 to WT 12-mer arrays in phosphate buffer (~40 mM Na^+) led to formation of rod-like structures with an average height of 2.79 nm, whereas Sir3 addition to H4-K16Q arrays maintained a partially compacted structure with an average height of 1.72 nm (Figure 2.14c). Similar results were obtained when Sir3 was incubated with arrays in phosphate buffer that contained 150 mM Na^+ (Figure 2.12b,c). Detailed

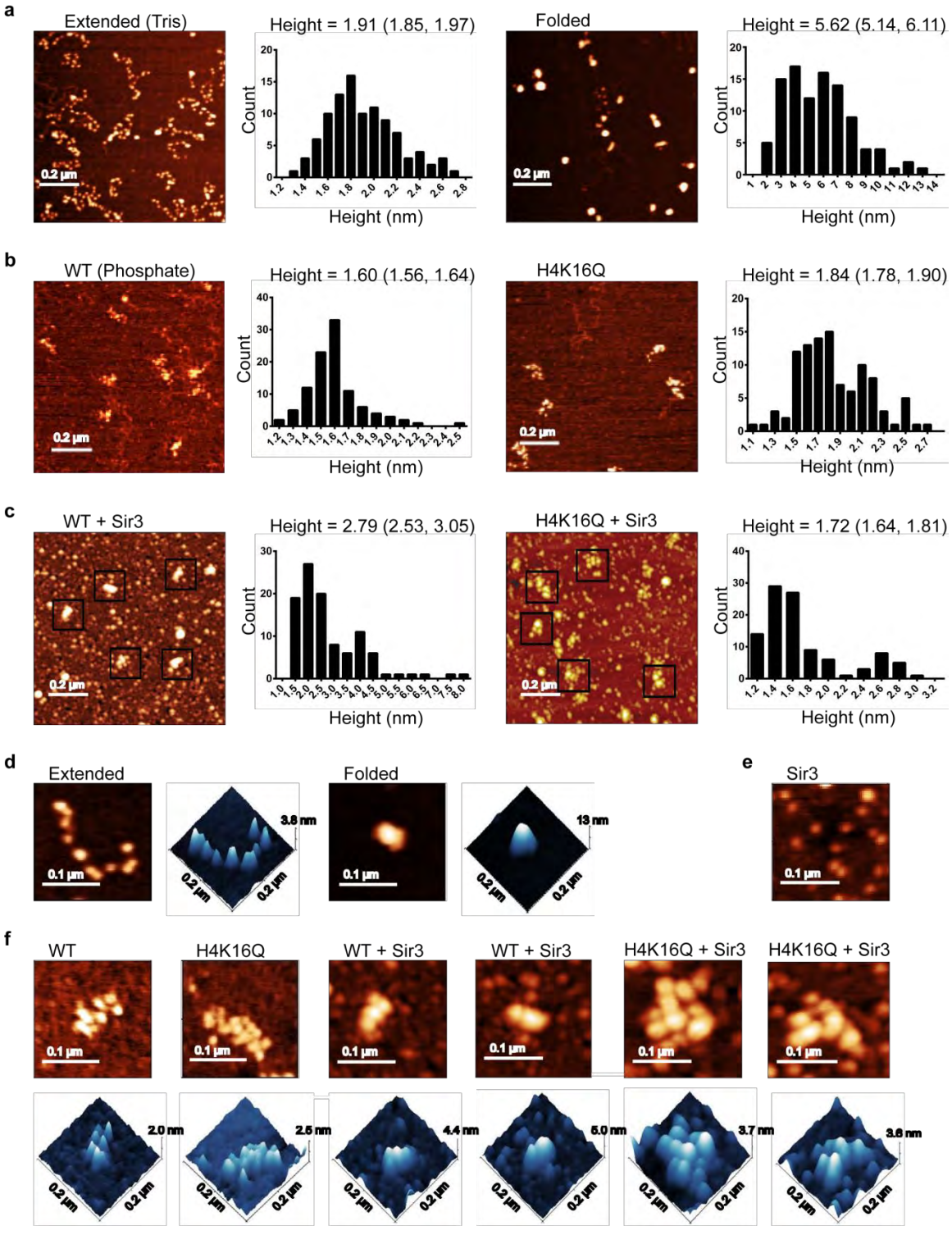
a
Extended (Tris)
Height = 1.91 (1.85, 1.97)
Folded
Height = 5.62 (5.14, 6.11)
0.2 µm
Count
Height (nm)
b
WT (Phosphate)
Height = 1.60 (1.56, 1.64)
H4K16Q
Height = 1.84 (1.78, 1.90)
c
WT + Sir3
Height = 2.79 (2.53, 3.05)
H4K16Q + Sir3
Height = 1.72 (1.64, 1.81)
d
Extended
Folded
3.8 nm
13 nm
0.1 µm
e
Sir3
f
WT
H4K16Q
WT + Sir3
WT + Sir3
H4K16Q + Sir3
H4K16Q + Sir3
2.0 nm
2.5 nm
4.4 nm
5.0 nm
3.7 nm
3.6 nm

Figure 2.14 Sir3 heterochromatin arrays are less compact than 30 nm fibers. **(a)** AFM images and height measurements of arrays in Tris (extended) and in Tris with 1 mM $MgCl_2$ (folded). The mean heights and 95% confidence intervals are shown above the height histograms. **(b)** Images and height histograms as in (**a**) of WT and H4-K16Q arrays in phosphate buffer. **(c)** Images and height histograms as in (**a**) of WT and H4-K16Q arrays in phosphate buffer with Sir3. Structures in black boxes are arrays bound or unbound by Sir3. **(d)** Representative, detailed 2D and 3D images of extended and folded arrays in low salt Tris buffer. **(e)** Representative, detailed image of Sir3 protein alone. **(f)** Representative, detailed 2D and 3D images of WT and H4-K16Q arrays in phosphate +/- Sir3. Note that AFM heights are generally less than crystallographic values (but proportional to them) because of sample compression, adsorption of ions and small molecules on the substrate adjacent to the complexes being measured and chemical interactions between the probe and molecules.

images indicate that the Sir3 chromatin fiber is more compact than the array without Sir3, but these fibers have a more linear structure than the Mg^{++}-compacted fibers (compare Figure 2.14d and Figure 2.14f).

Sir3 contains a BAH (Bromo-Associated Homology) domain within its N-terminus that binds to the nucleosomal surface that includes histone H4-K16 (Connelly et al. 2006; Onishi et al. 2007; Armache et al. 2011a). Several studies have demonstrated that Sir3 also contains a dimerization domain within its C-terminus, and that dimerization plays an essential role in assembly of heterochromatin (Liou et al. 2005; King et al. 2006; Oppikofer, Kueng, Keusch, et al. 2013). Indeed, as expected, the isolated Sir3 BAH domain is entirely monomeric in phosphate buffer, sedimenting at 2.22 S (Figure 2.15a, b). To investigate whether Sir3 dimerization impacts the structure of Sir3 chromatin fibers, WT and H4-K16Q nucleosomal arrays were reconstituted with increasing amounts of the isolated Sir3 BAH domain (Figure 2.16) and array structure was analyzed by AFM. As the Sir3 BAH domain was titrated to 10 molecules per nucleosome (where optimal binding was seen), the arrays retained an extended conformation with linkers between each nucleosome still apparent. Interestingly, the average height of the WT arrays increased from 1.62 nm to 3.05 nm following Sir3-BAH binding (Figure 2.16a). This value compares well to 2.79-3.29 nm for arrays containing full-length Sir3 (Figure 2.14c and Figure 2.12c). These data suggest that the increase in nucleosomal height seen upon full-length Sir3 binding is primarily a result of the Sir3-BAH domain binding to the nucleosomal

a

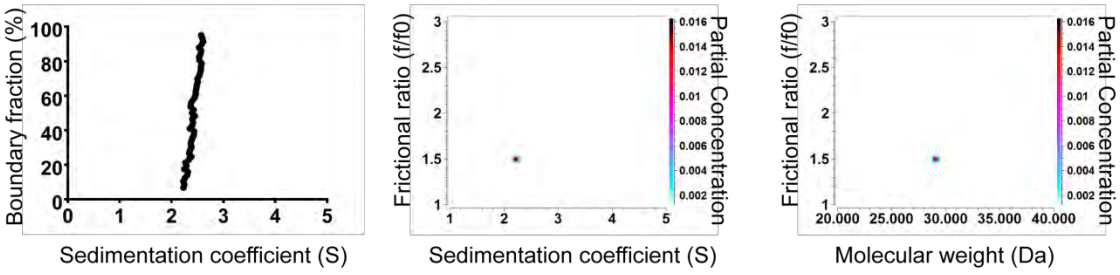

b

	Sed. Coefficient (S)	Mol. Weight (kDa)	Frictional Ratio
Monomer	2.224 (2.222, 2.226)	29.119 [26.336] (28.965, 29.274)	1.498 (1.492, 1.503)

Figure 2.15 Sir3 BAH exists as a monomer in solution. (a) Left panel, vHW analysis Sir3 BAH at 1.71 μM in phosphate buffer. Middle and right panels, GA-MC plots of S vs. molecular weight and *f/f0* vs. molecular weight. **(b)** 2DSA/GA-MC statistics show 100% of Sir3 BAH in solution is a monomer. Number in brackets is the expected molecular weight.

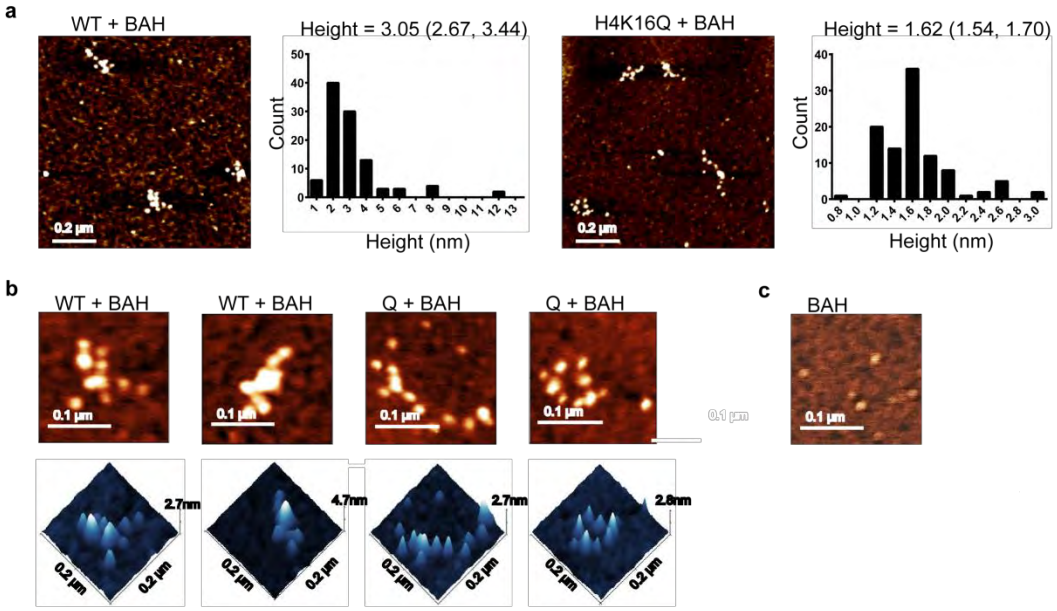
a
WT + BAH
Height = 3.05 (2.67, 3.44)
H4K16Q + BAH
Height = 1.62 (1.54, 1.70)
Count
Height (nm)
0.2 µm
b
WT + BAH
WT + BAH
Q + BAH
Q + BAH
0.1 µm
2.7nm
4.7nm
2.7nm
2.8nm
0.2 µm
c
BAH
0.1 µm

Figure 2.16 The Sir3 BAH domain binds nucleosomes but does not coat or occlude linker DNA. (a) AFM images and height measurements of WT and H4-K16Q arrays bound by the Sir3 BAH domain. The mean heights and 95% confidence intervals are shown above the height histograms. **(b)** Representative, detailed 3D and 3D images of WT and H4K16Q arrays in the presence of the Sir3 BAH doman in both 2D and 3D.

surface, whereas dimerization via the Sir3 C-terminal domain appears to promoter nucleosome-nucleosome interactions that occlude linker DNA.

Discussion

In *Saccharomyces cerevisiae*, heterochromatin formation is mediated by the Sir proteins, which deacetylate nucleosomes at telomeres and silent mating type loci and assemble a chromatin fiber that results in the transcriptional and recombinational silencing of these regions (Rusche et al. 2003). Previous biochemical studies have disagreed both as to the nature of this repressive structure, as well as to the stoichiometry of Sir proteins necessary for its formation (Onishi et al. 2007; McBryant et al. 2008; Martino et al. 2009; Sinha et al. 2009). Here, we have found that by transitioning to a buffer system with a moderate amount of monovalent cation, we are able to shield Sir3 from non-specific interactions with DNA. Consequently, our assay conditions result in a heterochromatin fiber of discrete composition, which is highly sensitive to the integrity of H4-K16, a hallmark of yeast heterochromatin. By adapting the 2DSA/GA modeling algorithms, we have taken full advantage of analytical ultracentrifugation to describe both the native molecular weight and conformation of Sir3 chromatin fibers. Coupled with AFM and chromatin binding analyses, our results indicate that Sir3 binds to model nucleosomal arrays with a stoichiometry of 2 monomers of Sir3 per nucleosome and that Sir3 creates a chromatin fiber

that is distinct from and less compact than fibers condensed with divalent cations.

SV-AUC experiments provide information about the conformational states of particles in solution, but can be difficult to interpret in situations where binding events may lead to conformational changes. By using 2DSA/GA-MC modeling to fit molecular weight and frictional properties to SV-AUC data, we were able to separate contributions to *S* derived from changes in size and changes in asymmetry. While these modeling methods have been used successfully for analyzing the sedimentation parameters of simple proteins and small nucleic acids, our study was the first to apply this approach to the analysis of chromatin fibers. During our initial studies, it was found that experimental determination of the $\bar{v}$ parameter was essential for the 2DSA/GA-MC method to provide accurate determinations for the molecular weight of chromatin fibers. Using a density contrast approach, we found that the $\bar{v}$ parameter, which is a measure of the solvated volume of a macromolecule, increased in direct proportion to the number of nucleosomes assembled on a template DNA. Furthermore, the $\bar{v}$ provided a measurement of the shape of a chromatin fiber, as it decreased dramatically as an extended nucleosomal array folded into a 30 nm fiber (i.e. due to Mg^{++}). Surprisingly, the $\bar{v}$ of a nucleosomal array that was bound by 24 molecules of Sir3 did not change dramatically, which, in combination with AFM imaging, provided further evidence that Sir3 does not induce extensive

nucleosomal array condensation but rather may “coat” the chromatin fiber while occluding linker DNA.

In wildtype yeast, the Sir2, Sir3, and Sir4 proteins co-localize at heterochromatin domains, and biochemical studies have demonstrated high affinity interactions between each of the Sir proteins (Liou et al. 2005). In yeast whole cell extracts, however, the majority of Sir3 is not associated with either Sir2 or Sir4, whereas Sir2 and Sir4 form a stable complex (Hoppe et al. 2002). Notably, a Sir2/Sir3/Sir4 complex can be assembled with recombinant proteins, either by combining the purified Sir2/Sir4 complex and Sir3, or by co-overexpression in baculovirus-infected cells (Hoppe et al. 2002; Rudner et al. 2005; Oppikofer et al. 2011). Surprisingly however, the Sir2/Sir3/Sir4 complex formed in solution binds with nearly equal affinity to acetylated nucleosomes or nucleosomes harboring H4-K16Q (Oppikofer et al. 2011). Thus, it is unclear if this complex interacts with chromatin in a physiologically relevant manner.

Recently, it was suggested that a preassembled Sir2/Sir3/Sir4 complex might play a role in the initial establishment stage of heterochromatin formation, and that the subsequent assembly and spreading of Sir proteins may require an ordered, stepwise assembly pathway (Norris & Boeke 2010). In this model, the initial binding of an intact Sir2/Sir3/Sir4 complex to silencing regions via interactions with sequence-specific DNA binding factors would promote deacetylation of H4-K16 on an adjacent nucleosome. This would lead to binding of Sir3 to the nucleosome, which would then facilitate binding of a Sir2-Sir4

complex that would deacetylate an adjacent nucleosome and repeat the cycle. Interestingly, both Sir3 and Sir4 bind to DNA, and each also binds to similar or overlapping histone surfaces with high affinity (Liou et al. 2005; Johnson et al. 2009), including the histone residues flanking H4-K16. Likewise, Sir2 must also interact with this region of the H4 N-terminus during histone deacetylation, and must then dissociate prior to Sir3 binding. These complex binding interactions support the view that a stepwise assembly mechanism may be required to ensure assembly of a *bona fide* heterochromatin fiber.

Several studies have demonstrated that Sir3 contains a dimerization domain within its C-terminus, and that dimerization plays an essential role in assembly of heterochromatin (Liou et al. 2005; McBryant et al. 2006; King et al. 2006; Oppikofer, Kueng, Keusch, et al. 2013). Although, Sir3 forms dimers and higher oligomers at high protein concentrations (McBryant et al. 2006), we found that Sir3 is present primarily as a mixture of monomers and dimers at concentrations used for heterochromatin assembly *in vitro* (<200 nM) and in buffers containing 40-150 mM Na^+. Together with our stoichiometry measurements, these data suggest a model in which two monomers of Sir3 bind to a single nucleosome, with each BAH domain of Sir3 occupying the nucleosomal surface exemplified by H4-K16. In this model, the antiparallel nature of the Sir3 dimerization domain could then facilitate interactions between neighboring nucleosomes (Figure 2.17). This model is consistent with our AFM imaging of nucleosomal arrays bound by the isolated BAH domain that shows a

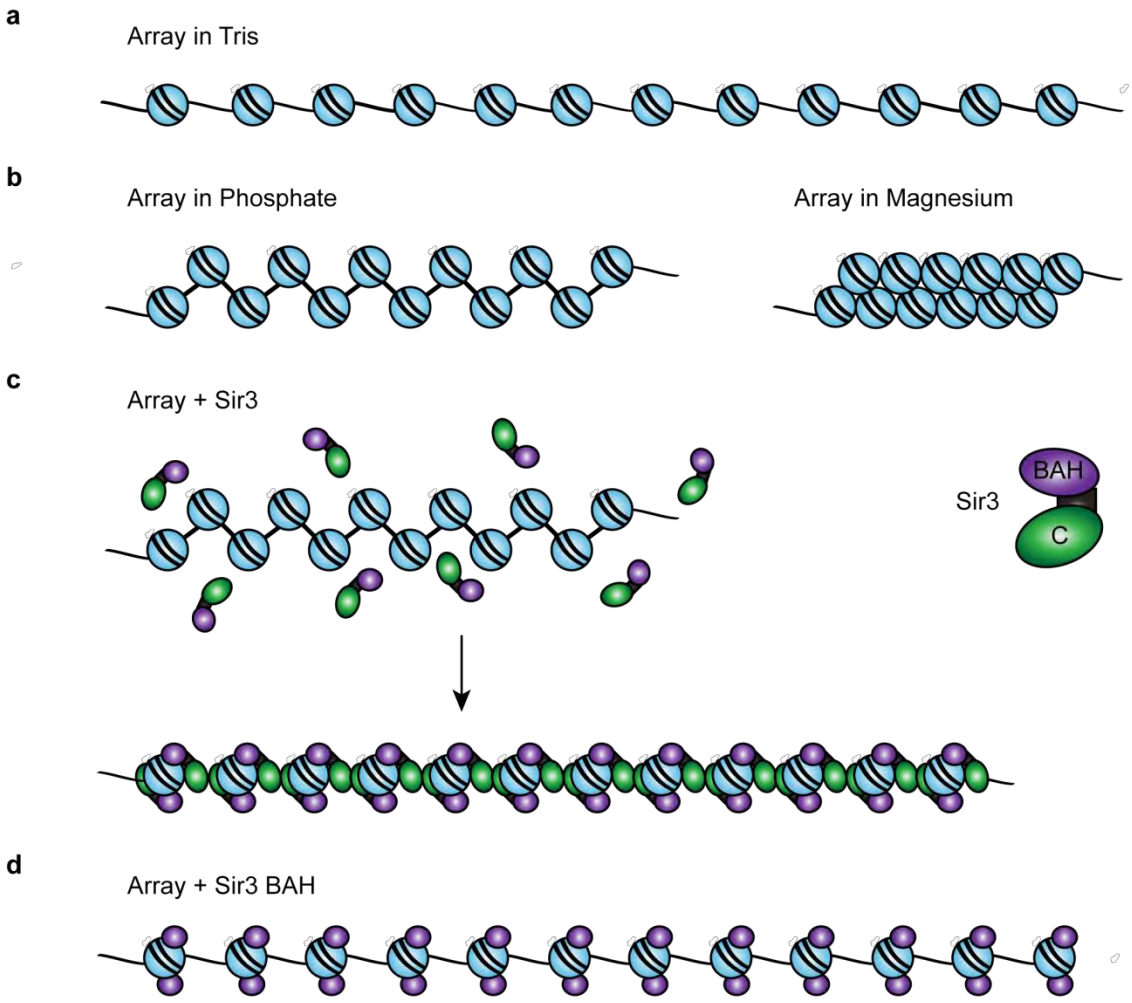
a
Array in Tris
b
Array in Phosphate
Array in Magnesium
c
Array + Sir3
Sir3
BAH
C
d
Array + Sir3 BAH

Figure 2.17 Model for a Sir3 chromatin fiber. (a) Diagram of a 12-mer array in low-salt Tris buffer. **(b)** Arrays in 20 mM phosphate buffer pH 8.0 (containing ~40 mM Na^+) are partially folded. Arrays in 1 mM $MgCl_2$ buffer fold into 30 nm fibers. **(c)** Sir3 binds to arrays as a monomer, then subsequent dimerization via the Sir3 c-terminus bridges neighboring nucleosomes. Sir3 dimerization leads to array compaction distinct from 30 nm folding. **(d)** The Sir3 BAH domain binds to nucleosomes but cannot occlude linker DNA due to the absence of the C-terminal dimerization domain.

"balls-on-a-string" structure rather than the more homogenous, elongated fiber observed for wildtype Sir3. The known interaction of Sir4 with the Sir3 C-terminal domain might also direct a Sir2-Sir4 complex to bridge adjacent nucleosomes. Interestingly, the binding of Sir2/Sir4 to the linker region is consistent with a previous prediction of the stoichiometry of a Sir2/Sir3/Sir4 complex bound to a 6-mer array (Martino et al. 2009).

The Mg^{++}-dependent folding of model 12-mer nucleosomal arrays creates a two-start helical fiber with a diameter of ~30 nm (Dorigo et al. 2004). We find that this condensation reaction is accompanied by a large decrease in the solvated volume of the fiber as well as an increase in asymmetry of the array. Furthermore, AFM analysis confirms the formation of a fiber with a greatly increased height compared to an unfolded array. In contrast, addition of Sir3 to a nucleosomal array leads to little change in the solvated volume, although the Sir3 chromatin fiber is more asymmetric than arrays that lack Sir3. AFM analyses also indicate that Sir3 creates a linear structure that is less extended than the unbound nucleosomal array, but also more rodlike and rigid. Interestingly, a model in which Sir3 monomers bridge adjacent nucleosomes closely resembles the crystal packing interactions observed for a Sir3-nucleosome x-ray structure (Armache et al. 2011b), and it is consistent with EM images demonstrating long linear filaments of Sir proteins bound to yeast chromatin (Onishi et al. 2007). This linear model of heterochromatin structure is in stark contrast to the existing dogma that heterochromatin is composed of tightly-compacted chromatin fibers

(Woodcock & Ghosh 2010). Instead, it suggests that heterochromatin proteins function by stabilizing interactions between underlying nucleosomes and DNA, and by serving as a physical barrier to the actions of chromatin remodeling enzymes.

Materials and Methods

Proteins

Lysozyme from chicken egg white was obtained from Sigma/Aldrich as a 10 mg/mL solution, and dialyzed into 20 mM sodium phosphate buffer pH 8.0. Final concentration was determined via spectroscopy. FLAG-tagged Sir3 protein was overexpressed and affinity purified from yeast (Sinha et al. 2009; Buchberger et al. 2008). Briefly, yeast cultures transformed with a plasmid containing 3xFLAG-tagged Sir3 under a galactose-inducible promoter were grown to OD 0.6 and induced with 2% galactose for 8 hours. Cultures were pelleted, resuspended in E Buffer (20 mM HEPES pH 7.4, 350 mM NaCl, 10% glycerol, 0.1% Tween 20, and protease inhibitors), and frozen in liquid nitrogen. Pellets were ground using a cold mortar and pestle with frequent additions of liquid nitrogen until approximately 50% of cells appeared lysed under a microscope. Cells were incubated on ice in E buffer for 30 min, then spun at 3,000 rpm for 15 minutes to remove debris. Supernatant was spun down at 40,000 rpm for 1 hour, then the aqueous layer was removed from the lipid layer

using a syringe. Lysate was incubated with anti-Flag resin from Sigma for three hours at 4°C. Resin was washed in E buffer, then Sir3 was eluted in batch via four 30 minute incubations of resin with E Buffer containing 100 µg/mL 3xFLAG peptide from Sigma. Concentration was determined by comparison to known concentrations of BSA electrophoreses on the same Coomassie-stained SDS-PAGE gel. 6xHis-tagged Sir3 D205N BAH was expressed in Rosetta cells and purified using Qiagen Ni-NTA resin according to the manufacturer protocol. It was quantified spectroscopically using an extinction coefficient predicted by UltraScan3 software (40,090 OD/mol*cm). Recombinant *Xenopus laevis* histones were expressed in BL21 cells, purified, and assembled into histone octamers according to standard protocols (Luger et al. 1999). Biotinylated octamers contained a H2A derivative where serine 113 was changed to a cysteine. H2A-S113C-containing octamers were dialyzed into biotinylation buffer (35mM Tris pH=7.4, 1mM EDTA, 2M NaCl) and reacted at 20 µM octamer with 800µM Maleimide-PEG2-Biotin (Thermo Fisher Scientific Inc. Cat# 21902; dry powder reconstituted immediately before use into biotinylation buffer). Reaction proceeded on ice for 48 hours.

DNA

The 601-177-12 nucleosomal array template containing twelve copies of the Widom 601 nucleosome positioning sequence was digested from its plasmid backbone using EcoRV and purified by size-exclusion chromatography. 601-

177-1 DNA was generated by digestion of the 601-177-12 template with ScaI. DNA fragments were dialyzed into 20 mM sodium phosphate pH 8.0 prior to SV-AUC.

Nucleosomal array assembly

Nucleosomal arrays were assembled by combining recombinant histone octamers and 601-177-12 DNA template at varying molar ratios of octamer to nucleosome positioning sequence in 2 M NaCl, and step-wise salt dialysis was performed until completion into either 2.5 mM NaCl and TE, or 20 mM sodium phosphate pH. 8.0 with 0.1 mM EDTA. Arrays are in phosphate buffer unless otherwise indicated. Array saturation was determined by ScaI digestion followed by analysis via native PAGE and by SV-AUC. To construct partially biotinylated nucleosomal arrays, WT and biotinylated octamers were mixed at an 85:15 molar ratio and reconstituted as above, using the 208-12 DNA template.

Nucleosomal array capture

16nM biotinylated nucleosomal array (192 nM nucleosomes) was bound to 384 nM Sir3p (unless experimentally varied) in pulldown buffer (35mM Tris pH 7.4, 50mM NaCl unless experimentally varied, 1.75 mM MgCl2, 0.05% Tween-20, 1 mM DTT) for 25 minutes at 22°C. For Figure 2.2, 20 mM phosphate buffer pH 8.0 containing was used in placed of pulldown buffer. This reaction was then bound to 10µg/µl Streptavidin-coated magnetic beads (Invitrogen™ Cat#

11205D) for 5 minutes at 22°C. The magnetic beads had been washed twice in pulldown buffer and blocked for 15 minutes at 22°C in pulldown buffer supplemented with 100µg/mL BSA. During blocking and array binding, beads were kept continually suspended by gentle rotation. After binding, the beads were magnetically captured and the supernatant "unbound" fraction was removed. The beads were resuspended in 1x SDS-PAGE sample buffer, heated for 5' at 95°C, and care was taken to magnetically extract the stripped beads from the supernatant "bound" fraction. These fractions were subjected to SDS-PAGE, electroblotted onto nitrocellulose, and detected by HRP-FLAG (Sigma-Aldrich® Cat# A8592) immunoblotting.

EMSA

300 ng WT or H4-K16Q nucleosomal array in Tris buffer containing 2.5 mM NaCl or 20 mM phosphate buffer containing approximately 40 mM Na^+ was combined with Sir3 at a range of 0-8 monomers per nucleosome to a final concentration of 10 ng/ul array and 5% glycerol. Binding reactions were incubated at room temperature for 30 minutes, run on 1% TBE agarose gels, and stained with ethidium bromide.

SV-AUC

SV-AUC was carried out using 400 µl sample loaded into two-sector Epon centerpieces in an An60 Ti rotor in a Beckman Optima XL-I analytical

ultracentrifuge, and run at 20°C. Measurement was completed in intensity mode. Nucleosomal arrays were run at 10 ng/ul concentrations with the indicated amount of Sir3 or $MgCl_2$ at 20,000 RPM, and were measured at 215 nm (for arrays in phosphate buffer) or 260 nm (for samples containing Tris or Sir3). All arrays were run in 20 mM phosphate unless otherwise indicated. Lysozyme was loaded to an OD of 0.4, and run at 41,000 RPM and measured at 280 nm. DNA fragments were run at 10 ng/ul in phosphate buffer with 300 mM NaCl added to reduce concentration-dependent nonideality, and measured at 260 nm. The 601-177-12 fragment was run at 30,000 RPM and the 601-177-1 fragment at 48,000 RPM. Sir3 alone was run in the indicated solution at 171 nM and 40,000 RPM and measured at 215 nm, and Sir3 BAH alone was run at 1.71 μM and 48,000 RPM. For $\bar{\nu}$ determination, three preparations of sample were run as above, with 0, 30, or 60% $H_2{}^{18}O$ (obtained from Cambridge Istotope Laboratories, Andover, MA) added in place of $H_2{}^{16}O$. The obtained S values were then plotted as a function of solvent densities, linear regression was performed, and the $\bar{\nu}$ was calculated by dividing the slope of the resulting line by the y-intercept. Solvent densities and viscosities were obtained from the literature.(Brown et al. 2011) Linear regression was performed using GraphPad Prism software.

2DSA/GA-MC

All SV-AUC data were analyzed using UltraScan3 software, version 2.1 and release 1706 (Demeler et al. 2014), and fitting procedures were completed

on XSEDE clusters at the Texas Advanced Computing Center (Lonestar, Stampede) and at the San Diego Supercomputing Center (Trestles) through the UltraScan Science Gateway (https://www.xsede.org/web/guest/gateways-listing). Raw intensity data were converted to pseudo-absorbance by using the intensity of the air above the meniscus as a reference and edited. Next, 2DSA was performed to subtract time-invariant noise and the meniscus was fit using 10 points in a 0.05 cm range. Arrays were fit using an S range of 5-60 S, an f/f_0 range of 1-10 with 64 or 100 grid points for each, 10 uniform grid repetitions, and 400 simulation points. 2DSA was then repeated at the determined meniscus to fit radially-invariant and time-invariant noise together using 5 iterations. vHW analysis was completed using these noise subtraction profiles to determine S. Where indicated, GA was initialized by binning major solutes in the 2DSA dataset, and run via LIMS. Major solutes from GA analysis were then binned and run again using GA with 50 MC iterations.

AFM

For atomic force microscopic experiments, an Agilent AFM 5500 instrument and silicon nitride cantilevers were used (force constant 25-75 N/m, resonant frequency 332 kHz). Imaging was done in air using the acoustic AC mode with an amplitude of ~10 nm and a set-point reduction of about 10%, scanning at 1 line per second. Immobilization of chromatin arrays on mica surface was done as follows. First, 1 µL of Sir3 protein solution (39 ng/µL) was

added to the phosphate or Tris buffer (7 µL) followed by addition of 1 µL of chromatin array (10 ng/µL) and mixed gently, maintaining a ratio of 4 Sir3 molecules/nucleosome. For Sir3 BAH D205N experiments, BAH was added at 4 (data not shown) and 10 monomers per nucleosome as above. After 30 minutes, 0.5% glutaraldehyde solution (1 µL) was added to this mixture for crosslinking and incubated for 10 minutes. APTES was deposited on freshly cleaved mica substrate using vapor deposition. The crosslinked chromatin solution was diluted to 1 ng/µL and 3 µL was added to this APTES modified mica surface and after 5 minutes the surface was cleaned three times using 400 µL of buffer solution, dried carefully using argon gas and immediately used for imaging. To image only chromatin arrays, the first mixing step with Sir3 was omitted.

CHAPTER III: SOLUTION-STATE BEHAVIOR OF RECONSTITUTED SIR HETEROCHROMATIN FIBERS

Abstract

Heterochromatin is a silenced chromatin region essential for maintaining genomic stability in eukaryotes and for driving developmental processes in higher organisms. Although heterochromatin formation is known to be mediated by the binding of heterochromatin-specific architectural proteins, the structural features of heterochromatin are poorly understood. In budding yeast, heterochromatin assembly requires the Sir proteins: Sir3, believed to be the major structural component of SIR heterochromatin, and the Sir2/4 complex, responsible for SIR recruitment to silencing regions and deacetylation of lysine 16 of the H4 tail, a mark associated with active chromatin. Previous work from our group found that Sir3 binds to, but does not compact nucleosomal arrays, and that this interaction is sufficient to block chromatin remodeling and the early stages of homologous recombination. Here, we reconstitute nucleosomal arrays with all three Sir proteins and apply sedimentation velocity, modeling, and atomic force microscopy methods to characterize their solution state behavior, stoichiometry, and structure.

Introduction

Eukaryotic cells regulate the accessibility of their genome to enzymatic processes by organizing it into two functionally distinct compartments, known as euchromatin and heterochromatin. Euchromatin consists of actively transcribed gene regions, whereas heterochromatin is refractory to processes such as transcription and recombination (Woodcock & Ghosh 2010). Heterochromatin organizes and protects centromeres and telomeres, guards against the spreading of transposons, and prevents aberrant homologous recombination within repetitive regions that can lead to chromosomal abnormalities such as deletions, inversions, and translocations (Grewal & Jia 2007; Beisel & Paro 2011; Saksouk et al. 2015). Additionally, heterochromatin formation is an essential developmental process that drives the differentiation and maintenance of cell types (Grewal & Jia 2007; Beisel & Paro 2011; Simon & Kingston 2013). Although heterochromatin carries a distinct subset of histone modifications and protein complexes, the mechanism by which heterochromatin maintains its silent state is poorly understood.

The most thoroughly-characterized form of heterochromatin exists in the budding yeast *Saccharomyces cerevisiae*, which requires the Sir proteins for silencing (Rine & Herskowitz 1987). The formation of SIR heterochromatin is believed to be a step-wise process in which the Sir2/4 complex is recruited to silencing regions via interactions between the Sir4 protein and sequence-specific DNA binding factors such as Rap1, Orc1, and Abf1 (Diffley & Stillman 1989; Moretti et al. 1994; Hecht et al. 1996; Triolo & Sternglanz 1996; Mishra & Shore

1999; Roy et al. 2004). Sir2, an NAD^+-dependent histone deacetylase, then deacetylates the H4 tail of an adjacent nucleosome at lysine 16 (H4-K16), which promotes the binding of the Sir3 protein to the nucleosome, in turn recruiting additional Sir2/4 complex (Hecht et al. 1995; Hecht et al. 1996; Imai et al. 2000; Rusche et al. 2002). As this cycle of deacetylation and binding continues, the Sir proteins spread away from the nucleation site, creating a silent heterochromatin domain (Rusche et al. 2003).

The importance of H4-K16 to SIR heterochromatin was initially discovered when its mutation to glutamine (H4-K16Q) was found to disrupt the repression of the silent mating loci, and compensatory mutations in the Sir3 protein were identified (Johnson et al. 1990). The physical interaction between Sir3 and H4-K16 has been explored at length both *in vivo* and *in vitro* (Hecht et al. 1995; Onishi et al. 2007; Sinha et al. 2009; Swygert et al. 2014), with several crystal structures of the Sir3 BAH domain bound to the nucleosome displaying the H4 tail interacting with an electronegative patch of Sir3 containing a specific binding pocket for K16 (Armache et al. 2011b; Wang et al. 2013; Arnaudo et al. 2013). Interestingly, while Sir3 alone demonstrates a clear preference for binding unmodified versus acetylated or mutated H4-K16, this preference is lost in presence of Sir2/4 (Johnson et al. 2009; Oppikofer et al. 2011; Johnson et al. 2013). However, a single amino acid substitution within the coiled-coil region of Sir4 that interacts with Sir3 (Sir4-I1311N) restores Sir3's binding specificity, suggesting that Sir3's presence at modified or mutated H4-K16 chromatin is

mediated primarily by interactions with Sir4 rather than with the chromatin itself (Chang et al. 2003; Rudner et al. 2005; Johnson et al. 2009). Further, although all three Sir proteins can be detected as bound to H4-K16Ac chromatin templates, they are unable to prevent the binding of transcriptional activators or block transcriptional elongation in the absence of NAD^+ (Johnson et al. 2009; Johnson et al. 2013). This suggests that although interaction between modified H4-K16 and Sir proteins is possible, the presence of H4-K16Ac prevents the formation of functionally repressed heterochromatin structure. However, the structural change that occurs to mediate silencing on unmodified chromatin remains unclear.

Recently, we established experimental conditions in which Sir3 displays a strong preference for wild type (WT) versus H4-K16Q chromatin (Swygert et al. 2014). We used a combination of sedimentation velocity analytical ultracentrifugation (SV-AUC), modeling, and atomic force microscopy (AFM) to demonstrate that these physiologically-relevant reconstituted heterochromatin fibers are surprisingly less compact compared to condensed 30 nm fibers. The moderate occlusion of linker DNA observed required the C-terminal dimerization domain of Sir3, suggesting that the oligomerization of Sir3 mediates cross-nucleosomal interactions (Swygert et al. 2014). Here, we apply these methods to reconstituted heterochromatin fibers containing all three Sir proteins. We find that although all three proteins are capable of interacting with both WT and H4-K16Q chromatin, only WT chromatin is sufficient to form a condensed structure

consistent with an inaccessible heterochromatin fiber. Additionally, this structure required the interaction of Sir3 with Sir4.

Results

Sir2/4 binds to both WT and H4-K16Q arrays

We previously established ionic conditions that diminished nonspecific binding interactions between Sir3 and DNA in order to create heterochromatin fibers sensitive to H4-K16Q (Swygert et al. 2014). In order to examine the binding of Sir2/4 to nucleosomal arrays under these conditions, chromatin fibers were reconstituted via salt dialysis using a DNA template containing twelve sequential repeats of the synthetic 601 nucleosome positioning sequence with a 30 base pair linker (601-177-12) with either WT or H4-K16Q recombinant *Xenopus laevis* histone octamers, and a tandem affinity purification (TAP) strategy was used to purify the Sir2/4 complex from yeast. Binding was first analyzed via electrophoretic mobility shift assay (EMSA), in which increasing amounts of Sir2/4 complex were added to chromatin and binding was monitored by the decrease in mobility of bands on an agarose gel (Figure 3.1a). Consistent with previous studies, Sir2/4 bound WT and H4-K16Q arrays at similar concentrations, with an apparent slight preference for H4-K16Q (Oppikofer et al. 2011).

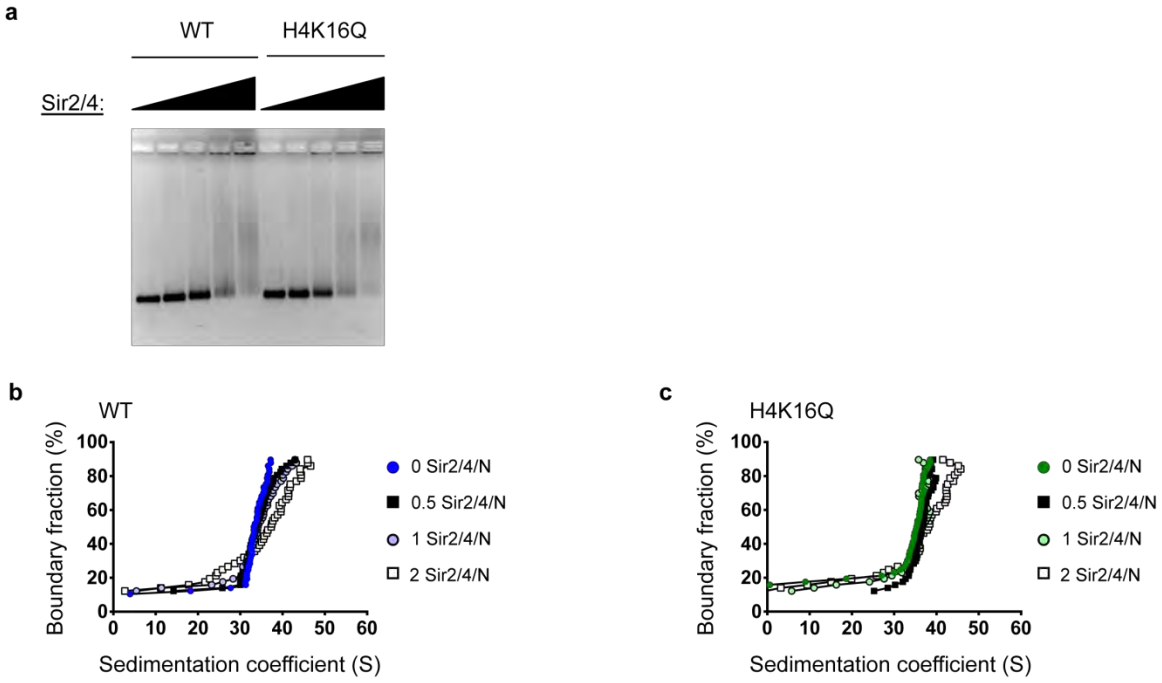
a
WT
H4K16Q
Sir2/4:
b
WT
Boundary fraction (%)
Sedimentation coefficient (S)
0 Sir2/4/N
0.5 Sir2/4/N
1 Sir2/4/N
2 Sir2/4/N
c
H4K16Q
Boundary fraction (%)
Sedimentation coefficient (S)
0 Sir2/4/N
0.5 Sir2/4/N
1 Sir2/4/N
2 Sir2/4/N

Figure 3.1 The Sir2/4 complex binds both WT and H4K16Q arrays. (a) EMSA of Sir2/4 binding to WT and H4K16Q arrays. **(b-c)** vHW plots of Sir2/4 complex titrated onto WT and H4K16Q arrays. Numbers indicate the molar ratio of Sir2/4 complex per nucleosome.

Next, Sir2/4 was titrated onto arrays and interactions were monitored via SV-AUC. Sir2/4 bound maximally to WT and H4-K16Q arrays at 1-2 Sir2/4 molecules per nucleosome (Figure 3.1a and b), with further additions leading to aggregation and loss of solubility (data not shown). For both WT and H4-K16Q, arrays, the sedimentation coefficient shifted from 33 to 38 S upon addition of 2 molecules of Sir2/4 per nucleosome, in contrast to the increase in sedimentation coefficient to 45-50 S seen on addition of Sir3 to WT arrays previously and in Figure 3.2a and Figure 3.6a.

SIR interactions with WT and H4-K16Q arrays are distinct

After determining the range of binding of Sir2/4 to arrays, the binding of Sir3 in the presence of Sir2/4 complex was determined via EMSA (Figure 3.2a). Although Sir3 alone bound with much greater affinity to WT than H4-K16Q arrays as seen previously, titrating Sir3 in the presence of Sir2/4 led to the formation of a band of similar mobility on both WT and H4-K16Q. Notably, this species remained at constant mobility despite further additions of Sir3. This suggests that these ionic conditions allow formation of a discrete SIR heterochromatin fiber. This is in stark contrast to previous studies in which the addition of increasing concentrations of Sir proteins led to continual decreases in the mobility of SIR-nucleosome complexes suggestive of nonspecific DNA binding or aggregation (Martino et al. 2009; Oppikofer et al. 2011).

a

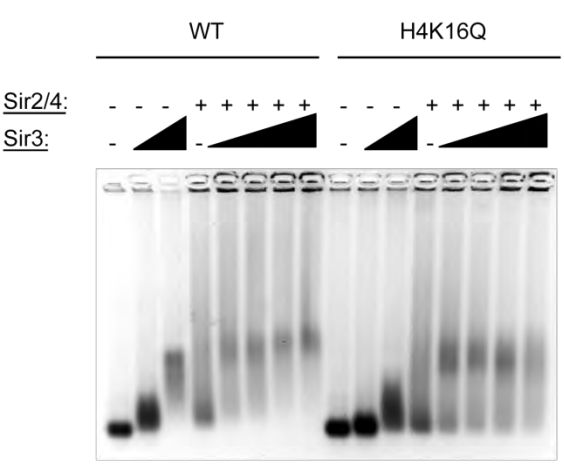

b

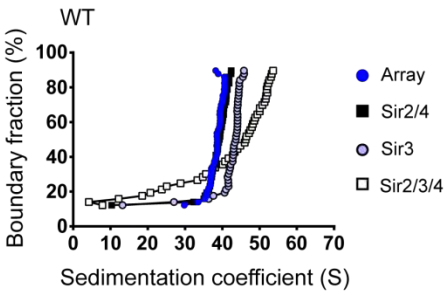

c

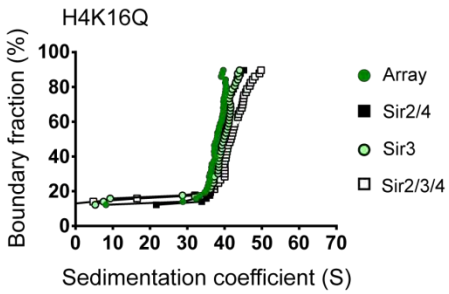

d

	$\overline{v}$ (mL/g)	Mol. Weight (MDa)	Sir3	Sir2/4	Frictional Ratio
WT	0.701	2.461 [2.614] (2.399, 2.524)	-	-	2.018 (1.983, 2.052)
WT + Sir2/4	0.701	3.263 (3.202, 3.325)	-	4	2.256 (2.228, 2.284)
WT + Sir3	0.715	4.942 (4.865, 5.020)	22	-	2.591 (2.565, 2.618)
WT + Sir2/3/4	0.776	7.307 (7.036, 7.577)	22	11	2.927 (2.856, 2.998)
H4K16Q	0.700	2.531 [2.614] (2.498, 2.565)	-	-	2.053 (2.035, 2.072)
H4K16Q + Sir2/4	0.717	7.334 (7.026, 7.642)	-	22	3.730 (3.626, 3.835)
H4K16Q + Sir3	0.702	3.551 (3.490, 3.613)	9	-	2.240 (2.215, 2.265)
H4K16Q + Sir2/3/4	0.679	7.230 (7.064, 7.396)	22	10	3.997 (3.938, 4.056)

Figure 3.2 SIR interactions with WT and H4K16Q arrays are distinct. (a) EMSA of Sir3 titrated onto WT and H4K16Q arrays in the absence or presence of Sir2/4 complex. **(b-c)** vHW plots of Sir2/4, Sir3, and Sir3 and Sir2/4 complex added to WT and H4K16Q arrays. **(d)** 2DSA/GA-MC modeling results of the sedimentation data in **(b-c)**. Numbers in brackets represent expected molecular weights. Numbers in parentheses are 95% confidence intervals. Stoichiometries upon addition of Sir2/3/4 are speculative.

SIR heterochromatin fibers were next examined via SV-AUC (Figure 3.2b and c). As in Figure 3.1, the addition of Sir2/4 onto WT and H4-K16Q arrays led to small changes in S. Similar to our previous study (Swygert et al. 2014), the addition of Sir3 to WT arrays led to a substantial change in S, from ~35 to 45 S, but did not alter the sedimentation distribution of H4-K16Q arrays, consistent with binding of Sir3 to WT but not H4-K16Q nucleosomes. Interestingly, despite the formation of a band of similar mobility in the EMSA, the addition of all three Sir proteins to WT arrays led to a shift to ~50 S, whereas binding of all three Sir proteins to H4-K16Q led to a very modest shift to ~42 S. These data suggest that although the levels of SIR binding to WT and H4-K16Q arrays are similar, the structure of WT and H4-K16Q SIR fibers may be markedly different.

In order to ascertain the differences in structure formed by Sir proteins on WT and H4-K16Q chromatin, the SV-AUC data were further analyzed using two dimensional spectrum analysis, genetic algorithm, and Monte Carlo (2DSA/GA-MC) modeling implemented in UltraScan3 software (see Swygert et al. 2014 for extensive discussion). These modeling algorithms fit molecular weight and shape parameters to the sedimentation profiles (Demeler & Brookes 2007; Brookes & Demeler 2007; Brookes et al. 2010; Gorbet et al. 2014). As before, this modeling required the experimental determination of the partial specific volumes ($\bar{\nu}$) of each of the chromatin fibers analyzed (Figure 3.3).

2DSA/GA-MC results (Figure 3.2d) show the molecular weights of both WT and H4-K16Q arrays were approximately 2.5 MDa, indicating the presence of

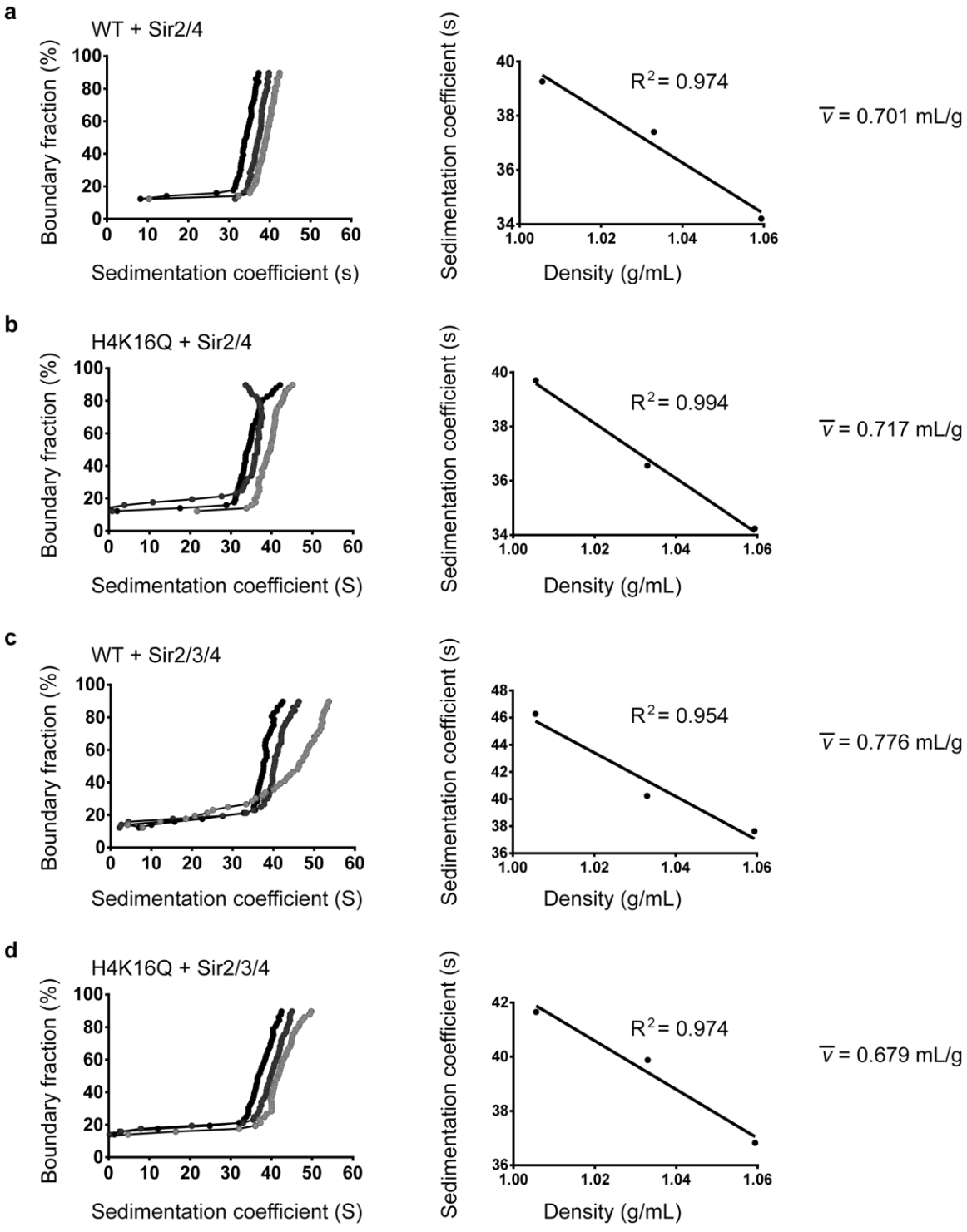
a
WT + Sir2/4
Boundary fraction (%)
Sedimentation coefficient (s)
Sedimentation coefficient (s)
R2 = 0.974
Density (g/mL)
v̄ = 0.701 mL/g
b
H4K16Q + Sir2/4
Boundary fraction (%)
Sedimentation coefficient (S)
Sedimentation coefficient (s)
R2 = 0.994
Density (g/mL)
v̄ = 0.717 mL/g
c
WT + Sir2/3/4
Boundary fraction (%)
Sedimentation coefficient (S)
Sedimentation coefficient (s)
R2 = 0.954
Density (g/mL)
v̄ = 0.776 mL/g
d
H4K16Q + Sir2/3/4
Boundary fraction (%)
Sedimentation coefficient (S)
Sedimentation coefficient (s)
R2 = 0.974
Density (g/mL)
v̄ = 0.679 mL/g

Figure 3.3 The partial specific volume of WT and H4K16Q arrays with Sir2/4. (a-d) vHW plots showing the sedimentation of molecules in 0% (light gray), 25% (dark gray), and 50% H2O18 (black) and plots of sedimentation coefficient vs. density. The $\bar{v}$ is calculated by dividing the slope of the fit line by the y-intercept.

11 nucleosomes on the 12mer template. The addition of Sir3 to WT arrays led to an increase in molecular weight to 4.9 MDa, consistent with the binding of 22 molecules of the 113 kDa Sir3-FLAG protein, or a stoichiometry of two Sir3 molecules per nucleosome. In accordance with low levels of binding, the increase in molecular weight on H4-K16Q arrays upon Sir3 addition indicated the presence of approximately 9 molecules of Sir3. In contrast, the molecular weight of the Sir2/4 H4-K16Q fiber indicated binding of 22 molecules of Sir2/4, or two molecules per nucleosome, whereas the molecular weight of the Sir2/4 WT fiber increased only modestly over the array alone, suggesting binding of only four molecules of Sir2/4. However, in the presence of all three Sir proteins, the molecular weight of WT arrays increased to 7.3 MDa, which could correspond to the binding of 22 molecules of Sir3 and 11 molecules of Sir2/4, or a stoichiometry of 2 Sir3's and 1 Sir2/4 per nucleosome. Interestingly, the addition of all three Sir proteins to H4-K16Q arrays did not lead to an increase in molecular weight over Sir2/4 alone, with the molecular weight remaining stable at 7.2 and 7.3 MDa, respectively. These results suggests one of three possibilities: 1) as the molecular weights of the WT and H4-K16Q SIR fibers were quite similar, Sir proteins on H4-K16Q could also exist at a stoichiometry of 2 Sir3's and 1 Sir2/4 per nucleosome, consistent with the similar levels of binding seen via EMSA, 2) as the molecular weight of the Sir2/4 H4-K16Q fiber did not increase upon addition of Sir3, it is possible that no Sir3 bound at all, or that Sir3 binding was not stable during centrifugation, and 3) that the stoichiometry of Sir2/4 and Sir3

exists somewhere in between, with more Sir2/4 bound to H4-K16Q arrays than WT, but with some Sir3 molecules present as well.

Despite a nearly identical increase in molecular weight on addition of Sir proteins, WT arrays sedimented much more rapidly than H4-K16Q arrays (Figure 3.2d). This suggests that WT arrays adopted a more compacted, symmetric structure than H4-K16Q arrays, which is reflected in the frictional ratio (f/f_0). The f/f_0 is the ratio of the coefficient of friction of the molecule studied to the coefficient of friction of a perfectly spherical molecule of the same volume and mass (Hansen et al. 1995; Demeler 2010). Thus, as f/f_0 increases from 1, the molecule moves from being spherical, to globular, to disordered, to rodlike. As Sir proteins were added to WT arrays, the f/f_0 increased from 2.0, to 2.3 with Sir2/4, to 2.6 with Sir3, and finally to 2.9 in the presence of all three Sirs. In contrast, the f/f_0 of H4-K16Q increased from 2.1 to 3.7 in the presence of Sir2/4 to 4.0 in the presence of all three Sirs. This indicates that whereas the WT SIR fiber remained globular, the H4-K16Q SIR fiber adopted a highly asymmetric extended conformation incompatible with compaction. This difference was also reflected in the $\bar{v}$ of the chromatin, as the WT SIR fiber adopted a higher and more protein-like 0.776 mL/g, whereas the H4-K16Q fiber $\bar{v}$ remained low and more nucleic acid-like at 0.679 mL/g, which could reflect the existence of exposed linker DNA in the structure.

Sir proteins condense WT but not H4-K16Q arrays

In order to explore the structural differences between WT and H4-K16Q SIR fibers, 36mer 601-177 arrays (601-177-36) were generated and imaged by AFM (Figure 3.4 and Figure 3.5). Although SIR binding experiments were completed in sodium phosphate buffer, which has a sodium ion concentration of approximately 40 mM ideal for promoting specific SIR binding to chromatin (Swygert et al. 2014), arrays were initially imaged in low salt Tris buffer in order to visualize structural differences between extended arrays and arrays compacted into 30 nm fibers (Figure 3.4a and Figure 3.5a). On addition of 1 mM $MgCl_2$, which induces folding into the 30 nm fiber (Finch & Klug 1976; Widom 1986; Schwarz & Hansen 1994), the arrays changed from a beads-on-a-string structure to a highly compacted globular structure, with a proportional increase in height from 1.88 to 5.43 nm. In buffer containing moderate salt (Figure 3.4b), both WT and H4-K16Q arrays adopted a zig-zag structure consistent with an intermediate folding state reflective of the two-start helix of 30 nm fibers with 30 bp DNA linkers (Routh et al. 2008), with a height of approximately 1.9 nm. The addition of Sir3 (Figure 3.4c and Figure 3.5b) increased the height of WT arrays to 4.06 nm, whereas H4-K16Q arrays increased only slightly to 2.29 nm, corresponding to binding to WT but not H4-K16Q. As previously, although Sir3 binding appeared to occlude linker DNA (as evidenced by the loss of a beads-on-a-string structure), Sir3 fibers remained significantly uncompacted compared to 30 nm fibers (Swygert et al. 2014). However, the addition of Sir2/4 to WT arrays appeared to lead to the formation of a more condensed structure, with the height

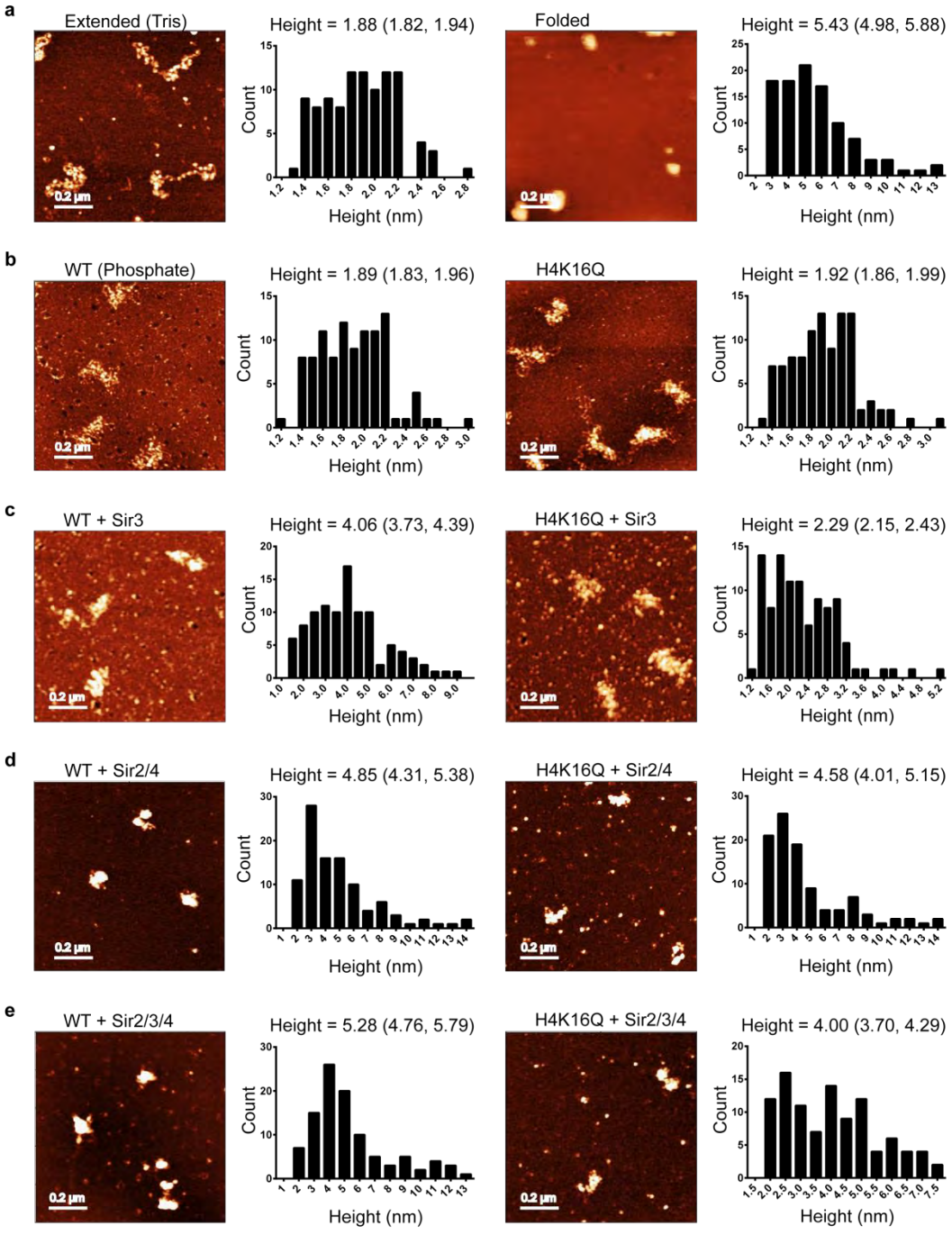
a
Extended (Tris)
Height = 1.88 (1.82, 1.94)
Folded
Height = 5.43 (4.98, 5.88)
b
WT (Phosphate)
Height = 1.89 (1.83, 1.96)
H4K16Q
Height = 1.92 (1.86, 1.99)
c
WT + Sir3
Height = 4.06 (3.73, 4.39)
H4K16Q + Sir3
Height = 2.29 (2.15, 2.43)
d
WT + Sir2/4
Height = 4.85 (4.31, 5.38)
H4K16Q + Sir2/4
Height = 4.58 (4.01, 5.15)
e
WT + Sir2/3/4
Height = 5.28 (4.76, 5.79)
H4K16Q + Sir2/3/4
Height = 4.00 (3.70, 4.29)
Count
Height (nm)
0.2 µm

Figure 3.4 SIR heterochromatin is compact. (a) AFM images of WT 601-177-36 arrays in low salt Tris buffer in the absence (left) or presence (right) of 1 mM $MgCl_2$. Histograms are of 100 individual measurements. Mean height and 95% confidence intervals are shown above. **(b-e)** WT and H4K16Q 601-177-36 arrays in sodium phosphate buffer incubated with indicated SIR proteins.

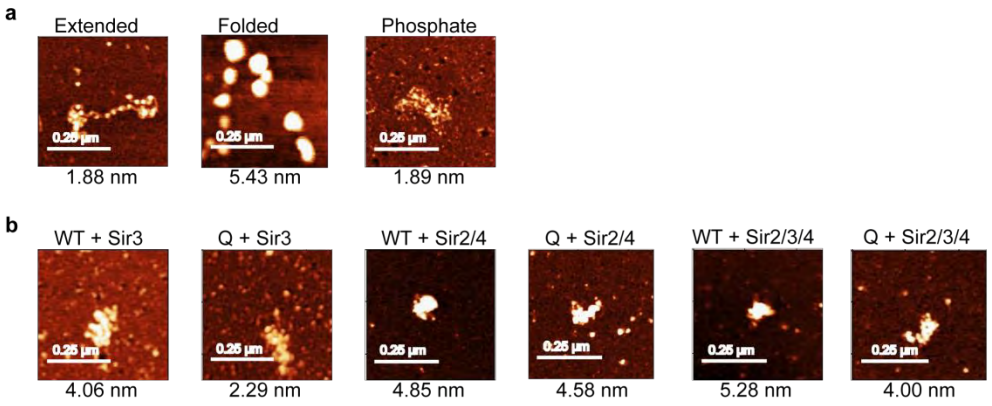
a
Extended
Folded
Phosphate
0.25 µm
1.88 nm
5.43 nm
1.89 nm
b
WT + Sir3
Q + Sir3
WT + Sir2/4
Q + Sir2/4
WT + Sir2/3/4
Q + Sir2/3/4
4.06 nm
2.29 nm
4.85 nm
4.58 nm
5.28 nm
4.00 nm

Figure 3.5 SIR heterochromatin is compact compared to Sir3 fibers. (a-b) Detail of AFM images shown in Figure 4.

increasing to 4.85 nm, and finally to 5.28 nm in the presence of all three Sir proteins (Figure 3.4d-e, and Figure 3.5b). In contrast, although the height of H4-K16Q arrays increased on addition of Sir2/4 and all three Sirs, the H4-K16Q SIR fibers appeared extended and individual nucleosomes could still be identified, suggesting that while Sir proteins bound at similar levels to H4-K16Q nucleosomes, they were unable to occlude linker DNA and form a compact structure.

The compaction of SIR chromatin requires Sir3-Sir4 interaction

Finally, the contribution of the Sir4 coiled-coil domain responsible for binding Sir3 to WT and H4-K16Q SIR structure was examined. Sir2/4 complex in which isoleucine 1311 of Sir4 was mutated to asparagine was purified from yeast, and its contribution to SIR array binding was monitored via EMSA. This mutation is known to abolish the interaction of the Sir4 with Sir3 *in vitro* and *in vivo* (Chang et al. 2003; Rudner et al. 2005), and was found to eliminate the pull-down of Sir3 on H4-K16A arrays (Johnson et al. 2009). As expected, in the presence of Sir2/4-I1311N, Sir3 binding on H4-K16Q arrays was reduced compared to WT (Figure 3.6a), although binding was still observed at higher concentrations of Sir3. Intriguingly, although the mobility of the Sir proteins on WT arrays was similar with WT and mutant Sir2/4, the addition of Sir2/4-I1311N produced a more discrete, darkly-staining band, suggesting that though the levels of binding were similar, the structure of the fibers were different.

a

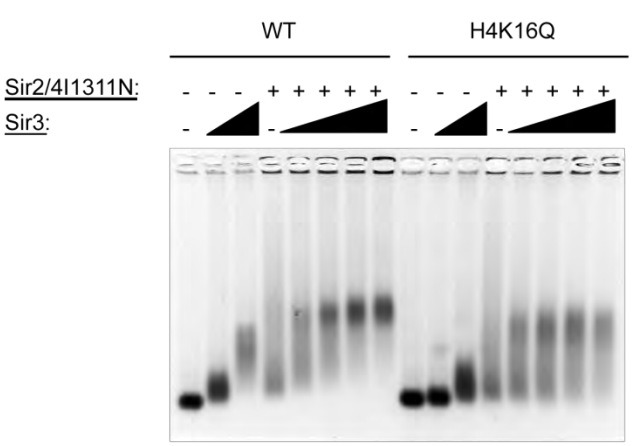

b

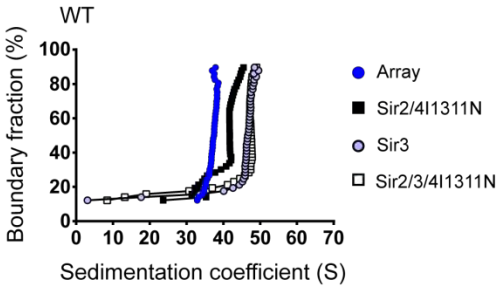

c

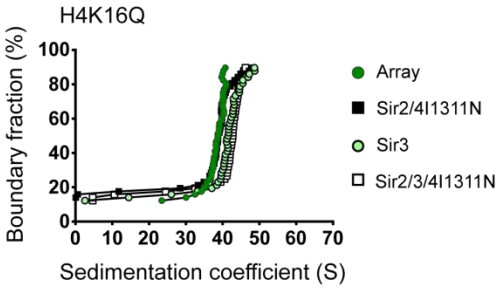

d

	$\bar{v}$ (mL/g)	Mol. Weight (MDa)	Sir3	Sir2/4	Frictional Ratio
WT	0.699	2.370 [2.614] (2.316, 2.425)	-	-	1.968 (1.938, 1.999)
WT + Sir2/4N	0.692	10.59 (9.856, 10.33)	-	38	4.465 (4.262, 4.667)
WT + Sir3	0.715	5.591 (5.404, 5.777)	29	-	2.709 (2.649, 2.769)
WT + Sir2/3/4N	0.679	8.019 (7.889, 8.149)	29	11	3.755 (3.715, 3.795)
H4K16Q	0.701	2.520 [2.614] (2.479, 2.561)	-	-	1.867 (1.847, 1.886)
H4K16Q + Sir2/4N	0.633	5.960 (5.452, 6.468)	-	16	3.717 (3.510, 3.924)
H4K16Q + Sir3	0.702	2.332 (2.233, 2.431)	0	-	1.628 (1.583, 1.673)
H4K16Q + Sir2/3/4N	0.726	5.253 (5.233, 5.273)	0	13	2.537 (2.532, 2.542)

Figure 3.6 SIR-mediated compaction requires the interaction between Sir3 and Sir4. (a) EMSA of Sir3 titrated onto WT and H4K16Q arrays in the absence or present of Sir2/4I1311N. **(b-c)** vHW plots of Sir3, Sir2/4I1311N, and Sir3 and Sir2/4I1311N complex added to WT and H4K16Q arrays. **(d)** 2DSA/GA-MC modeling results of the sedimentation data in **(b-c)**. Numbers in brackets represent expected molecular weights. Numbers in parentheses are 95% confidence intervals. Stoichiometries upon addition of Sir2/3/4 are speculative.

To address the possibility of a distinct structure in the absence of Sir3-Sir4 interaction, SIR WT and H4-K16Q fibers bearing Sir4-I1311N were studied via SV-AUC, $\bar{v}'s$ were determined (Figure 3.7), and 2DSA/GA-MC modeling was completed on the data (Figure 3.6b-d). Interestingly, although Sir2/4-I1311N induced a greater increase in S than WT Sir2/4 (~42 S vs 38 S), Sir2/4-I1311N did not increase the rate of sedimentation over WT arrays bound by Sir3 alone (Figure 3.6b). In concordance with this finding, 2DSA/GA-MC modeling revealed that although the increase in molecular weight upon mutant SIR addition to WT was similar to WT SIR (8 MDa versus 7.3 MDa, respectively), the f/f_0 increased dramatically in the presence of the Sir4 mutation, from 2.0 to 3.8. Similarly, the $\bar{v}$ decreased to 0.679, rather than increased as in the presence of WT Sir2/4. Fascinatingly, an f/f_0 of 3.8 and $\bar{v}$ of 0.679 are nearly identical to the numbers obtained for the H4-K16Q SIR fiber. This strongly suggests that although binding is not inhibited by Sir2/4-I1311N, the resulting structure most closely resembles that of H4-K16Q SIR chromatin, with Sir proteins bound to nucleosomes but unable to compact arrays.

Discussion

Previously, we identified ionic conditions in which *in vitro* reconstituted Sir3 heterochromatin fibers displayed a physiologically relevant preference for forming on WT versus H4-K16Q chromatin (Swygert et al. 2014). Sir3 was found

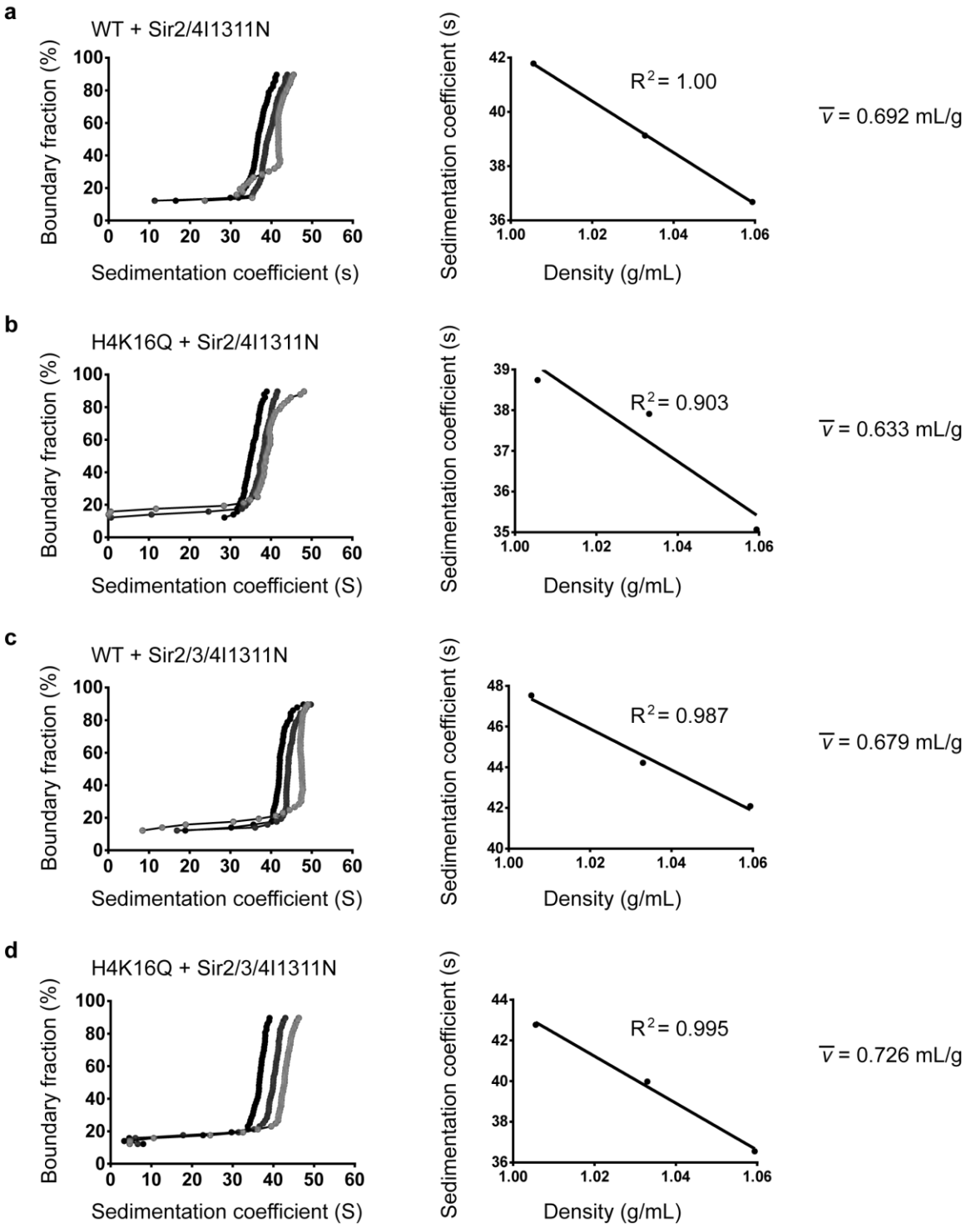
a
WT + Sir2/4I1311N
Boundary fraction (%)
Sedimentation coefficient (s)
Sedimentation coefficient (s)
R2= 1.00
Density (g/mL)
v̄ = 0.692 mL/g
b
H4K16Q + Sir2/4I1311N
Boundary fraction (%)
Sedimentation coefficient (S)
Sedimentation coefficient (s)
R2= 0.903
Density (g/mL)
v̄ = 0.633 mL/g
c
WT + Sir2/3/4I1311N
Boundary fraction (%)
Sedimentation coefficient (S)
Sedimentation coefficient (s)
R2= 0.987
Density (g/mL)
v̄ = 0.679 mL/g
d
H4K16Q + Sir2/3/4I1311N
Boundary fraction (%)
Sedimentation coefficient (S)
Sedimentation coefficient (s)
R2= 0.995
Density (g/mL)
v̄ = 0.726 mL/g

Figure 3.7 The partial specific volume of WT and H4K16Q arrays with Sir2/4I1311N. (a-d) vHW plots showing the sedimentation of molecules in 0% (light gray), 25% (dark gray), and 50% H_2O^{18} (black) and plots of sedimentation coefficient vs. density. The $\bar{v}$ is calculated by dividing the slope of the fit line by the y-intercept.

to bind at a stoichiometry of two molecules per nucleosome, and although it did not dramatically compact chromatin in comparison to 30 nm fibers, the dimerization of Sir3 molecules across nucleosomes was seen to occlude linker DNA. Here, we have applied these experimental conditions to heterochromatin fibers containing all three Sir proteins. We found that although Sir proteins are capable of interacting with both WT and H4-K16Q arrays, only WT chromatin is compatible with the formation of a condensed structure. Additionally, binding of Sir proteins to WT arrays was consistent with a stoichiometry of two molecules of Sir3 and one molecule of Sir2/4 bound per nucleosome (Figure 3.8). Finally, the formation of compacted SIR heterochromatin structure required the binding interactions between Sir3 and Sir4.

Although the overexpression of Sir3 can create extended silenced domains depleted in Sir2/4 and can compensate for the Sir4-I1311N mutation (Hecht et al. 1996; Wang et al. 2013), it appears that all three Sir proteins are required for the formation of a compacted heterochromatin structure. This suggests that heterochromatic silencing functions at two levels: 1) by Sir3-mediated stabilization of nucleosomes, perhaps by mediating contacts between arginines 17 and 19 of the H4 tail (suggested in Wang *et. al*) and DNA, and 2) by folding of chromatin into an inaccessible structure. This two-fold mechanism of structural repression explains both why the presence of Sir proteins on a single nucleosome is capable of blocking transcriptional elongation, and how the formation of the large pre-initiation complex at heterochromatin fibers is sterically

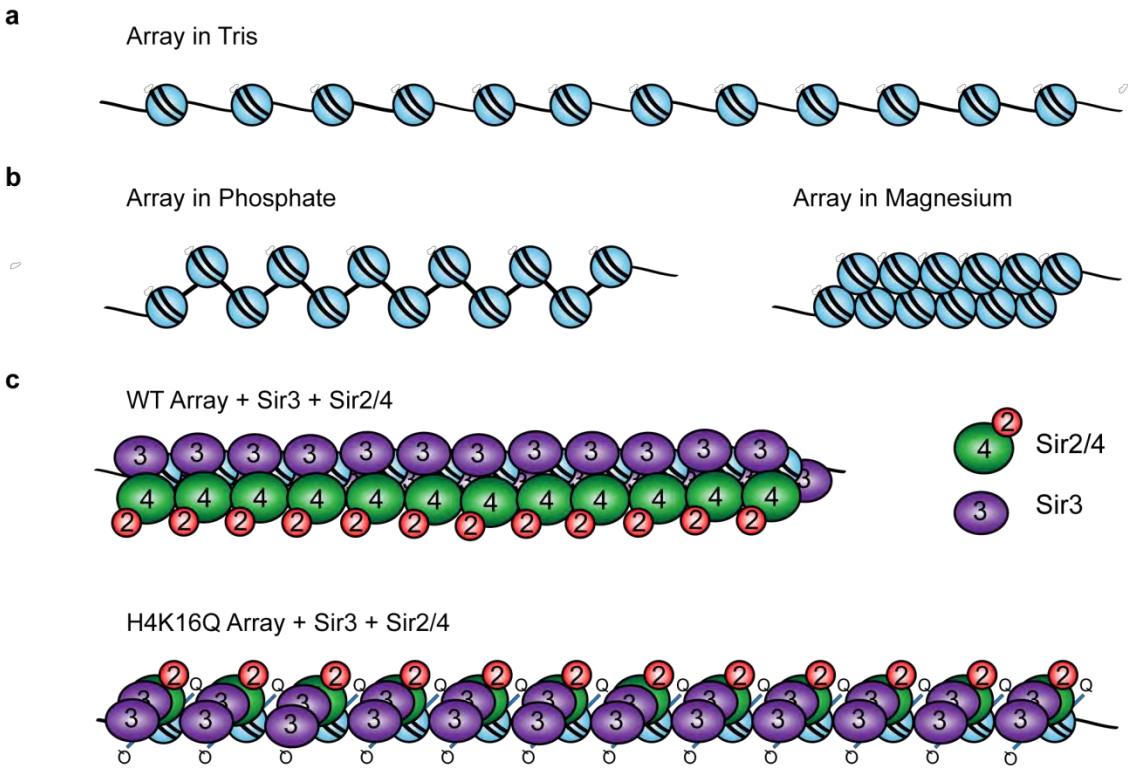
a
Array in Tris
b
Array in Phosphate
Array in Magnesium
c
WT Array + Sir3 + Sir2/4
Sir2/4
Sir3
H4K16Q Array + Sir3 + Sir2/4

Figure 3.8 Model for a SIR chromatin fiber. (a) Diagram of a 12-mer array in low-salt Tris buffer. **(b)** Arrays in 20 mM phosphate buffer pH 8.0 (containing ~40 mM Na^+) are partially folded. Arrays in 1 mM $MgCl_2$ buffer fold into 30 nm fibers. **(c)** SIR proteins bind and condense WT arrays, though to a lesser extent than 30 nm fibers, with two molecules of Sir3 and likely one molecule of Sir2/4 per nucleosome. Although Sir proteins also bind H4K16Q arrays, linker DNA is not occluded.

hindered (Johnson et al. 2013). Additionally, this model may shed light on the different roles and binding modes of Sir3 within SIR heterochromatin and of Sir3 binding independently at euchromatic sites throughout the genome (Radman-Livaja et al. 2011).

While Sir proteins were found to bind to H4-K16Q chromatin at similar rates and with potentially equivalent stoichiometry as WT, the H4-K16Q mutation prevented the occlusion of linker DNA (Figure 3.8c). Despite the affinity of Sir2/4 for H4-K16Q nucleosomes (an interaction perhaps mirroring the initial steps of SIR heterochromatin assembly, in which Sir2/4 binds and deacetylates H4-K16Ac nucleosomes), Sir3 recruitment to H4-K16Q required the presence of Sir2/4. The lack of condensation seen on H4-K16Q SIR fibers and the diminished binding of SIRs bearing the Sir4-I1311N mutant suggests that cross-nucleosomal interactions are blocked in the absence of K16, likely due to Sir3's failure to bind nucleosomes. Thus, H4-K16Q or H4-K16Ac prevents both modes of SIR repression- the nucleosome-stabilizing Sir3 interaction, and the chromatin-folding cross-nucleosomal SIR interactions.

Interestingly, although the Sir4-I1311N mutation abolishes silencing *in vivo* (Rudner et al. 2005), the function of the Sir3-Sir4 binding interaction was believed primarily to be to drive the recruitment and polymerization of SIRs across chromatin (Moretti et al. 1994; Cockell et al. 1995; Hoppe et al. 2002; Rudner et al. 2005; Kueng et al. 2013). Here, we have found that on WT chromatin, Sir4-I1311N does not prevent SIR binding across arrays in the

steady-state, but does block formation of a condensed fiber, indicating Sir4 may serve a more important structural role in repression than previously thought. As the Sir4 coiled-coil domain binds neither DNA nor nucleosomes (Rudner et al. 2005), it likely serves as a bridge, perhaps by mediating the cross-nucleosomal Sir3-Sir3, and Sir3-Sir4 interactions that drive folding.

In conclusion, we propose a model of SIR heterochromatic silencing in which two molecules of Sir3 bind to each surface of the nucleosome and one molecule of Sir2/4 binds primarily within each linker, and fiber compaction is completed via cross-nucleosomal Sir3-Sir4 and Sir3-Sir3 interactions. This structure represses activities such as transcription and recombination both by creating stable, remodeling-resistant nucleosomes, and by sterically excluding the binding of external factors to DNA.

Materials and Methods

Proteins

FLAG-tagged Sir3 protein and TAP-tagged Sir2/4 complex were individually overexpressed and affinity purified from yeast. Briefly, yeast cultures transformed with plasmids contained tagged proteins under a galactose-inducible promoter were grown to OD 0.6 and induced with 2% galactose for 5 hours. Cultures were pelleted, resuspended in E Buffer (20 mM HEPES pH 7.4, 350 mM

NaCl, 10% glycerol, 0.1% Tween 20, and protease inhibitors), and frozen in liquid nitrogen. Pellets were ground using a cold mortar and pestle with frequent additions of liquid nitrogen until approximately 50% of cells appeared lysed under a microscope. Cells were incubated on ice in E buffer for 30 min, then spun at 3,000 rpm for 15 minutes to remove debris. Supernatant was spun down at 40,000 rpm for 1 hour, then the aqueous layer was removed from the lipid layer using a syringe. For Sir3 purification, lysate was incubated with anti-Flag resin from Sigma for three hours at 4°C. Resin was washed in E buffer, then Sir3 was eluted in batch via four 30 minute incubations of resin with E Buffer containing 100 µg/mL 3xFLAG peptide from Sigma. For Sir2/4 purification, lysate was incubated with IgG resin for 2 hours, washed in E buffer, then eluted in batch via the addition of purified TEV protease overnight. Eluted Sir2/4 was then bound in batch to Calmodulin resin for 2 hours in the presence of Ca^{2+}, washed in E buffer, and eluted with EGTA. Concentrations were determined by comparison to known concentrations of BSA electrophoreses on the same Coomassie-stained SDS-PAGE gel. The Sir4-I1311N plasmid was generated by site-directed mutagenesis, and purified as above. All Sir2/4 was dialyzed into 20 mM sodium phosphate buffer pH 8.0 prior to use in order to maintain moderate concentrations of salt across experiments. Recombinant *Xenopus laevis* histones were expressed in BL21 cells, purified, and assembled into histone octamers according to standard protocols.

DNA

The 601-177-12 nucleosomal array template containing twelve copies of the Widom 601 nucleosome positioning sequence was digested from its plasmid backbone using EcoRV and purified by size-exclusion chromatography. The 601-177-36 fragment was generated by digestion of the 601-177-36 plasmid (a generous gift from Scot Wolfe's group, who generated it using a Golden Gate cloning strategy) was digested by HaeII and XbaI and purified as above.

Nucleosomal array assembly

Nucleosomal arrays were assembled by combining recombinant histone octamers and 601-177-12 or 601-177-12 DNA template at varying molar ratios of octamer to nucleosome positioning sequence in 2 M NaCl, and step-wise salt dialysis was performed until completion into 20 mM sodium phosphate pH. 8.0 with 0.1 mM EDTA. Array saturation was determined by ScaI digestion followed by analysis via native PAGE and by SV-AUC.

EMSA

300 ng WT or H4-K16Q nucleosomal array was combined with Sir2/4 at a ratio of 1, 2, or 3 molecules per nucleosome to a final concentration of 10 ng/ul array and 5% glycerol. For combined Sir2/4 and Sir3 EMSA, Sir2/4 or Sir2/4I1311N was added at 2 molecules per nucleosome, and Sir3 was titrated at 1, 2, 4, and 6 molecules per nucleosome. Binding reactions were incubated at

room temperature for 30 minutes, run on 1% TBE agarose gels, and stained with ethidium bromide.

SV-AUC

SV-AUC was carried out using 400 µl sample loaded into two-sector Epon centerpieces in an An60 Ti rotor in a Beckman Optima XL-I analytical ultracentrifuge, and run at 20°C. Measurement was completed in intensity mode. Nucleosomal arrays were run at 10 ng/ul concentrations with the indicated amounts of Sir3 or Sir2/4 at 20,000 RPM, and were measured at 215 nm (for arrays alone) or 260 nm (for samples containing SIR proteins). For experiments containing all three Sir proteins, Sir2/4 was added first, followed by array, followed by Sir3. For $\bar{\nu}$ determination, three preparations of sample were run as above, with 0, 25, or 50% $H_2{}^{18}O$ (obtained from Cambridge Istotope Laboratories, Andover, MA) added in place of $H_2{}^{16}O$. The obtained S values were then plotted as a function of solvent densities, linear regression was performed, and the $\bar{\nu}$ was calculated by dividing the slope of the resulting line by the y-intercept. Solvent densities and viscosities were obtained from the literature (Brown et al. 2011). Linear regression was performed using GraphPad Prism software.

2DSA/GA-MC

All SV-AUC data were analyzed using UltraScan3 software, version 3.3 and release 1977, and fitting procedures were completed on XSEDE clusters at the Texas Advanced Computing Center (Lonestar, Stampede) and at the San Diego Supercomputing Center (Trestles) through the UltraScan Science Gateway (https://www.xsede.org/web/guest/gateways-listing). Raw intensity data were converted to pseudo-absorbance by using the intensity of the air above the meniscus as a reference and edited. Next, 2DSA was performed to subtract time-invariant noise and the meniscus was fit using 10 points in a 0.05 cm range. Arrays were fit using an S range of 5-60 S, an f/f_0 range of 1-10 with 100 grid points for each, 10 uniform grid repetitions, 400 simulation points, and meniscus fitting within a 0.6 cm range with 10 points. 2DSA was then repeated at the determined meniscus to fit radially-invariant and time-invariant noise together using 5 iterations. vHW analysis was completed using these noise subtraction profiles to determine S. Where indicated, GA was initialized by binning major solutes in the 2DSA dataset, and run via LIMS. Major solutes from GA analysis were then binned and run again using GA with 50 MC iterations.

AFM

For atomic force microscopic experiments, an Agilent AFM 5500 instrument and silicon nitride cantilevers were used (force constant 25-75 N/m, resonant frequency 332 kHz). Imaging was done in air using the acoustic AC mode with an amplitude of ~10 nm and a set-point reduction of about 10%,

scanning at 1 line per second. Immobilization of chromatin arrays on mica surface was done as follows. First, Sir3 or Sir2/4 was added to phosphate buffer followed by addition of 10 ng/ul chromatin array and mixed gently, maintaining a ratio of 4 Sir3 or Sir2/4 molecules/nucleosome. For imaging with both Sir3 and Sir2/4, Sir2/4 was added first, then arrays, followed by Sir3, at a ratio of 2 Sir3's and 2 Sir2/4's per nucleosome. After 30 minutes, 0.5% glutaraldehyde solution (1 µL) was added to this mixture for crosslinking and incubated for 10 minutes. APTES was deposited on freshly cleaved mica substrate using vapor deposition. The crosslinked chromatin solution was diluted to 1 ng/µL and 3 µL was added to this APTES modified mica surface and after 5 minutes the surface was cleaned three times using 400 µL of buffer solution, dried carefully using argon gas and immediately used for imaging. To image only chromatin arrays, the first mixing step with Sir proteins was omitted, and imaging was carried out in the indicated buffer.

CHAPTER IV: THE PAST, PRESENT, AND FUTURE OF SILENCE

Final Summary

The organization of genomes into chromatin regulates all eukaryotic nuclear processes. On a local scale, chromatin dictates the accessibility of the underlying DNA sequences to the enzymes responsible for transcription, replication, and repair (Rando & Winston 2012; Papamichos-Chronakis & Peterson 2013; Zentner & Henikoff 2013). On the global scale, chromatin partitions genomic regions in specific manners to facilitate the efficient utilization of *trans* factors, the maintenance of developmental states, and the even distribution of chromosomes among daughter cells during mitosis and meiosis (Woodcock & Ghosh 2010; Bickmore & van Steensel 2013). Although of profound relevance to development and disease, much of chromatin structure remains controversial. While *in vivo* approaches such as fluorescent cell imaging and 3-C based experiments have discovered much about the organization of chromosomes within the nucleus, and methods such as chromatin immunoprecipitation followed by tiling microarray or deep sequencing analysis have elucidated many details about nucleosome positioning and the distribution of histone modifications across genomes, most of our knowledge of the structures of chromatin fibers has necessarily arisen from *in vitro* experiments (Woodcock & Ghosh 2010; Luger et al. 2012; Ozer et al. 2015). These studies

have revealed that *in vitro* reconstituted nucleosomal arrays are capable of compacting into 30 nm fibers, and that uncompacted 10 nm fibers are able to interdigitate into higher-order oligomers (Schwarz & Hansen 1994; Schwarz et al. 1996). Although recent *in vivo* and *in vitro* experiments using purified chromatin tend to favor a predominance of the latter structure within euchromatin, the structure of heterochromatin is completely unknown (van Holde & Zlatanova 2007; Eltsov et al. 2008; Dekker 2008; Lieberman-Aiden et al. 2009; Nishino et al. 2012; Fussner et al. 2012; Maeshima et al. 2014).

Heterochromatin is a heritably silent compartment of the genome located mostly around the nuclear periphery (Woodcock & Ghosh 2010; Beisel & Paro 2011; Saksouk et al. 2015). Constitutive heterochromatin exists at repetitive sequences such as telomeres and centromeres, where it functions to protect chromosome ends; suppress aberrant homologous recombination which could lead to chromosomal deletions, inversions, or translocations; and prevents the spreading of transposable elements (Grewal & Jia 2007; Saksouk et al. 2015). Facultative heterochromatin suppresses developmental genes in order to promote the differentiation and maintenance of cell types (Grewal & Jia 2007; Beisel & Paro 2011; Simon & Kingston 2013). Taken together, heterochromatin is essential for maintaining genomic stability and cellular identity, and is thus responsible for guarding higher organisms against developmental abnormalities and cancer. While the mechanism of heterochromatic repression is poorly understood, it is known that its formation involves the binding of heterochromatin-

specific architectural proteins, the deacetylation of histones, and, in higher organisms, the propagation of specific methylation marks (Rusche et al. 2003; Woodcock & Ghosh 2010; Grewal & Jia 2007; Beisel & Paro 2011; Kueng et al. 2013).

The most-thoroughly characterized form of heterochromatin exists in *S. cerevisiae*, which requires the Sir proteins. SIR heterochromatin formation is believed to be a step-wise process in which the Sir2/4 complex is recruited to silencing nucleation regions via direct interactions with sequence-specific DNA binding factors, Sir2 deacetylates H4-K16, providing a high-affinity binding site for Sir3, and subsequent cycles of recruitment and deacetylation lead to the spreading of heterochromatin along the chromosome (Hecht et al. 1996; Imai et al. 2000; Rusche et al. 2002). Although SIR heterochromatin has been studied at length both *in vivo* and *in vitro*, its structural mechanism of silencing continues to be controversial, with some groups advocating a model in which Sir proteins bind chromatin and compact it in a manner resembling and complementary to 30 nm fiber folding, and others favoring a model in which Sir proteins bind arrays forming a linear structure in which DNA is occluded but the intrinsic folding pathway is inhibited (Onishi et al. 2007; McBryant et al. 2008; Johnson et al. 2009; Thurtle & Rine 2014). Even the stoichiometry of the SIR/chromatin complex is contested, with some groups finding the Sir proteins in a 1:1:1 ratio per nucleosome, and others suggesting a need for a greater ratio of Sir3 (Chang et al. 2003; Liou et al. 2005; Martino et al. 2009; Sinha et al. 2009). A major

issue confounding biochemical studies of SIR fibers has been the high nonspecific binding affinity of Sir3 and Sir4 for DNA, with many experiments resulting in the binding of excessive and endlessly additive quantities of Sir proteins more closely resembling aggregation than the formation of a biological complex (Georgel et al. 2001; McBryant et al. 2008; Adkins et al. 2009; Martino et al. 2009; Oppikofer et al. 2011). Further, many early structural studies failed to replicate Sir3's preference for interacting with WT versus H4-K16Q or H4-K16 acetylated chromatin, despite the known ability of this modification to abrogate Sir3 binding and silencing *in vivo* (Martino et al. 2009).

In this work, I have described the development of physiologically-relevant *in vitro* reconstituted SIR heterochromatin fibers. The simple addition of a moderate amount of salt to experimental buffers shields against nonspecific charged-based interactions between Sir proteins and DNA, leading to Sir3 binding that is highly specific for WT versus H4-K16Q arrays. Additionally, these ionic conditions promote the formation of a discrete SIR chromatin complex, in which Sir protein binding to nucleosomal arrays saturates and subsequent additions do not lead to aggregation. These SIR heterochromatin fibers were then analyzed via SV-AUC and AFM in order to reveal their conformation and stoichiometry.

Sedimentation velocity ultracentrifugation has been a popular means of studying chromatin structure, as it is one of the few structural methods available for the analysis of MegaDalton macromolecules such as the ubiquitously studied

12mer nucleosomal arrays (Hansen et al. 1995). SV-AUC separates molecules based on their size and shape, and has thus been an excellent approach to studying chromatin conformational changes, such as the compaction of the 10 nm fiber into the 30 nm fiber, or the oligomerization of 10 nm fibers into interdigitated structures sedimenting at hundreds S (Schwarz & Hansen 1994; Schwarz et al. 1996). However, in situations in which both the molecular weight and the shape of molecules may change, SV-AUC results can be confounding. Here, I have described the application of 2DSA/GA-MC modeling algorithms to the sedimentation profiles of chromatin in order to distinguish between changes in S resulting from conformational changes versus changes in mass (Demeler & Brookes 2007; Brookes & Demeler 2007; Brookes et al. 2010; Gorbet et al. 2014). This modeling required the development of an experimental method to determine the partial specific volume of each molecule studied, as current methods for estimating $\bar{\nu}$ are unable to account for complexes composed of both protein and nucleic acids (Swygert et al. 2014).

SV-AUC followed by 2DSA/GA-MC modeling and AFM imaging revealed that Sir3 binds specifically to unmodified chromatin at a ratio of two molecules per nucleosome, and that the subsequent dimerization of Sir3 molecules across nucleosomes leads to the occlusion of linker DNA. However, this structure is nowhere near as compacted as 30 nm fibers. When all three Sir proteins are added, they increase the molecular weight of both WT and H4-K16Q arrays to an extent that suggests a complex stoichiometry of two molecules of Sir3 and one

molecule of Sir2/4 per nucleosome. Despite approximately equivalent binding to both WT and H4-K16Q chromatin, the conformation of SIR chromatin on these varying templates was distinct. On WT arrays, additional occlusion of linker DNA was seen when compared to Sir3 fibers alone, though the frictional ratios of these fibers did not change dramatically, suggesting all three Sir proteins interact across nucleosomes in an additive but similar manner. However, this was not the case on H4-K16Q arrays; instead, the f/f_0 ratio nearly doubled on addition of all three Sirs, whereas linker DNA was not seen to be fully occluded by AFM. This suggests that although the Sir proteins are able to bind to H4-K16Q arrays, they are not able to mediate contacts across nucleosomes. This is likely due to Sir3's inability to bind H4-K16Q nucleosomes themselves. Rather, it may be bound primarily to Sir4, hanging off away from the nucleosome and subjecting arrays to greater friction during sedimentation.

These findings have led us to propose a model in which SIR heterochromatic silencing is mediated via two distinct but complementary mechanisms. First, Sir3 binds to chromatin but does not compact it. Instead, it enhances the stability of the underlying nucleosomes, rendering them resistant to processes such as chromatin remodeling. This stability may rely on the creation of intranucleosomal contacts between arginines 17 and 19 of the H4 tail and DNA, which were identified in a crystal structure of the Sir3 BAH domain bound to the nucleosome (Figure 4.1) (Wang et al. 2013). Second, the binding of all three Sir proteins to arrays induces cross-nucleosomal interactions more closely

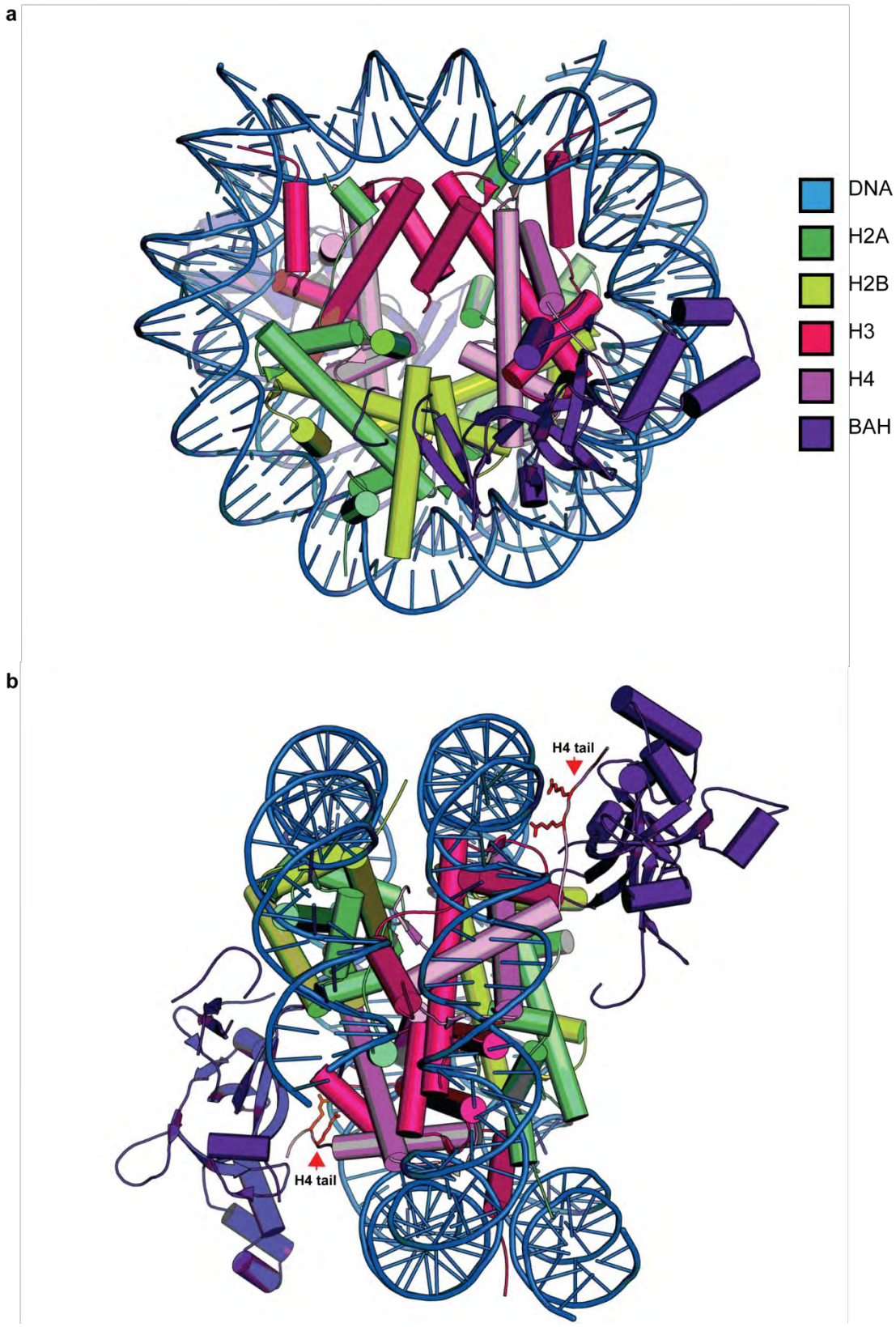
a
DNA
H2A
H2B
H3
H4
BAH
b
H4 tail
H4 tail

Figure 4.1 Binding of the Sir3 BAH to the nucleosome induces contacts between H4-K17 and H4-K19 and nucleosomal DNA. (a) Crystal structure of the Sir3 BAH domain bound to the face of the nucleosome. **(b)** Side view. The H4 tail is indicated, and H4-K17 and H4-K19 are in stick form colored in red (PDB # 4jjn, Wang et al. 2013).

resembling compaction. This two-step method of repression explains both how external factors are sterically excluded from heterochromatin, and how processes such as transcription are blocked even when binding is permitted (Gottschling 1992; Loo & Rine 1994; Weiss & Simpson 1998; Ansari & Gartenberg 1999; Sekinger & Gross 2001; Chen & Widom 2005; Johnson et al. 2013; Thurtle & Rine 2014).

Future Directions

SIR heterochromatin structure in detail

Although this work provides the overall conformation and stoichiometry of the SIR heterochromatin fiber, many structural details remain unknown. First, although chromatin fibers bound by all three Sir proteins appear globular and folded, it is unclear to what extent the DNA is compacted as compared to 30 nm fibers. Perhaps the most direct approach to answer this question would be a single-molecule optical tweezer experiment, in which each end of a nucleosomal array would be tethered within a flow cell, and changes in end-to-end difference could be measured as $MgCl_2$ or Sir proteins were added. This method has previously been used to distinguish between zigzag and solenoid 30 nm fiber structures (Kruithof et al. 2009), and has the potential to identify the force of the interactions of Sir proteins with chromatin, possibly confirming stoichiometry.

Several interactions have been identified between Sir proteins and nucleosomes, including the binding of Sir3 to the H4 tail and the nucleosomal surface (Hecht et al. 1995; Armache et al. 2011b; Wang et al. 2013), and the binding of Sir4 to H3 and H4 tails and DNA (Hecht et al. 1995; Liou et al. 2005; Johnson et al. 2009; Martino et al. 2009; Oppikofer et al. 2011; Kueng et al. 2012). Further, Sir4 is known to bind both to Sir2 and Sir3 (Moretti et al. 1994; Moazed et al. 1997; Hoppe et al. 2002; Chang et al. 2003; Liou et al. 2005; Hsu et al. 2013), and both Sir3 and Sir4 have dimerization domains essential for silencing (Moretti et al. 1994; Cockell et al. 1995; Chang et al. 2003; Murphy et al. 2003; King et al. 2006; Oppikofer, Kueng, Keusch, et al. 2013). However, how these interactions among Sir proteins and between Sir proteins and chromatin function together to dictate the final structure is unclear. Recently, a chemical cross-linking and mass spectrometry (XL-MS) strategy has been used to map interactions between subunits in the INO80 and SWR-C complexes (Herzog et al. 2012; Tosi et al. 2013; Nguyen et al. 2013). A similar method could be applied to Sir proteins bound to mononucleosomes or a small nucleosomal array to determine the sites of interactions within SIR heterochromatin.

It would further be interesting to determine the effect of DNA linker length on SIR heterochromatin structure. Although the experiments described in this work were completed on nucleosomal array templates with 30 base pair linkers, linker lengths in *S. cerevisiae* tend toward a 10*n*+5 periodicity, with 15 and 25

base pairs being most common (Wang et al. 2008; Brogaard et al. 2012). Additionally, the mapping of nucleosome positions at *HMR* revealed six pairs of very closely-spaced nucleosomes separated from each other by linkers of ~20 base pairs (Ravindra et al. 1999). As linker length has been shown to affect the binding affinity of Swi6 for arrays (Canzio et al. 2011), and both the length and periodicity of linkers has been shown to affect the folding pathway and compaction efficiency of 30 nm fibers (Correll et al. 2012), it is likely that linker length also plays some role in the structure of SIR heterochromatin.

Conformational dynamics within SIR heterochromatin

Several lines of evidence suggest that the conformation of SIR heterochromatin is dynamic. Interestingly, both the BAH and AAA domains of Sir3 bind both the H4 tail and the surface of the nucleosome near H3-K79 (Hecht et al. 1995; Buchberger et al. 2008; Ehrentraut et al. 2011; Armache et al. 2011b; Wang et al. 2013; Arnaudo et al. 2013). Additionally, the C-terminus of Sir4 has also been found to interact with the H4 tail (Hecht et al. 1995; Liou et al. 2005; Kueng et al. 2012), and Sir2's role in H4-K16 acetylation implies that it too must directly bind the H4 tail. However, the crystal structures of Sir3's BAH domain bound to the nucleosome show the entire base of the H4 tail and the nucleosomal surface near H3-K79 bound to Sir3 in a manner unlikely to permit additional interactions with this region (Armache et al. 2011b; Wang et al. 2013; Arnaudo et al. 2013). Interestingly, two amino acid substitutions in Sir3, D205N

in the BAH domain and L738P in the AAA domain, increase the binding affinity of Sir3 for the nucleosome but actually inhibit silencing (Connelly et al. 2006; Buchberger et al. 2008). Further, like HP1 proteins, Sir3 contains a central disordered region that may act as a flexible hinge, allowing Sir3 to adopt multiple forms (McBryant et al. 2006; Canzio et al. 2013). These data suggest that Sir3 may bind the nucleosome in multiple conformations, and that the dynamics of Sir3 nucleosomal interactions are crucial for silencing.

The most obvious role for a conformational change within SIR heterochromatin would be to mediate the contacts necessary before and after H4-K16 deacetylation. In this model, the Sir proteins would bind in a manner allowing Sir2 access to the H4 tail, possibly aided by Sir4 and the Sir3 AAA domain, then deacetylation would promote binding of BAH to the tail and nucleosomal surface. This change may be facilitated by the formation of *O*-AADPR. Although the structure of Sir3's AAA domain was found to be incompatible with *O*-AADPR binding (Ehrentraut et al. 2011), an EM study examining all three Sir proteins bound to an H4 tail peptide demonstrated that the complex shifted from a globular to a more linear conformation upon addition of *O*-AADPR, even in the absence of deacetylation (Liou et al. 2005). It is possible that *O*-AADPR actually stably binds within the active site of Sir2, promoting a conformational change. This model is supported by the fact that most crystal structures of sirtuins have *O*-AADPR bound in their active site, possibly indicating that this may represent their most stable state (Hsu et al. 2013). This would also

explain why an experiment in which Sir3 was fused to an NAD^+-independent deacetylation domain was able to restore silencing in a strain in which all NAD^+ deacetylases, including *sir2*, were deleted (Chou et al. 2008); in the absence of Sir2, *O*-AADPR was not required to induce a structural change in which Sir2 was shifted out of the way to promote Sir3 binding. Structural studies, perhaps using a combination of XL-MS and AFM or cryo-EM, should be completed on chromatin templates prior to and following deacetylation, or in the absence or presence of *O*-AADPR, in order to characterize conformational changes within SIR heterochromatin in greater detail.

HP1 heterochromatin

Ultimately, the next major step in heterochromatin biology is to understand the mechanism of silencing in vertebrate heterochromatin. Although the general principles of nucleation and spreading are known to persist in HP1 heterochromatin, little structural information about this form of chromatin currently exists (Grewal & Jia 2007; Beisel & Paro 2011; Canzio et al. 2014). Most biochemical data about HP1 chromatin have arisen from studies of the *S. pombe* paralog, Swi6. Swi6 has been found to preferentially bind nucleosomal arrays with 15 base pair linkers in which a tri-methyl group has been chemically added to H3K9 (Canzio et al. 2011). These *in vitro* studies represent a framework for further biophysical studies such as SV-AUC and 2DSA/GA-MC modeling, which could be used to identify the conformation and stoichiometry of Swi6 fibers using

chromatin containing unmodified H3K9 as a control (Simon et al. 2007; Armache et al. 2011b). Further work could also use purified Clr4 to examine more complete HP1-type fibers (Al-Sady et al. 2013). It would be of great interest to determine if HP1 paralogs mediate structural changes similar to Sir proteins as expected, or if heterochromatin in higher organisms makes use of different or more complex mechanisms.

Conclusion

Far more than a storage solution, chromatin organizes eukaryotic genomes in an intricate and dynamic way which facilitates all nuclear processes. In this work, I have described the groundwork of a structural understanding of the mechanisms of possibly the most complex form of chromatin. Heterochromatin is responsible for guarding the integrity of our genetic material and for defining the identity of our cells. Future work will extend our knowledge of the many ways in which chromatin structure and dynamics regulate and protect the building blocks of life.

BIBLIOGRAPHY

Abraham, J. et al., 1984. Regulation of mating-type information in yeast: negative control requiring sequences both 5' and 3' to the regulated region. *Journal of Molecular Biology*, 176(3), pp.307–331.

Adkins, N.L. et al., 2009. Role of nucleic acid binding in Sir3p-dependent interactions with chromatin fibers. *Biochemistry*, 48(2), pp.276–88.

Alberts, B. et al., 2002. *Molecular Biology of the Cell*, 4th edition. Garland Science, New York.

Allan, J. et al., 1980. The structure of histone H1 and its location in chromatin. *Nature*, 288(5792), pp.675–679.

Al-Sady, B., Madhani, H.D. & Narlikar, G.J., 2013. Division of labor between the chromodomains of HP1 and Suv39 methylase enables coordination of heterochromatin spread. *Molecular Cell*, 51(1), pp.80–91.

Altaf, M. et al., 2007. Interplay of chromatin modifiers on a short basic patch of histone H4 tail defines the boundary of telomeric heterochromatin. *Molecular Cell*, 28(6), pp.1002–1014.

Andrulis, E.D. et al., 2002. Esc1, a nuclear periphery protein required for Sir4-based plasmid anchoring and partitioning. *Molecular and Cellular Biology*, 22(23), pp.8292–8301.

Ansari, A. & Gartenberg, M.R., 1999. Persistence of an alternate chromatin structure at silenced loci in vitro. *Proceedings of the National Academy of Sciences of the United States of America*, 96(2), pp.343–8.

Aparicio, O.M., Billington, B.L. & Gottschling, D.E., 1991. Modifiers of position effect are shared between telomeric and silent mating-type loci in S. cerevisiae. *Cell*, 66(6), pp.1279–1287.

Arents, G. et al., 1991. The nucleosomal core histone octamer at 3.1 A resolution: a tripartite protein assembly and a left-handed superhelix. *Proceedings of the National Academy of Sciences of the United States of America*, 88(22), pp.10148–10152.

Armache, K.-J. et al., 2011a. Structural basis of silencing: Sir3 BAH domain in complex with a nucleosome at 3.0 Å resolution. *Science (New York, N.Y.)*, 334(6058), pp.977–82.

Armache, K.-J. et al., 2011b. Structural basis of silencing: Sir3 BAH domain in complex with a nucleosome at 3.0 Å resolution. *Science*, 334(6058), pp.977–82.

Arnaudo, N. et al., 2013. The N-terminal acetylation of Sir3 stabilizes its binding to the nucleosome core particle. *Nature Structural & Molecular Biology*, 20(9), pp.1119–21.

Bannister, A.J. et al., 2001. Selective recognition of methylated lysine 9 on histone H3 by the HP1 chromo domain. *Nature*, 410(6824), pp.120–124.

Bao, Y., White, C.L. & Luger, K., 2006. Nucleosome core particles containing a poly(dA/dT) sequence element exhibit a locally distorted DNA structure. *Journal of Molecular Biology*, 361(4), pp.617–624.

Beisel, C. & Paro, R., 2011. Silencing chromatin: comparing modes and mechanisms. *Nature reviews. Genetics*, 12(2), pp.123–35.

Bell, S.P. et al., 1995. The multidomain structure of Orc1p reveals similarity to regulators of DNA replication and transcriptional silencing. *Cell*, 83(4), pp.563–568.

Bickmore, W.A. & van Steensel, B., 2013. Genome architecture: domain organization of interphase chromosomes. *Cell*, 152(6), pp.1270–84.

Brand, A.H. et al., 1985. Characterization of a “silencer” in yeast: a DNA sequence with properties opposite to those of a transcriptional enhancer. *Cell*, 41(1), pp.41–48.

Brand, A.H., Micklem, G. & Nasmyth, K., 1987. A yeast silencer contains sequences that can promote autonomous plasmid replication and transcriptional activation. *Cell*, 51(5), pp.709–719.

Brasher, S. V et al., 2000. The structure of mouse HP1 suggests a unique mode of single peptide recognition by the shadow chromo domain dimer. *The EMBO Journal*, 19(7), pp.1587–1597.

Brogaard, K. et al., 2012. A map of nucleosome positions in yeast at base-pair resolution. *Nature*, 486(7404), pp.496–501.

Brookes, E., 2006. Genetic algorithm optimization for obtaining accurate molecular weight distributions from sedimentation velocity experiments. *Colloid & Polymer Science*, 131, pp.33–40.

Brookes, E., Cao, W. & Demeler, B., 2010. A two-dimensional spectrum analysis for sedimentation velocity experiments of mixtures with heterogeneity in molecular weight and shape. *European Biophysics Journal*, 39(3), pp.405–14.

Brookes, E.H. & Demeler, B., 2007. Parsimonious regularization using genetic algorithms applied to the analysis of analytical ultracentrifugation experiments. *Proceedings of the 9th Annual Conference on Genetic and Evolutionary Computation*, pp.361–368.

Brown, P.H. et al., 2011. Density contrast sedimentation velocity for the determination of protein partial-specific volumes. *PloS One*, 6(10), p.e26221.

Buchberger, J.R. et al., 2008. Sir3-nucleosome interactions in spreading of silent chromatin in Saccharomyces cerevisiae. *Molecular and Cellular Biology*, 28(22), pp.6903–18.

Bühler, M., Verdel, A. & Moazed, D., 2006. Tethering RITS to a Nascent Transcript Initiates RNAi- and Heterochromatin-Dependent Gene Silencing. *Cell*, 125(5), pp.873–886.

Canzio, D. et al., 2013. A conformational switch in HP1 releases auto-inhibition to drive heterochromatin assembly. *Nature*, 496(7445), pp.377–81.

Canzio, D. et al., 2011. Chromodomain-mediated oligomerization of HP1 suggests a nucleosome-bridging mechanism for heterochromatin assembly. *Molecular Cell*, 41(1), pp.67–81.

Canzio, D., Larson, A. & Narlikar, G.J., 2014. Mechanisms of functional promiscuity by HP1 proteins. *Trends in Cell Biology*, 24(6), pp.377–386.

Carmen, A.A., Milne, L. & Grunstein, M., 2002. Acetylation of the yeast histone H4 N terminus regulates its binding to heterochromatin protein SIR3. *The Journal of Biological Chemistry*, 277(7), pp.4778–81.

Chang, J.F. et al., 2003. Structure of the coiled-coil dimerization motif of Sir4 and its interaction with Sir3. *Structure*, 11(6), pp.637–649.

Chen, L. & Widom, J., 2005. Mechanism of transcriptional silencing in yeast. *Cell*, 120(1), pp.37–48.

Chou, C.-C., Li, Y.-C. & Gartenberg, M.R., 2008. Bypassing Sir2 and O-acetyl-ADP-ribose in transcriptional silencing. *Molecular Cell*, 31(5), pp.650–9.

Cockell, M. et al., 1995. The carboxy termini of Sir4 and RAP1 affect Sir3 localization: evidence for a multicomponent complex required for yeast telomeric silencing. *Journal of Cell Biology*, 129(4), pp.909–924.

Connelly, J.J. et al., 2006. Structure and function of the Saccharomyces cerevisiae Sir3 BAH domain. *Molecular and Cellular Biology*, 26(8), pp.3256–3262.

Conrad, M.N. et al., 1990. RAP1 protein interacts with yeast telomeres in vivo: overproduction alters telomere structure and decreases chromosome stability. *Cell*, 63(4), pp.739–750.

Correll, S.J., Schubert, M.H. & Grigoryev, S.A., 2012. Short nucleosome repeats impose rotational modulations on chromatin fibre folding. *The EMBO Journal*, 31(10), pp.2416–26.

Cowieson, N.P. et al., 2000. Dimerisation of a chromo shadow domain and distinctions from the chromodomain as revealed by structural analysis. *Current Biology*, 10(9), pp.517–525.

Cubizolles, F. et al., 2006. A homotrimer-heterotrimer switch in Sir2 structure differentiates rDNA and telomeric silencing. *Molecular Cell*, 21(6), pp.825–836.

Cutter, A.R. & Hayes, J.J., 2015. A brief review of nucleosome structure. *FEBS Letters*, pp.1–9.

Davey, C.A. et al., 2002. Solvent mediated interactions in the structure of the nucleosome core particle at 1.9 A resolution. *Journal of Molecular Biology*, 319(5), pp.1097–1113.

Dekker, J., 2008. Mapping in vivo chromatin interactions in yeast suggests an extended chromatin fiber with regional variation in compaction. *The Journal of Biological Chemistry*, 283(50), pp.34532–40.

Demeler, B., 2010. Methods for the design and analysis of sedimentation velocity and sedimentation equilibrium experiments with proteins. *Current Protocols in Protein Science*, 7(13), pp.1–24.

Demeler, B. et al., 2014. UltraScan-III version 2.1, release 1706: a comprehensive data analysis software package for analytical ultracentrifugation experiments. *http://www.ultrascan3.uthscsa.edu*.

Demeler, B. & Brookes, E., 2007. Monte Carlo analysis of sedimentation experiments. *Colloid and Polymer Science*, 286(2), pp.129–137.

Diffley, J.F.X. & Stillman, B., 1989. Similarity between the transcriptional silencer binding proteins ABF1 and RAP1. *Science*, 246(3), pp.1034–1038.

Dion, M.F. et al., 2007. Dynamics of replication-independent histone turnover in budding yeast. *Science*, 315(5817), pp.1405–1408.

Dorigo, B. et al., 2003. Chromatin fiber folding: requirement for the histone H4 N-terminal tail. *Journal of Molecular Biology*, 327(1), pp.85–96.

Dorigo, B., et al., 2004. Nucleosome arrays reveal the two-start organization of the chromatin fiber. *Science*, 306(5701), pp.1571–1573.

Edelstein, S.J. & Schachman, H.K., 1967. The simultaneous determination of partial specific volumes and molecular weights with microgram quantities. *The Journal of Bological Chemistry*, 242(2), pp.306–11.

Ehrentraut, S. et al., 2011. Structural basis for the role of the Sir3 AAA+ domain in silencing: interaction with Sir4 and unmethylated histone H3K79. *Genes & Development*, 25(17), pp.1835–46.

Eissenberg, J.C. et al., 1990. Mutation in a heterochromatin-specific chromosomal protein is associated with suppression of position-effect variegation in Drosophila melanogaster. *Proceedings of the National Academy of Sciences of the United States of America*, 87(24), pp.9923–9927.

Eltsov, M. et al., 2008. Analysis of cryo-electron microscopy images does not support the existence of 30-nm chromatin fibers in mitotic chromosomes in situ. *Proceedings of the National Academy of Sciences of the United States of America*, 105(50), pp.19732–19737.

Fan, J.Y. et al., 2002. The essential histone variant H2A.Z regulates the equilibrium between different chromatin conformational states. *Nature Structural Biology*, 9(3), pp.172–176.

Feldman, J.B., Hicks, J.B. & Broach, J.R., 1984. Identification of sites required for repression of a silent mating type locus in yeast. *Journal of Molecular Biology*, 178(4), pp.815–834.

Finch, J.T. & Klug, A., 1976. Solenoidal model for superstructure in chromatin. *Proceedings of the National Academy of Sciences of the United States of America*, 73(6), pp.1897–1901.

Fussner, E. et al., 2012. Open and closed domains in the mouse genome are configured as 10-nm chromatin fibres. *EMBO reports*, 13(11), pp.992–6.

Gabrielli, F., Hancock, R. & Faber, A.J., 1981. Characterisation of a chromatin fraction bearing pulse-labelled RNA. 2. Quantification of histones and high-mobility-group proteins. *European Journal of Biochemistry*, 120(2), pp.363–369.

Garcia, S.N. & Pillus, L., 2002. A unique class of conditional sir2 mutants displays distinct silencing defects in Saccharomyces cerevisiae. *Genetics*, 162(2), pp.721–736.

Garcia-Ramirez, M., Dong, F. & Ausio, J., 1992. Role of the histone “Tails” in the folding of oligonucleosomes depleted of histone H1. *Journal of Biological Chemistry*, 267(27), pp.19587–19595.

Georgel, P.T. et al., 2001. Sir3-dependent assembly of supramolecular chromatin structures in vitro. *Proceedings of the National Academy of Sciences of the United States of America*, 98(15), pp.8584–9.

Ghirlando, R. & Felsenfeld, G., 2008. Hydrodynamic studies on defined heterochromatin fragments support a 30-nm fiber having six nucleosomes per turn. *Journal of Molecular Biology*, 376(5), pp.1417–25.

Gohon, Y. et al., 2004. Partial specific volume and solvent interactions of amphipol A8-35. *Analytical Biochemistry*, 334Gohon, (2), pp.318–34.

Gorbet, G. et al., 2014. A parametrically constrained optimization method for fitting sedimentation velocity experiments. *Biophysical Journal*, 106, pp.1741–1750.

Gottschling, D.E. et al., 1990. Position effect at S. cerevisiae telomeres: reversible repression of Pol II transcription. *Cell*, 63(4), pp.751–762.

Gottschling, D.E., 1992. Telomere-proximal DNA in Saccharomyces cerevisiae is refractory to methyltransferase activity in vivo. *Proceedings of the National Academy of Sciences of the United States of America*, 89(9), pp.4062–4065.

Grewal, S.I.S. & Jia, S., 2007. Heterochromatin revisited. *Nature reviews. Genetics*, 8(1), pp.35–46.

Grigoryev, S.A. et al., 2009. Evidence for heteromorphic chromatin fibers from analysis of nucleosome interactions. *Proceedings of the National Academy of Sciences of the United States of America*, 106(32), pp.13317–22.

Grigoryev, S.A., 2004. Keeping fingers crossed: heterochromatin spreading through interdigitation of nucleosome arrays. *FEBS letters*, 564(1-2), pp.4–8.

Haber, J.E., 1998. Mating-type gene switching in Saccharomyces cerevisiae. *Annual Review of Genetics*, 32, pp.561–599.

Haber, J.E. & George, J.P., 1979. A mutation that permits the expression of normally silent copies of mating-type information in Saccharomyces cerevisiae. *Genetics*, 93(1), pp.13–35.

Haber, J.E., Rogers, D.T. & McCusker, J.H., 1980. Homothallic conversions of yeast mating-type genes occur by intrachromosomal recombination. *Cell*, 22(1), pp.277–289.

Hall, I.M. et al., 2002. Establishment and maintenance of a heterochromatin domain. *Science (New York, N.Y.)*, 297(5590), pp.2232–2237.

Hansen, J.C., van Holde, K.E. & Lohr, D., 1991. The mechanism of nucleosome assembly onto oligomers of the sea urchin 5 S DNA positioning sequence. *The Journal of biological chemistry*, 266(7), pp.4276–82.

Hansen, J.C., Lebowitz, J. & Demeler, B., 1995. Analytical ultracentrifugation of complex macromolecular systems. *Biochemistry*, 33(45), pp.13155–13163.

Hansen, J.C. & Wolffe, A.P., 1992. Influence of chromatin folding on transcription initiation and elongation by RNA Polymerase III. *Biochemistry*, 31(34), pp.7977–7988.

Hargreaves, D.C. & Crabtree, G.R., 2011. ATP-dependent chromatin remodeling: genetics, genomics and mechanisms. *Cell Research*, 21(3), pp.396–420.

Hearst, J.E., 1962. The specific volume of various cationic forms of deoxyribonucleic acid. *Journal of Molecular Biology*, 4, pp.415–7.

Hecht, A. et al., 1995. Histone H3 and H4 N-termini interact with SIR3 and SIR4 proteins: a molecular model for the formation of heterochromatin in yeast. *Cell*, 80(4), pp.583–92.

Hecht, A., Strahl-Bolsinger, S. & Grunstein, M., 1996. Spreading of transcriptional repressor SIR3 from telomeric heterochromatin. *Nature*, 383, pp.92–95.

Herzog, F. et al., 2012. Structural probing of a protein phosphatase 2A network by chemical cross-linking and mass spectrometry. *Science (New York, N.Y.)*, 337(6100), pp.1348–52.

Hicks, J.B. & Herskowitz, I., 1977. Interconversion of yeast mating types. II. Restoration of mating ability to sterile mutants in homothallic and heterothallic strains. *Genetics*, 85(3), pp.373–393.

Hicks, J.B., Strathern, J.N. & Herskowitz, I., 1977. Interconversion of yeast mating types. I. Direct observations of the action of the homothallism (HO) gene. *Genetics*, 85(3), pp.395–405.

Hicks, J.B., Strathern, J.N. & Herskowitz, I.R. a, 1977. Interconvension of yeast mating types III. Action of the homothallism (HO) gene in cells homozygous for the mating type locus. *Genetics*, 85, pp.395–405.

Van Holde, K. & Zlatanova, J., 2007. Chromatin fiber structure: Where is the problem now? *Seminars in Cell and Developmental Biology*, 18(5), pp.651–658.

Hoppe, G.J. et al., 2002. Steps in assembly of silent chromatin in yeast : Sir3-independent binding of a Sir2 / Sir4 complex to silencers and role for Sir2-dependent deacetylation. *Molecular and Cellular Bology*, 22(12), pp.4167–4180.

Hsu, H.-C. et al., 2013. Structural basis for allosteric stimulation of Sir2 activity by Sir4 binding. *Genes & Development*, 27(1), pp.64–73.

Hughes, A. & Rando, O.J., 2009. Chromatin “programming” by sequence--is there more to the nucleosome code than %GC? *Journal of Biology*, 8(11), pp.96.1–96.4.

Imai, S. et al., 2000. Transcriptional silencing and longevity protein Sir2 is an NAD-dependent histone deacetylase. *Nature*, 403(6771), pp.795–800.

Ivy, J.M., Klar, A.J. & Hicks, J.B., 1986. Cloning and characterization of four SIR genes of Saccharomyces cerevisiae. *Molecular and Cellular Biology*, 6(2), pp.688–702.

James, T.C. & Elgin, S.C., 1986. Identification of a nonhistone chromosomal protein associated with heterochromatin in Drosophila melanogaster and its gene. *Molecular and Cellular Biology*, 6(11), pp.3862–3872.

Jia, S., Noma, K. & Grewal, S.I.S., 2004. RNAi-independent heterochromatin nucleation by the stress-activated ATF/CREB family proteins. *Science*, 304(5679), pp.1971–1976.

Johnson, A. et al., 2013. Heterochromatic gene silencing by activator interference and a transcription elongation barrier. *The Journal of Biological Chemistry*.

Johnson, A. et al., 2009. Reconstitution of heterochromatin-dependent transcriptional gene silencing. *Molecular Cell*, 35(6), pp.769–81.

Johnson, L.M. et al., 1990. Genetic evidence for an interaction between SIR3 and histone H4 in the repression of the silent mating loci in Saccharomyces cerevisiae. *Proceedings of the National Academy of Sciences of the United States of America*, 87(16), pp.6286–90.

Kan, P.-Y. et al., 2007. The H3 tail domain participates in multiple interactions during folding and self-association of nucleosome arrays. *Molecular and Cellular Biology*, 27(6), pp.2084–2091.

Kan, P.-Y., Caterino, T.L. & Hayes, J.J., 2009. The H4 tail domain participates in intra- and internucleosome interactions with protein and DNA during folding and oligomerization of nucleosome arrays. *Molecular and Cellular Biology*, 29(2), pp.538–46.

Kanoh, J. et al., 2005. Telomere binding protein Taz1 establishes Swi6 heterochromatin independently of RNAi at telomeres. *Current Biology*, 15(20), pp.1808–1819.

Kaufman, P.D. & Botchan, M.R., 1994. Assembly of nucleosomes: do multiple assembly factors mean multiple mechanisms? *Current Opinion in Genetics & Development*, 4(2), pp.229–235.

King, D.A. et al., 2006. Domain structure and protein interactions of the silent information regulator Sir3 revealed by screening a nested deletion library of protein fragments. *The Journal of Biological Chemistry*, 281(29), pp.20107–19.

Kitada, T. et al., 2012. Mechanism for epigenetic variegation of gene expression at yeast telomeric heterochromatin. *Genes & Development*, 26(21), pp.2443–55.

Kostriken, R. & Heffron, F., 1984. The product of the HO gene is a nuclease: purification and characterization of the enzyme. *Cold Spring Harbor Symposia on Quantitative Biology*, 49, pp.89–96.

Kruithof, M. et al., 2009. Single-molecule force spectroscopy reveals a highly compliant helical folding for the 30-nm chromatin fiber. *Nature Structural & Molecular Biology*, 16(5), pp.534–40.

Kueng, S. et al., 2012. Regulating repression: roles for the sir4 N-terminus in linker DNA protection and stabilization of epigenetic states. *PLoS Genetics*, 8(5), p.e1002727.

Kueng, S., Oppikofer, M. & Gasser, S.M., 2013. SIR proteins and the assembly of silent chromatin in budding yeast. *Annual Review of Genetics*, 47, pp.275–306.

Lachner, M. et al., 2001. Methylation of histone H3 lysine 9 creates a binding site for HP1 proteins. *Nature*, 410(6824), pp.116–120.

Laroche, T. et al., 1998. Mutation of yeast Ku genes disrupts the subnuclear organization of telomeres. *Current Biology*, 8(11), pp.653–656.

Van Leeuwen, F., Gafken, P.R. & Gottschling, D.E., 2002. Dot1p modulates silencing in yeast by methylation of the nucleosome core. *Cell*, 109(6), pp.745–756.

Leuba, S.H. et al., 1998. Contributions of linker histones and histone H3 to chromatin structure: scanning force microscopy studies on trypsinized fibers. *Biophysical journal*, 74, pp.2823–2829.

Liaw, H. & Lustig, A.J., 2006. Sir3 C-terminal domain involvement in the initiation and spreading of heterochromatin. *Molecular and Cellular Biology*, 26(20), pp.7616–7631.

Lieberman-Aiden, E. et al., 2009. Comprehensive mapping of long-range interactions reveals folding principles of the human genome. *Science*, 326(5950), pp.289–93.

Liou, G.-G. et al., 2005. Assembly of the SIR complex and its regulation by O-acetyl-ADP-ribose, a product of NAD-dependent histone deacetylation. *Cell*, 121(4), pp.515–27.

Loo, S. & Rine, J., 1994. Silencers and domains of generalized repression. *Science*, 264(5166), pp.1768–1771.

Lowary, P.T. & Widom, J., 1998. New DNA sequence rules for high affinity binding to histone octamer and sequence-directed nucleosome positioning. *Journal of Molecular Biology*, 276, pp.19–42.

Lu, X. et al., 2006. In vitro chromatin self-association and its relevance to genome architecture. *Biochemical Cell Biology*, 84, pp.411–417.

Luger, K. et al., 1997. Crystal structure of the nucleosome core particle at 2.8 A resolution. *Nature*, 389, pp.251–260.

Luger, K., Dechassa, M.L. & Tremethick, D.J., 2012. New insights into nucleosome and chromatin structure: an ordered state or a disordered affair? *Nature Reviews. Molecular Cell Biology*, 13(7), pp.436–47.

Luger, K., Rechsteiner, T.J. & Richmond, T.J., 1999. Expression and purification of recombinant histones and nucleosome reconstitution. *Methods in molecular biology (Clifton, N.J.)*, 119(4), pp.1–16.

Mackay, V. & Manney, T.R., 1974. Mutations affecting sexual conjugation and related processes in Saccharomyces cerevisiae. I. Isolation and phenotypic characterization of nonmating mutants. *Genetics*, 76(2), pp.255–271.

Maeshima, K. et al., 2014. Chromatin as dynamic 10-nm fibers. *Chromosoma*, 123(3), pp.225–37.

Manning, B.J. & Peterson, C.L., 2014. Direct interactions promote eviction of the Sir3 heterochromatin protein by the SWI/SNF chromatin remodeling enzyme. *Proceedings of the National Academy of Sciences*, 111(50), pp.17827–17832.

Martino, F. et al., 2009. Reconstitution of yeast silent chromatin: multiple contact sites and O-AADPR binding load SIR complexes onto nucleosomes in vitro. *Molecular cell*, 33(3), pp.323–34.

McBryant, S.J. et al., 2008. The silent information regulator 3 protein, SIR3p, binds to chromatin fibers and assembles a hypercondensed chromatin

architecture in the presence of salt. *Molecular and Cellular Biology*, 28(11), pp.3563–72.

McBryant, S.J., Krause, C. & Hansen, J.C., 2006. Domain organization and quaternary structure of the Saccharomyces cerevisiae silent information regulator 3 protein, Sir3p. *Biochemistry*, 45(51), pp.15941–8.

Meehan, R.R., Kao, C.F. & Pennings, S., 2003. HP1 binding to native chromatin in vitro is determined by the hinge region and not by the chromodomain. *EMBO Journal*, 22(12), pp.3164–3174.

Meneghini, M.D., Wu, M. & Madhani, H.D., 2003. Conserved histone variant H2A.Z protects euchromatin from the ectopic spread of silent heterochromatin. *Cell*, 112(5), pp.725–736.

Mishra, K. & Shore, D., 1999. Yeast Ku protein plays a direct role in telomeric silencing and counteracts inhibition by Rif proteins. *Current Biology*, 9(19), pp.1123–1126.

Moazed, D. et al., 1997. Silent information regulator protein complexes in Saccharomyces cerevisiae: a SIR2/SIR4 complex and evidence for a regulatory domain in SIR4 that inhibits its interaction with SIR3. *Proceedings of the National Academy of Sciences of the United States of America*, 94(6), pp.2186–2191.

Moretti, P. et al., 1994. Evidence that a complex of SIR proteins interacts with the silencer and telomere-binding protein RAP1. *Genes & Development*, 8(19), pp.2257–2269.

Murphy, G.A. et al., 2003. The Sir4 C-terminal coiled coil is required for telomeric and mating type silencing in Saccharomyces cerevisiae. *Journal of Molecular Biology*, 334(4), pp.769–780.

Naumova, N. et al., 2013. Organization of the mitotic chromosome. *Science*, 342(6161), pp.948–53.

Neumann, F.R. et al., 2012. Targeted INO80 enhances subnuclear chromatin movement and ectopic homologous recombination. *Genes and Development*, 26(4), pp.369–383.

Nguyen, V.Q. et al., 2013. Molecular architecture of the ATP-dependent chromatin-remodeling complex SWR1. *Cell*, 154(6), pp.1220–1231.

Nishino, Y. et al., 2012. Human mitotic chromosomes consist predominantly of irregularly folded nucleosome fibres without a 30-nm chromatin structure. *The EMBO Journal*, 31(7), pp.1644–53.

Norris, A. & Boeke, J.D., 2010. Silent information regulator 3: the Goldilocks of the silencing complex. *Genes & development*, 24(2), pp.115–22.

Olins, A.L. & Olins, D.E., 1974. Spheroid chromatin units (v bodies). *Science*, 183(4122), pp.330–332.

Onishi, M. et al., 2007. Role of the conserved Sir3-BAH domain in nucleosome binding and silent chromatin assembly. *Molecular Cell*, 28(6), pp.1015–28.

Oppikofer, M. et al., 2011. A dual role of H4K16 acetylation in the establishment of yeast silent chromatin. *The EMBO Journal*, 30(13), pp.2610–21.

Oppikofer, M., Kueng, S., Keusch, J.J., et al., 2013. Dimerization of Sir3 via its C-terminal winged helix domain is essential for yeast heterochromatin formation. *The EMBO Journal*, 32(3), pp.437–49.

Oppikofer, M., Kueng, S. & Gasser, S.M., 2013. SIR-nucleosome interactions: structure-function relationships in yeast silent chromatin. *Gene*, 527(1), pp.10–25.

Ozer, G., Luque, A. & Schlick, T., 2015. The chromatin fiber: multiscale problems and approaches. *Current Opinion in Structural Biology*, 31, pp.124–139.

Palladino, F. et al., 1993. SIR3 and SIR4 proteins are required for the positioning and integrity of yeast telomeres. *Cell*, 75(3), pp.543–555.

Papamichos-Chronakis, M. & Peterson, C.L., 2013. Chromatin and the genome integrity network. *Nature reviews. Genetics*, 14(1), pp.62–75.

Patel, D.J. & Wang, Z., 2013. Readout of epigenetic modifications. *Annual Review of Biochemistry*, 82, pp.81–118.

Peng, J.C. & Karpen, G.H., 2008. Epigenetic regulation of heterochromatic DNA stability. *Current Opinion in Genetics & Development*, 18(2), pp.204–11.

Peng, J.C. & Karpen, G.H., 2007. H3K9 methylation and RNA interference regulate nucleolar organization and repeated DNA stability. *Nature Cell Biology*, 9(1), pp.25–35.

Pepenella, S., Murphy, K.J. & Hayes, J.J., 2014. Intra- and inter-nucleosome interactions of the core histone tail domains in higher-order chromatin structure. *Chromosoma*, 123(1-2), pp.3–13.

Platero, J.S., Hartnett, T. & Eissenberg, J.C., 1995. Functional analysis of the chromo domain of HP1. *The EMBO Journal*, 14(16), pp.3977–3986.

Radman-Livaja, M. et al., 2011. Dynamics of Sir3 spreading in budding yeast: secondary recruitment sites and euchromatic localization. *The EMBO Journal*, 30(6), pp.1012–1026.

Rando, O.J. & Winston, F., 2012. Chromatin and transcription in yeast. *Genetics*, 190(2), pp.351–87.

Ravindra, A., Weiss, K. & Simpson, R.T., 1999. High-resolution structural analysis of chromatin at specific loci: Saccharomyces cerevisiae silent mating-type locus HMRa. *Molecular and cellular biology*, 19(12), pp.7944–50.

Rea, S. et al., 2000. Regulation of chromatin structure by site-specific histone H3 methyltransferases. *Nature*, 406(6796), pp.593–599.

Richmond, T.J. et al., 1984. Structure of the nucleosome core particle at 7 A resolution. *Nature*, 311(5986), pp.532–537.

Richmond, T.J. et al., 2003. The structure of DNA in the nucleosome core. *Nature*, 423(6936), pp.145–50.

Rine, J. et al., 1979. A suppressor of mating-type locus mutations in Saccharomyces cerevisiae: Evidence for and identification of cryptic mating-type loci. *Genetics*, 93(4), pp.877–901.

Rine, J. & Herskowitz, I., 1987. Four genes responsible for a position effect on expression from HML and HMR in Saccharomyces cerevisiae. *Genetics*, 116(1), pp.9–22.

Roman, H. & Sands, S.M., 1953. Heterogeneity of clones of Saccharomyces derived from haploid ascospores. *Proceedings of the National Academy of Sciences of the United States of America*, 39(3), pp.171–179.

Routh, A., Sandin, S. & Rhodes, D., 2008. Nucleosome repeat length and linker histone stoichiometry determine chromatin fiber structure. *Proceedings of the National Academy of Sciences of the United States of America*, 105(26), pp.8872–7.

Roy, R. et al., 2004. Separation-of-function mutants of reast Ku80 reveal a Yku80p-Sir4p interaction involved in telomeric silencing. *Journal of Biological Chemistry*, 279(1), pp.86–94.

Rudner, A.D. et al., 2005. A nonhistone protein-protein interaction required for assembly of the SIR complex and silent chromatin. *Molecular and Cellular Biology*, 25(11), pp.4514–4528.

Rusche, L.N., Kirchmaier, A.L. & Rine, J., 2002. Ordered nucleation and spreading of silenced chromatin in Saccharomyces cerevisiae. *Molecular Biology of the Cell*, 13(July), pp.2207–2222.

Rusche, L.N., Kirchmaier, A.L. & Rine, J., 2003. The establishment, inheritance, and function of silenced chromatin in Saccharomyces cerevisiae. *Annual Review of Biochemistry*, 72, pp.481–516.

Rusche, L.N. & Lynch, P.J., 2009. Assembling heterochromatin in the appropriate places: A boost is needed. *Journal of Cellular Physiology*, 219(3), pp.525–8.

Saksouk, N., Simboeck, E. & Déjardin, J., 2015. Constitutive heterochromatin formation and transcription in mammals. *Epigenetics and Chromatn*, 8(3), pp.1–17.

Savitsky, M. et al., 2002. Heterochromatin Protein 1 is involved in control of telomere elongation in Drosophila melanogaster. *Molecular and Cellular Biology*, 22(9), pp.3204–3218.

Schotta, G. et al., 2002. Central role of Drosophila SU(VAR)3-9 in histone H3-K9 methylation and heterochromatic gene silencing. *EMBO Journal*, 21(5), pp.1121–1131.

Schwarz, P.M. et al., 1996. Reversible oligonucleosome self-association: dependence on divalent cations and core histone tail domains. *Biochemistry*, 35(13), pp.4009–15.

Schwarz, P.M. & Hansen, J.C., 1994. Formation and stability of higher order chromatin structures. *The Journal of Biological Chemistry*, 12(36), pp.16284–16289.

Sekinger, E.A. & Gross, D.S., 2001. Silenced chromatin is permissive to activator binding and PIC recruitment. *Cell*, 105(3), pp.403–14.

Shia, W.-J., Li, B. & Workman, J.L., 2006. SAS-mediated acetylation of histone H4 Lys 16 is required for H2A.Z incorporation at subtelomeric regions in Saccharomyces cerevisiae. *Genes & Development*, 20(18), pp.2507–12.

Shogren-Knaak, M. et al., 2006. Histone H4-K16 acetylation controls chromatin structure and protein interactions. *Science*, 311, pp.844–847.

Shogren-knaak, M. & Peterson, C.L., 2006. Switching on Chromatin: mechanistic role of histone H4-K16 Acetylation. *Cell Cycle*, 5(13), pp.1361–1365.

Simon, J.A. & Kingston, R.E., 2013. Occupying chromatin: polycomb mechanisms for getting to genomic targets, stopping transcriptional traffic, and staying put. *Molecular Cell*, 49(5), pp.808–824.

Simon, M.D. et al., 2007. The site-specific installation of methyl-lysine analogs into recombinant histones. *Cell*, 128(5), pp.1003–12.

Simpson, R.T., 1986. Nucleosome positioning in vivo and in vitro. *BioEssays*, 4(4), pp.172–176.

Simpson, R.T., 1978. Structure of the chromatosome, a chromatin particle containing 160 base pairs of DNA and all the histones. *Biochemistry*, 17(25), pp.5524–5531.

Simpson, R.T., Thoma, F. & Brubaker, J.M., 1985. Chromatin reconstituted from tandemly repeated cloned DNA fragments and core histones: a model system for study of higher order structure. *Cell*, 42(3), pp.799–808.

Singer, M.S. et al., 1998. Identification of high-copy disruptors of telomeric silencing in Saccharomyces cerevisiae. *Genetics*, 150(2), pp.613–632.

Sinha, D. & Shogren-Knaak, M., 2010. Role of direct interactions between the histone H4 Tail and the H2A core in long range nucleosome contacts. *The Journal of Biological Chemistry*, 285(22), pp.16572–81.

Sinha, M. et al., 2009. Recombinational repair within heterochromatin requires ATP-dependent chromatin remodeling. *Cell*, 138(6), pp.1109–21.

Smothers, J.F. & Henikoff, S., 2000. The HP1 chromo shadow domain binds a consensus peptide pentamer. *Current Biology*, 10(1), pp.27–30.

Staynov, D.Z. & Crane-Robinson, C., 1988. Footprinting of linker histones H5 and H1 on the nucleosome. *The EMBO Journal*, 7(12), pp.3685–3691.

Strahl-Bolsinger, S. et al., 1997. SIR2 and SIR4 interactions differ in core and extended telomeric heterochromatin in yeast. *Genes & Development*, 11(1), pp.83–93.

Strick, R. et al., 2001. Cation-chromatin binding as shown by ion microscopy is essential for the structural integrity of chromosomes. *Journal of Cell Biology*, 155(6), pp.899–910.

Sugiyama, T. et al., 2005. RNA-dependent RNA polymerase is an essential component of a self-enforcing loop coupling heterochromatin assembly to siRNA production. *Proceedings of the National Academy of Sciences of the United States of America*, 102(1), pp.152–157.

Suka, N. et al., 2001. Highly specific antibodies determine histone acetylation site usage in yeast heterochromatin and euchromatin. *Molecular Cell*, 8(2), pp.473–479.

Suka, N., Luo, K. & Grunstein, M., 2002. Sir2p and Sas2p opposingly regulate acetylation of yeast histone H4 lysine16 and spreading of heterochromatin. *Nature Genetics*, 32(3), pp.378–83.

Swygert, S.G. et al., 2014. Solution-state conformation and stoichiometry of yeast Sir3 heterochromatin fibres. *Nature Communications*, 5(May), p.4751.

Swygert, S.G. & Peterson, C.L., 2014. Chromatin dynamics: interplay between remodeling enzymes and histone modifications. *Biochimica et Biophysica Acta - Gene Regulatory Mechanisms*, 1839(8), pp.728–736.

Taddei, A. et al., 2004. Separation of silencing from perinuclear anchoring functions in yeast Ku80, Sir4 and Esc1 proteins. *The EMBO Journal*, 23(6), pp.1301–12.

Taddei, A. & Gasser, S.M., 2004. Multiple pathways for telomere tethering: Functional implications of subnuclear position for heterochromatin formation. *Biochimica et Biophysica Acta - Gene Structure and Expression*, 1677(1-3), pp.120–128.

Takano, I. & Oshima, Y., 1970. Mutational nature of an allele-specific conversion of the mating type by the homothallic gene HO alpha in Saccharomyces. *Genetics*, 65(3), pp.421–427.

Tanner, K.G. et al., 2000. Silent information regulator 2 family of NAD-dependent histone/protein deacetylases generates a unique product, 1-O-

acetyl-ADP-ribose. *Proceedings of the National Academy of Sciences of the United States of America*, 97(26), pp.14178–14182.

Tanny, J.C. et al., 1999. An enzymatic activity in the yeast Sir2 protein that is essential for gene silencing. *Cell*, 99(7), pp.735–745.

Tanny, J.C. & Moazed, D., 2001. Coupling of histone deacetylation to NAD breakdown by the yeast silencing protein Sir2: evidence for acetyl transfer from substrate to an NAD breakdown product. *Proceedings of the National Academy of Sciences of the United States of America*, 98(2), pp.415–420.

Thoma, F., Koller, T.H. & A, K., 1979. Involvement of histone H1 in the organization of the nucleosome and of the salt-dependent superstructures ofchromatin. *Journal of Cell Biology*, 83, pp.403–427.

Thurtle, D.M. & Rine, J., 2014. The molecular topography of silenced chromatin in Saccharomyces cerevisiae. *Genes & Development*, 28(3), pp.245–258.

Tosi, A. et al., 2013. Structure and subunit topology of the INO80 chromatin remodeler and its nucleosome complex. *Cell*, 154(6), pp.1207–1219.

Triolo, T. & Sternglanz, R., 1996. Role of interactions between the origin recognition complex and SIR1 in transcriptional silencing. *Nature*, 381(6579), pp.251–253.

Tse, C. & Hansen, J.C., 1997. Hybrid trypsinized nucleosomal arrays: identification of multiple functional roles of the H2A/H2B and H3/H4 N-termini in chromatin fiber compaction. *Biochemistry*, 36(38), pp.11381–11388.

Wang, F. et al., 2013. Heterochromatin protein Sir3 induces contacts between the amino terminus of histone H4 and nucleosomal DNA. *Proceedings of the National Academy of Sciences of the United States of America*, 110(21), pp.8495–500.

Wang, J.-P. et al., 2008. Preferentially quantized linker DNA lengths in Saccharomyces cerevisiae. *PLoS Computational Biology*, 4(9), p.e1000175.

Wang, X. et al., 2004. Importance of the Sir3 N terminus and its acetylation for yeast transcriptional silencing. *Genetics*, 168(1), pp.547–551.

Ward, K., 1976. Partial specific volume, expansibility, heat capacity of aqueous lysozyme solutions. *The Journal of Biological Chemistry*, 251(13), pp.4001–4004.

Weiss, K. & Simpson, R.T., 1998. High-resolution structural analysis of chromatin at specific loci : Saccharomyces cerevisiae silent mating type locus HMLα. *Molecular and Cellular Biology*, 18(9), pp.5392–5403.

White, S.A. & Allshire, R.C., 2008. RNAi-mediated chromatin silencing in fission yeast. *Current Topics in Microbiology and Immunology*, 320, pp.158–178.

Widom, J., 1986. Physicochemical studies of the folding of the 100 A nucleosome filament into the 300 A filament: cation dependence. *Journal of Molecular Biology*, 190(3), pp.411–424.

Widom, J., 1985. Structure of the 300Å chromatin filament: X-ray diffraction from oriented samples. *Cell*, 43(1), pp.207–213.

Woodcock, C.L. & Ghosh, R.P., 2010. Chromatin higher-order structure and dynamics. *Cold Spring Harbor Perspectives in Biology*, 2(5), p.a000596.

Woodcock, C.L.F., Frado, L.L.Y. & Rattner, J.B., 1984. The higher-order structure of chromatin: evidence for a helical ribbon arrangement. *Journal of Cell Biology*, 99(1 I), pp.42–52.

Yamada, T. et al., 2005. The nucleation and maintenance of heterochromatin by a histone deacetylase in fission yeast. *Molecular Cell*, 20(2), pp.173–185.

Yang, D. et al., 2013. Nα-acetylated Sir3 stabilizes the conformation of a nucleosome-binding loop in the BAH domain. *Nature Structural & Molecular Biology*, 20(9), pp.1116–1119.

Zentner, G.E. & Henikoff, S., 2013. Regulation of nucleosome dynamics by histone modifications. *Nature Structural & Molecular Biology*, 20(3), pp.259–66.

Zheng, C. et al., 2005. Salt-dependent intra- and internucleosomal interactions of the H3 tail domain in a model oligonucleosomal array. *The Journal of Biological Chemistry*, 280(39), pp.33552–7.